NASA CR-72793
PWA FR-4541

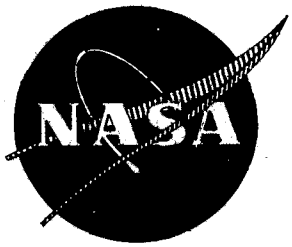

SINGLE-STAGE EXPERIMENTAL EVALUATION OF COMPRESSOR BLADING WITH SLOTS AND VORTEX GENERATORS

PART V - FINAL REPORT

by J. A. Brent

PRATT & WHITNEY AIRCRAFT
DIVISION OF UNITED AIRCRAFT CORPORATION
FLORIDA RESEARCH AND DEVELOPMENT CENTER

Prepared for
NATIONAL AERONAUTICS AND SPACE ADMINISTRATION

NASA Lewis Research Center
Contract NAS3-10481

(NASA-CR-72793) SINGLE-STAGE EXPERIMENTAL EVALUATION OF COMPRESSOR BLADING WITH SLOTS AND VORTEX GENERATORS, PART 5 Final Report J.A. Brent (Pratt and Whitney Aircraft) 31 Mar. 1972 135 p CSCL 21E G3/28
N72-22791
Unclas 22936

CAT. 28

32

1. Report No. NASA CR-72793	2. Government Accession No.	3. Recipient's Catalog No.
4. Title and Subtitle "SINGLE-STAGE EXPERIMENTAL EVALUATION OF COMPRESSOR BLADING WITH SLOTS AND VORTEX GENERATORS", PART V - FINAL REPORT		5. Report Date 31 March 1972 6. Performing Organization Code
7. Author(s) J. A. Brent		8. Performing Organization Report No. PWA FR-4541 10. Work Unit No.
9. Performing Organization Name and Address Pratt & Whitney Aircraft Florida Research and Development Center West Palm Beach, Florida 33402		11. Contract or Grant No. NAS3-10481 13. Type of Report and Period Covered Contractor Report
12. Sponsoring Agency Name and Address National Aeronautics and Space Administration Washington, D. C. 20546		14. Sponsoring Agency Code

15. Supplementary Notes

Project Manager, L. Joseph Herrig, Fluid System Components Division, NASA - Lewis Research Center, Cleveland, Ohio 44135

16. Abstract

An experimental investigation was conducted to determine the extent that slots and vortex generators can increase the efficiency and stable operating range of highly loaded compressor stages. With slots in the rotor and stator, the stage perfromance both with and without vortex generators was inferior to that achieved with the unslotted blading. However, with vortex generators, stator slots, and an unslotted rotor, the stable operating range increased 25% and the stage peak efficiency increased 2.1% over the values achieved with the unslotted rotor and stator without vortex generators, at design equivalent rotor speed.

17. Key Words (Suggested by Author(s))	18. Distribution Statement
Blading with slots and vortex generators Compressor	Unclassified - Unlimited

19. Security Classif. (of this report)	20. Security Classif. (of this page)	21. No. of Pages	22. Price*
Unclassified	Unclassified	135	$3.00

* For sale by the National Technical Information Service, Springfield, Virginia 22151

PRECEDING PAGE BLANK NOT FILMED

CONTENTS

ILLUSTRATIONS

ILLUSTRATIONS (Continued)

ILLUSTRATIONS (Continued)

ILLUSTRATIONS (Continued)

ILLUSTRATIONS (Continued)

TABLES

TABLES (Continued)

SUMMARY

An experimental investigation was conducted with an 0.8 hub-tip ratio single-stage compressor to determine the extent that slots and vortex generators can be applied to reduce losses in the wall regions and increase the efficiency and stable operating range of highly loaded compressor stages. A secondary objective of this investigation was to determine the effects of loading level and boundary layer suction on stage efficiency and operating range. Two compressor stages, each comprising a rotor and a stator, were designed with different work levels and corresponding radial work gradients for this investigation. After reviewing the test data for the unslotted baseline configurations, endwall slots and vortex generators were designed for the more lightly loaded stage. Because of the poor performance of the more highly loaded stage, and because of a rotor blade failure near the end of the baseline test program, slots and vortex generators were not designed for this stage.

Both stages were designed with zero rotor prewhirl, axial discharge flow, and constant exit total pressure across the span. The design velocity diagrams and predicted performance were based on the assumption that the rotor and stator losses would be reduced by the addition of slots and vortex generators. All rotors and stators were designed with NACA 65-series airfoil sections with A = 1.0 meanlines. Table I summarizes the stage designs.

Table I. Summary of Stage 4 and 5 Designs

Factors	Stage 4	Stage 5
Tip Speed, fps (mps)	757 (230.7)	757 (230.7)
Pressure Ratio	1.325	1.375
Adiabatic Efficiency, %	84	82
Difussion Factor:		
Rotor Tip	0.60	0.68
Rotor Hub	0.74	0.82
Stator Tip	0.50	0.61
Stator Hub	0.69	0.81

Porous walls were located at the rotor tip and the stator hub and tip for boundary layer suction. With the exception of several points where the bleed flow was intentionally reduced to determine the effect of boundary layer suction on stage efficiency and operating range, the maximum obtainable bleed flow was maintained throughout the test program. Table II summarizes the configurations that were tested.

Table II. Summary of Configurations Tested

Configuration	Rotor Inlet Vortex Generators	Stator Inlet Vortex Generators	Exploratory Tests With Reduced Rotor and Stator Wall Bleed
Unslotted Rotor 4 - Unslotted Stator 4	No	No	No
Unslotted Rotor 5 - Unslotted Stator 5	No	No	No
Slotted Rotor 4 - Slotted Stator 4	No	No	Yes
Slotted Rotor 4 - Slotted Stator 4	Yes	No	Yes
Unslotted Rotor 4 - Slotted Stator 4	Yes	Yes	Yes

The maximum adiabatic efficiency and the corresponding pressure ratio achieved by the unslotted configurations without vortex generators at design equivalent rotor speed are summarized in table III.

Table III. Maximum Adiabatic Efficiency and Corresponding Pressure Ratio

Configuration	Adiabatic Efficiency	Pressure Ratio
Rotor 4	0.874	1.324
Stage 4	0.748	1.274
Rotor 5	0.843	1.367
Stage 5	0.700	1.299

At design equivalent rotor speed the pressure ratio and efficiency of slotted stage 4, both with and without vortex generators, were lower than the performance obtained with the unslotted stage. However, the stator blade element performance data indicate lower losses near the walls for the slotted stator at the same or higher incidence angles than those for the unslotted stator. The addition of rotor inlet vortex generators to the slotted stage produced a slight decrease in the rotor tip region losses near stall. With vortex generators upstream of the rotor and between the rotor and stator, stator slots, and an unslotted rotor 4, the stable operating range was increased by 25% relative to the unslotted baseline operating range. The increase in stable operating range was accompanied by 0.8 and 2.1% increases in peak rotor and stage efficiencies, respectively, at approximately the same peak pressure ratios.

Reducing the wall boundary layer bleed flow in the rotor and stator reduced the rotor and stage pressure ratio and efficiency and changed the pressure ratio-flow characteristic at constant rotor speed.

INTRODUCTION

Experience with highly loaded axial-flow compressors has shown that the region of the flow path most critical to achieving high performance is that area adjacent to the walls. In the wall region of these stages the flow is predominantly three-dimensional, whereas at midspan the flow is more nearly two-dimensional. The three-dimensional aspects of the flow result in marked reductions in total pressure ratio, adiabatic efficiency, and flow near the walls. Because these factors generally represent a conversion of kinetic energy into internal energy at an increase in entropy, the diffusion limits for a conventional blade row are reached near the wall and stall or compressor surge is induced. Further, the wall diffusion limits prevent the utilization of the full loading capacity of the midstream portion of the blade, since the reduction in flow near the walls causes an increase in the midspan velocity with a resultant decrease in midspan loading. These factors indicate that advanced compressor design concepts for the increase of allowable stage loading and stable low-loss operating range should be concerned with the problem of three-dimensional flow near the walls.

Previous attempts to increase allowable stage loading limits by means of slotted blading under NASA Contract NAS3-7603 (Reference 1) indicated good performance for the blade midspan regions, but poor performance near the walls. The relative effectiveness of the slots at midspan and their ineffectiveness near the wall was attributed to the chordal placement of the slots and their inability to sufficiently reduce the three-dimensional flows in the wall region. To further investigate methods of decreasing end wall losses, a two-part single-stage experimental investigation was initiated to evaluate several methods of improving the blade element performance in the wall region. The first part of the program involved adding blade-end slots and secondary flow fences to stage 3 of Contract NAS3-7603. The second part of the program entailed designing two new stages, designated 4 and 5, for evaluation of the effects of slots and vortex generators on stage efficiency and stable operating range. Investigation of the effects of rotor and stator loading level and boundary layer suction on stage efficiency and operating range were secondary objectives of the second part of the program. Because of the poor performance of unslotted stage 5 and because a rotor blade failed near the end of the baseline test program, slots and vortex generators were not investigated in stage 5.

The design modifications, test data, and the test results for stage 3 modified with blade-end slots and secondary flow fences are summarized in Reference 2. Discussion of the aerodynamic and mechanical design of stages 4 and 5 is presented in Reference 3, and the data and performance reports for these stages are listed as References 4 and 5. This report summarizes the experimental results obtained during the second part of the program and discusses these results relative to the program design intent.

DESIGN SUMMARY

Selection of Velocity Diagrams

The initial phase of the design was the correlation of the rotor and stator blade element performance data from References 6 through 11. These data, which were used in the design of stages 4 and 5, were comprised of loss parameter, diffusion factor, deviation angle, and minimum-loss incidence angle. An important premise used for the design velocity diagram selection was the assumption that slots and vortex generators would reduce the blade element losses in the end regions by reducing the secondary flow. (See Reference 3.) Additionally, it was specified that the rotor inlet and stator exit velocities were to be axial, and that the stator exit total pressure was to be constant across the span.

The velocity diagrams were selected through an iteration procedure involving a streamline analysis calculation and the selected loss parameter vs diffusion factor distributions. An iteration procedure was required because the velocity diagrams are dependent upon losses that, in turn, are dependent upon the velocity diagrams and associated diffusion factors. The streamline analysis procedure solved the continuity, energy, and radial equilibrium equations for an axisymmetric flow. Radial gradients of enthalpy and entropy were included in the calculation, and the influence of streamline curvature on the radial distribution of static pressure was accounted for in the design. During these iterations the flow path to be used for both stage 4 and 5 was altered by varying the outer wall diameters to maintain a nearly constant average axial velocity. The tip speed was varied to provide the desired (0.8) tip inlet relative Mach number, and the specific flow was held constant at 33 lb/sec-ft^2 (161.1 kg/sec-m^2), a value that is representative of current middle stage design practice. The pressure ratio was varied to bring the loading to the desired levels (D max = 0.7 for rotor 4 and D max = 0.8 for rotor 5) to produce two stages with different levels of work input. Both stages 4 and 5 were designed with relatively high work input near the walls to compensate for the high losses that were predicted in these regions. Different work gradients resulted for the two stages because as average work coefficient (and hence diffusion factor) increased, the radial work gradient had to be greater to compensate for the increased slope of the predicted loss curve.

Design velocity diagram data and predicted performance for the stages that were selected to fulfill the design intent are summarized in Appendix A. Symbols and performance variables are defined in Appendix B. Stages 4 and 5 have design pressure ratios of 1.325 and 1.375, respectively, at a rotor tip velocity of 757 ft/sec (230.7 m/sec) and a corrected weight flow of 110 lb/sec (49.9 kg/sec).

Selection of Blading Geometry

NACA 65-series airfoil sections with an A = 1.0 meanline were selected for both the rotors and stators of stages 4 and 5 to be consistent with the blading used in Reference 1, since these stages represent a continuation of that work. Similarly, the number of rotor and stator blades were established to be 60 and 58, respectively. Other blade geometry variables such as chord length, aspect ratio, solidity, and maximum thickness were the same as, or very similar to, those for the blading used in Reference 1. Slight departures

in aspect ratio and hub/tip ratio resulted from the wall convergence at the rotor and stator tip that was provided to limit the diffusion factor, and to maintain an average axial velocity ratio of approximately 1.0.

Since the slope of the A = 1 meanline is theoretically infinite at the airfoil leading and trailing edges, the blade geometry data were calculated in terms of an equivalent circular arc meanline of the same maximum camber as the actual (A = 1.0) meanline. Design incidence (minimum loss) and deviation angles were calculated using equations 286 and 287 in Reference 12. For the rotor, 2 degrees were subtracted from the calculated incidence angles in accordance with the minimum loss incidence results obtained in Reference 1. The resultant radial distributions of rotor and stator equivalent circular arc meanline camber angles are shown in figures 1 and 2. The blade geometry data (inlet and exit metal angles, chord angles, camber angles, solidities, and maximum thickness) are summarized in terms of an equivalent circular arc meanline in tables A-1 through A-4 of Appendix A. Hub, midspan, and tip sections of the stage 4 and 5 blading are shown in figures 3 and 4. Photographs of the stage 4 and 5 blading are shown in figures 5 and 6 for the rotors and stators, respectively.

Stage 4 Slot Design

Four factors were considered for the selection of stage 4 rotor and stator slot configurations:

1. Spanwise extent
2. Chordal location
3. Number
4. Geometry

Spanwise extent, chordal location, and the number of slots were established on the basis of the axial velocity and loss coefficient distributions obtained from the unslotted (baseline) stage 4 test results (Reference 4). The slot geometry was determined for the stator 85% span location from calculated pressure coefficient distributions for this section. Two-dimensional, steady, incompressible, and inviscid potential flow was assumed for these calculations. Slot geometries for the rotor hub and tip and the stator tip sections were made geometrically similar to the configuration selected for the stator at 85% span. Details of the slot designs are given in Reference 3. Final slot geometries and locations are shown for the rotor in figures 7 and 8, and for the stator in figure 9. Photographs of the slotted rotor and slotted stator are shown in figures 10 and 11, respectively.

Vortex Generator Design

Based on the presence of severe secondary flows in both the rotor and stator blade rows, as indicated by the stage 4 baseline test results, it was concluded that vortex generators should be designed for the inner and outer walls of both blade rows. The vortex generators were intended, by means of turbulent mixing, to induce high momentum air from the mainstream into the wall boundary layer flow and low momentum air from the wall region into the mainstream flow, thus helping to unload the blades in the wall region and load the midspan region. The vortex generator design criteria are presented in Reference 3. The resulting configurations for the rotor and stator are shown in figures 12 through 14.

TEST EQUIPMENT

Compressor Test Rig

A schematic of the single-stage compressor rig is shown in figure 15, and the flow path dimensions are given in figure 16. The hub/tip ratio at the rotor inlet is 0.789, the test section has a constant hub diameter of 32.85 inches (0.834 m), and the outer wall converges from a diameter of 41.14 inches (1.045 m) at the rotor leading edge to 39.99 inches (1.016 m) at the stator exit. Relatively high convergence was provided at the rotor and stator tips to control the axial velocity and minimize the diffusion factor. Rotor bearing loads are transmitted to the rig support through struts located in the inlet and exhaust case assemblies. The inlet struts are sufficiently far upstream so their wakes are dissipated ahead of the rotor. The stage design specifications of zero rotor prewhirl and axial discharge flow eliminated the need for inlet and exit guide vanes. Flowrate was varied with a set of motor-driven throttle vanes located in the exhaust case.

Porous walls were installed for boundary layer suction at the rotor tip and the stator hub and tip as shown in figure 17. The porous wall was 0.060 inches (0.0015 m) thick and had 0.066 inch (0.0017 m) diameter holes on 0.187 inch (0.0047 m) centers, providing an 11% open area.

Instrumentation

The instrumentation utilized for the stage 4 and stage 5 test programs is described in detail in References 4 and 5, respectively. A general description of the instrumentation is given in this report to identify the source of measurements for the calculated performance variables.

Compressor flowrate was measured with a thin-plate orifice in the inlet duct, and compressor inlet pressure and temperature were recorded from measurements in the inlet plenum. Compressor inlet wall static pressures were recorded as the compressor was operated into and out of stall and were used to determine the stall limit flow from a correlation between these static pressures and weight flow. Rotor speed was measured by means of an electro-magnetic sensor mounted adjacent to a 60-tooth gear on the rotor shaft. Gear tooth passing frequency was displayed as RPM on a digital counter and recorded on magnetic tape.

Total pressure profiles ahead of and behind the rotor were measured with 20-degree wedge traverse probes. The measurements downstream of the rotor were verified by means of redundant measurements obtained with a radial rake with Kiel head sensing elements at 10, 30, 50, 70, and 90% span. Stage (stator) exit total pressure measurements were obtained using pitot-type wake probes of sufficient circumferential extent to encompass the vane gap. Static pressure ahead of and behind each blade row was measured by means of 8-degree wedge traverse probes. Four inner wall and four outer wall static pressure taps, approximately equally spaced, were located on extensions of the mid-channel streamlines ahead of and behind each blade row. Four additional inner and outer wall static pressure taps were also distributed across the vane gap ahead of and behind the stator to define the static pressure variations across the gap. Air angle measurements were obtained from 20-degree wedge traverse probes located ahead of and behind each blade row.

Stage exit total temperature was measured downstream of the stator at nine radial positions at each of four circumferential locations using shielded thermocouples installed in radial rakes. The stage exit temperature distributions measured with these rakes were also used for the rotor performance calculations.

Redundant instrumentation was provided so that the loss of any one instrument would not necessitate repeating the test and to provide a method of accounting for circumferential variations in performance. The axial locations of the instrumentation stations are shown in figure 15.

A high response pressure transducer, mounted in a total pressure probe behind the rotor at 10% span from the tip, was used to detect the initiation of rotating stall. Bellmouth static pressure, plenum pressure, rotor speed, and selected stage exit pressures were recorded on magnetic tape using high response instrumentation to aid in the determination of stall transient characteristics. These values were correlated in time with the output from the high response pressure transducer.

Steady-state pressure and temperature data were measured with a multichannel transducer scanning system that includes automatic data recording on computer cards. The temperature measurements were taken in conjunction with a temperature reference oven and a digital voltmeter. The steady-state pressure and temperature data were subsequently stored on tape for data processing. Traverse probe and transient data were recorded on tape in digital form.

Facility

The compressor test facility is shown schematically in figure 18. The compressor is driven by a single-stage turbine, powered by exhaust gases from a J75 slave engine, with compressor speed controlled by means of the engine throttle. The slave engine exhaust gas is also used to power an ejector for compressor wall boundary layer suction. Air enters the compressor test rig through a 103 ft (31.39 m) long combined inlet duct, plenum, and bellmouth inlet, and is exhausted through an exit diffuser to the atmosphere. The inlet duct contains a flow measuring orifice designed and installed in accordance with ASME standards. An area contraction ratio from plenum to compressor inlet of approximately 10:1 provided essentially stagnation conditions in the plenum. The inlet duct and plenum were mounted on a track and could be rolled away from the compressor rig inlet to facilitate configuration changes.

PROCEDURES

Test Procedures

Overall and blade element performance data were obtained at 50, 70, 90, 100 and 110% design equivalent rotor speed for unslotted stage 4, and at 70 and 100% of design equivalent rotor speed for slotted stage 4 and for the two configurations with vortex generators. Overall and blade element performance data were also recorded at 50, 70, 90, and 100% design equivalent rotor speed for unslotted stage 5. At each speed the flow was varied and data were recorded to define the speed characteristic between maximum flow and near-stall

conditions. With the exception of several points where the bleed flow was intentionally reduced, the rotor and stator bleed valves were left in the full-open position, thus providing the maximum obtainable bleed flow (limited by shroud effective flow area) throughout the test program. At each speed and flow setting, data from the fixed instrumentation were recorded and then the traverse probes were immersed to the hub, and traverse data were recorded as the probes were withdrawn at a travel rate of 3.0 in/min (0.0013 m/sec). Stall transient measurements were obtained at each rotor speed while operating the stage into and out of stall to define the stall point.

Data Reduction Procedures

Definitions of symbols and the overall and blade element performance variables are given in Appendix B. Total pressures and temperatures at each axial station were mass-averaged to obtain pressure ratio and efficiency. The mass-average temperature determined from the stage exit temperature and flow distribution was used as the rotor exit average temperature.

Performance and velocity diagram calculations were performed for each blade row along design streamlines that pass through 5, 10, 15, 30, 50, 70, 85, 90, and 95% span at the rotor exit instrumentation station. The values were calculated directly from the measurements obtained at the instrumentation stations. Translation of these measurements to the blade row leading and trailing edges was not considered necessary because, with the small wall convergence, the data at the instrumentation stations very nearly approximates that at the leading and trailing edges. Rotor loss coefficients were calculated using the measured values of pressure, temperature, and air angle at the blade inlet and exit. The stator loss coefficients were calculated using selected free-stream pressures from the respective downstream wake probe data for the upstream pressures to avoid biasing the results because of flow shifts through the stator blade row.

RESULTS AND DISCUSSION

Performance of Unslotted Stages 4 and 5

Unslotted stages 4 and 5 were tested to establish a performance baseline for comparison with the results of the subsequent tests with the addition of slots and vortex generators. The overall and blade element performance results, including the effects of rotor work level, inlet Mach number, and boundary layer bleed flow on rotor efficiency and stable operating range for these stages, are discussed in the following paragraphs. Complete tabulation of overall and blade element performance data for stages 4 and 5 are presented in references 4 and 5.

To provide a datum for the test results obtained with the unslotted stages, overall and blade element performance and velocity diagram values were predicted for the design blading geometry without assuming reduced losses due to slots and vortex generators. The results of these calculations are presented in tables A-5 through A-8 of Appendix A. These results are based on the assumptions that the rotor and stator deviation angles would be the same both with and without slots and that the unslotted stator blade elements would be operating close to minimum loss. The first assumption is consistent with

the results obtained in Reference 1, whereas the second assumption is based on the premise that the redistribution of the rotor exit flow, due to the higher rotor losses, would result in only a slight change in stator incidence angles. In the following discussion of the unslotted stage results any reference to the blading implies the unslotted rotor or stator.

Overall Performance

The overall performance for the two unslotted configurations is compared for the rotor in figure 19 and for the stage in figure 20. As shown, both stages failed to achieve their predicted pressure ratio and efficiency. The difference between predicted and measured efficiency was greater for stage 5 than for the lower loaded stage 4. At approximately design equivalent rotor speed and corrected flow, the efficiency of rotor 4 was 0.7% below its predicted value, whereas the efficiency of rotor 5 was 4.8% below its predicted value. The stage 4 and 5 efficiencies were 6.7% and 10.0%, respectively, below the predicted values.

Blade Element Performance for Unslotted Rotors

The low rotor pressure ratios, relative to the predicted values shown in figure 19, are attributed to high losses near the walls and low rotor work input. The high losses near the walls are evident from the radial distributions of loss coefficient shown in figure 21 for near design flow at design equivalent rotor speed. Radial distributions of diffusion factor, also shown in figure 21, indicate high levels of loading in the wall regions, particularly in the tip region. The loading level of rotor 5 and consequently the losses are substantially larger than those of rotor 4 in the tip region. At 10% span from the tip the diffusion factor and corresponding loss coefficient for rotor 4 are 0.66 and 0.23, respectively. For rotor 5 the diffusion factor and loss coefficient are 0.73 and 0.33, respectively. The difference between the predicted and measured loss is larger for the more highly loaded rotor.

Radial distributions of rotor work input are compared with the predicted distributions in figure 22. The difference between the measured and predicted values of rotor work shown in figure 22 are attributed to high rotor deviation angles and high midspan axial velocity, shown in figure 23. High deviation angles in the hub region were the primary cause of low work for rotor 4; whereas, for rotor 5, the low work was caused by both high deviation angles across the span and high midspan axial velocity.

The difference between the design rotor relative inlet velocity distributions and the actual velocity distributions (figures 24 and 25) may have been partially responsible for the high losses near the walls. The low velocities near the walls resulted in an increase in the rotor relative inlet air angles and caused the rotor to operate at higher than design incidence angles in these regions (figures 26 and 27). A nonuniform velocity profile also results in a streamline component of the passage vorticity that induces secondary flow within the blade row (Reference 13).

To illustrate the effect of the higher than design incidence angle on the losses near the walls, the cascade loss coefficient vs incidence angle distributions for the rotor 4 blade sections at 0% and 5% span, the rotor 4 test data at 5% span, and the range of actual incidence angles between 0% and 5% span

are compared in figure 28. Based on the cascade data shown in figure 28, the range of incidence angles between 0% and 5% span (figure 26) is large enough to stall the blade sections near the wall and, together with the wall/blade boundary layer interaction, induce large secondary flow gradients that may affect the blade row performance over a large portion of the blade span. The secondary flow gradients near the wall probably contributed to the large difference between the actual and cascade loss levels shown in figure 28, even though the incidence angle at 5% span is within the low loss range of the cascade data. The camber angles for the hub section of rotor 4 and the hub and tip sections of rotor 5 exceed the values for which cascade data are available, thus precluding a direct comparison of the range of incidence angles within 5% of the wall or the cascade loss vs angle for these locations. However, it is considered that the difference in the predicted and actual incidence angles near the walls for the hub of rotor 4 and the hub and tip of rotor 5, shown in figures 26 and 27, may also have been large enough to stall the blade sections in these regions.

The loss coefficient and deviation angle distributions shown in figures 21 and 23, respectively, also suggest strong secondary flow in the wall regions. The displacement of the rotor 5 hub maximum loss coefficient from the wall suggests very strong secondary flow and the existence of a vortex (References 14 and 15).

Rotor loss parameter vs diffusion factor is presented in figures 29a through c for the hub, mean, and tip (90, 50 and 10% span) sections of rotors 4 and 5. The correlation curves, based on the minimum loss data from References 6 through 8 that were used to predict the rotor performance, are included for comparison with the test data. The minimum loss parameter values for the hub of rotor 4 and the hub and tip of rotor 5 are above the correlation curves. The minimum loss parameter values for the midspan sections of both rotors and the tip section of rotor 4 are approximately on the correlation curves.

Blade Element Performance for Unslotted Stators

The stator inlet velocity and incidence angle distributions for approximately design equivalent rotor speed and flow are shown in figure 30. With the exception of the hub region, the stator 4 incidence angle data agree closely with the predicted values. Stator 5 was operating with less than design incidence angle across most of the span due to the combination of high rotor exit axial velocity in the midspan region and higher than predicted rotor deviation angles (figure 23) across the entire span. Although the rotor deviation angles were higher than predicted near both walls for rotor 4 and across the entire span of rotor 5, the reduction in axial velocity near the walls was large enough to result in higher than predicted incidence angles at the hub and tip of stator 4 and the tip of stator 5. To the extent that these blade elements operate like two-dimensional blade elements, these variations in the stator inlet conditions should not have adversely affected stator performance, since as indicated in figures 31a through 31i, the stator incidence angles at design equivalent rotor speed and corrected flow are within the low loss incidence operating ranges for the individual blade elements. However, the concept of blade element performance was derived for two-dimensional flow, and the existence of the low rotor exit axial velocity ratios near the walls reflects a highly non-two-dimensional

flow field. Previous results from highly loaded blade rows (Reference 1) indicate that these secondary flows have a substantial effect on the blade element performance.

The blade element performance for stators 4 and 5 is summarized in figure 32, which presents the radial distributions of loss coefficient, deviation angle, and diffusion factor for approximately design equivalent flow. The stator diffusion factors are less than the predicted values across the entire span primarily because of the relatively large deviation angles seen in the figure and the associated high exit tangential velocities. In general, the loss coefficient values for both stators are larger than predicted from 5% to 30% span and less than predicted from 50% to 95% span. But as previously noted the diffusion factors are less than the predicted values and blade element loss is a function of the blade element loading.

Loss parameter vs diffusion factor for unslotted stators 4 and 5 is presented in figures 33a through c for the hub, mean, and tip (90, 50, and 10% span) sections. Correlation curves for the minimum loss data of References 9 through 11, that were used to predict the stator performance, are included on figures 33a through c for comparison with the test data. The stator 4 and 5 loss parameter values are below the correlation curves for diffusion factors of 0.63 and 0.725, respectively, at the hub; whereas, at the tip, the loss parameter values are above the data correlation curves. The values of the loss parameter at midspan are approximately on the correlation curve. The unslotted stator 5 loss parameter data, shown in figure 33, are generally above the values for the unslotted stator 4 data, which suggests that additional variables must be considered when selecting the loss correlation for highly cambered blade rows. The camber of both stators (figure 2) far exceeds that used for state-of-the-art stator designs with the camber of stator 5 being 8 to 25 degrees greater across the span than stator 4. The camber of stator 4 varies from approximately 58 degrees at midspan to approximately 75 degrees at the hub and tip, whereas the camber of stator 5 varies from 66 degrees at midspan to over 85 degrees at the hub and tip.

Effect of Rotor Work Level on Efficiency

The hub, mean, and tip adiabatic efficiencies at near design flow conditions as functions of a design loading parameter, $L = \left[\Delta V_\theta \cos \beta_m / \sigma V_Z \text{ avg}\right]$ Design, for unslotted stages 4 and 5 are compared with the results of the Reference 1 program in figure 34. The equation for the loading parameter, although not rigorously derived, is similar in form to the equation for the lift coefficient. For two-dimensional incompressible flow, the lift coefficient would be equal to two times the loading parameter. Although stages 4 and 5 were designed with higher work input than the Reference 1 stages (i.e., more turning and consequently higher loading near the walls to compensate for the high wall losses and maintain more nearly two-dimensional flow), the results shown in figure 34 illustrate that as the design loading level was increased the blade element efficiency continued to decrease. The results in figure 34 also illustrate that as the design loading level was increased the efficiency near the walls decreased at a faster rate than the efficiency at midspan, and that for the same loading level the efficiency near the walls was substantially less than the efficiency at midspan. These results suggest that the stage efficiency might be optimized by the proper selection of radial work distribution. However, as

shown in figure 35, there are apparent upper limits to the amount of turning that will result in useful work output at near design flow conditions, i.e., $J_g C_p T_1 \left[(P_2/P_1)^{\gamma-1/\gamma}-1\right]/U^2 = f\left[\phi+i_m\right]$, and these limits must be observed when selecting an improved work distribution.

Effect of Mach Number and Boundary Layer Bleed Flow on Rotor Performance

As indicated in figures 36 and 37, there is a variation in loss coefficient with rotor speed. To determine which data were affected by high inlet relative Mach numbers and the associated shock losses, the calculated Mach numbers were compared with the limiting or cascade critical Mach numbers based on a P&WA cascade correlation. The hub and tip camber angles (95% and 5% span) for rotor 5 exceeded the range of available cascade data; therefore, the cascade critical Mach numbers for these locations were obtained by extrapolating the data to the appropriate camber angle. The data which have inlet relative Mach numbers greater than the cascade critical value are indicated in figures 36 and 37. In general, the loss coefficient values for the data with inlet relative Mach numbers above the cascade critical Mach number are higher than those for the lower Mach numbers. However, the variation in loss coefficient with rotor speed cannot be completely attributed to operation above the cascade critical Mach number since some variation in loss coefficient was still present at Mach numbers below the cascade critical value. Since the rotor bleed flow also varied with rotor speed, the effect of rotor bleed flow on loss coefficient was also investigated and the results are shown in figures 38 and 39 for rotors 4 and 5, respectively. The more pronounced effect of the bleed flow on the tip losses, indicated by the more negative slope of the loss coefficient vs bleed flow curve, results from the bleed flow being removed at the tip and not the hub. Based on the Mach number and bleed flow comparisons, the increase in loss coefficient with increased rotor speed is attributed to the following three causes: (1) inlet Mach numbers above cascade critical Mach number, (2) decreased bleed flow as a percentage of the primary flow, and (3) critical Mach numbers in a three-dimensional flow environment are lower than the initial Mach numbers in a two-dimensional flow environment. Items 1 and 2 are apparent from figures 36 and 39, whereas item 3 is hypothesized because the variation in loss coefficient was still present at the hub (where the boundary layer was not removed) at Mach numbers below the cascade critical value.

Effect of Slots on Stage 4 Performance

The overall performance for the slotted and unslotted stage 4 configurations are compared for the rotor and stage in figures 40 and 41, respectively. In general, the pressure ratio, efficiency, and stall flow for both slotted rotor 4 and slotted stage 4 are lower than those for the unslotted configuration; the reductions in pressure ratio and efficiency were greater at the higher flows. Although the stall flow was lower for slotted stage 4, the maximum flow was also reduced so that the maximum to stall flow range was approximately the same for both slotted and unslotted stage 4. A detailed discussion of the stage stall flows is given in the section entitled "Comment on Stage Stall Flow Comparisons," below. The reduced pressure ratio is attributed to higher rotor total pressure losses near the walls and lower rotor work input because of the increased midspan axial velocity and higher tip deviation angles.

The rotor loss coefficient, deviation angles, and diffusion factor distributions at design equivalent rotor speed are compared for the slotted and unslotted configurations at near stall, near design, and maximum flow in figures 42 through 44, respectively. These results and the loss parameter values shown in figures 45a through c indicate that slotting the rotor not only failed to provide a reduction in loss, but actually increased the hub and tip losses. However, the midspan losses for the slotted rotor are lower than the unslotted rotor losses at the lower loading levels and comparable to the unslotted rotor losses at the highest diffusion factor (figure 45b). The deviation angles for the slotted rotor are higher than those for the unslotted rotor in the tip region at all flow conditions (figures 42 through 44), and slightly lower than those for the unslotted rotor in the midspan to hub region at the design and stall flows (figures 42 and 43). It is also noted from figure 42 that the rotor tip diffusion factor for the slotted rotor at near-stall flow is greater than that for the unslotted rotor.

Evaluation of the influence of slots on stator blade element performance is confounded by the largely different rotor exit flow distributions that were produced by the slotted and the unslotted rotor. Unslotted and slotted rotor exit axial velocities and corresponding stator incidence angle distributions are compared for near-stall flow conditions in figure 46. The axial velocity distributions indicate a general flow shift from tip to hub for the slotted rotor, which results in comparatively high incidence angles in the tip region for the slotted stator.

Radial distributions of slotted stator blade element loss coefficient, deviation angle, and diffusion factor are compared with the unslotted configuration results in figures 47 through 49 for near stall, near design, and maximum flow, respectively. These data are presented for general information purposes. It is noted that the slotted stator tip region diffusion factor is greater and the losses and deviation angle are equal to or lower than the respective tip region values for the unslotted stator at both the near stall and design corrected flow conditions. The discontinuity in the radial loss coefficient distribution at 30% span for the slotted stator is attributed to the flow discontinuity associated with the slot end. Blade element data were not recorded at the end of the hub slot (80% span), but the same general trend toward higher loss coefficients near the end of the slot is observed at 85% span for the near design and near stall flow conditions.

A more generalized assessment of the influence of slots on stator performance is provided by the envelopes of loss coefficient and deviation angle data (as functions of incidence angle) for the hub region (85, 90, and 95% span) in figure 50 and for the tip region (5, 10, and 15% span) in figure 51. As seen in figure 50, the levels of hub region loss coefficient and deviation angle were in general higher for the slotted stator than for the unslotted stator. Figure 51 indicates that the average levels of the slotted stator tip region loss and deviation angle were lower than those of the unslotted stator, and that the slotted stator was operated to higher incidence angles than the unslotted stator. The higher incidence angles for the slotted stator tip resulted from the lower rotor tip exit axial velocity for the slotted rotor, as shown previously in figure 46. Although one might conclude that the stator slots were responsible

for the lower stator losses, the data for the same slotted stator tested behind the unslotted rotor do not indicate lower losses for the slotted stator. (This is discussed later in the report.) Therefore, the lower losses and deviation angles for the slotted stator tip when tested behind the slotted rotor are apparently associated with the rotor exit flow redistribution for this configuration, as shown by the exit axial velocity profile in figure 46. A similar effect of stator inlet flow field on stator losses is discussed in Reference 2.

Loss parameter vs diffusion factor values for unslotted and slotted stator 4 are compared in figures 52a through c. The slotted stator had slightly lower loss parameter values at the hub with little change in the magnitude of the loss parameter value at the tip.

Effect of Vortex Generators on Rotor Performance

Vortex generators were tested upstream of the rotor for the slotted rotor 4-slotted stator 4 stage and both upstream of the rotor and between the rotor and stator for the unslotted rotor 4-slotted stator 4 stage. The overall rotor performance for slotted rotor 4 with and without vortex generators is presented in figure 53. The addition of the vortex generators increased the maximum flow and efficiency at design equivalent rotor speed by approximately 2.0 lb/sec (0.907 ks/sec) and 0.5%, respectively, without changing the stall flow or peak pressure ratio. Although these changes may be considered within the accuracy of the data, the blade element performance data described in the following paragraph substantiates the slight improvement in efficiency.

Radial distributions of the rotor loss coefficient, deviation angle, and diffusion factor are compared for slotted rotor 4 with and without vortex generators in figures 54 through 56 for near stall, near design, and maximum flow. These results indicate that the addition of vortex generators reduced the rotor tip region diffusion factor and loss with the largest reduction in tip loss occurring at the near stall flow condition. The reduced diffusion factors in the tip region are apparently associated with a radial flow shift toward the tip, as indicated by the higher rotor tip exit axial velocities shown in figure 57 for slotted rotor 4 with vortex generators. For the near stall flow condition, the radial flow shift toward the tip also resulted in slightly higher loading levels from 30% to 95% span. The reduced losses are consistent with the previously mentioned increase in efficiency.

As shown in figure 58a, the addition of the rotor tip vortex generators ahead of the slotted rotor resulted in slightly reduced values of the tip loss parameter at the higher loading levels. Little or no change in the slotted rotor hub loss parameter (figure 58b) was observed with the addition of the rotor hub vortex generators. The loss parameter values for the midspan region (figure 58c) are comparable for slotted rotor 4 both with and without vortex generators. The previously discussed reduction in the tip loading (i.e., diffusion factor) and the increases in the maximum midspan and hub loading with the addition of vortex generators ahead of slotted rotor 4 are apparent in figure 58.

Since the addition of the rotor tip inlet vortex generators unloaded the tip region of slotted rotor 4 and reduced the losses in that area (figures 54 through 56), an additional test was scheduled with vortex generators ahead of unslotted rotor 4 and between the rotor and slotted stator 4 to determine if the unslotted

stage operating range could be improved without a reduction in efficiency. The combination of the unslotted rotor and slotted stator was selected because unslotted rotor 4 had lower hub and tip losses (figures 42 through 44) than slotted rotor 4 and the slotted stator tip was operated at higher incidence angles than the unslotted stator with losses equal to or less than the minimum values measured for the unslotted stator (figure 51). During the testing of this configuration, one-third of the stator inlet vortex generators separated from the wall. Since the time at which the separation occurred could not be determined and since the relationship of the remaining vortex generators to the instrumentation locations was such that sufficient pressure, temperature, and air angle data were not available for vane passages with vortex generators, the influence of stator inlet vortex generators on the stator performance could not be evaluated. Because of their small size, the effect of the nonuniform distribution of the remaining stator inlet vortex generators on rotor performance is considered negligible.

The overall rotor and stage performance for unslotted stage 4 without vortex generators and the stage comprised of unslotted rotor 4 and slotted stator 4 with vortex generators ahead of the rotor and between the rotor and stator are compared in figures 59 and 60. The peak rotor and stage efficiencies for the latter stage at design equivalent rotor speed were 0.8 and 2.1 percentage points, respectively, higher than those for the unslotted stage.

As shown by the radial distributions of the rotor loss coefficient, deviation angle, and diffusion factor in figure 61 at the near stall flow condition, the addition of the vortex generators upstream of the unslotted rotor unloaded the rotor blade end regions and reduced the losses near the walls. The diffusion factor distribution also indicates that the reduced loading in the wall regions resulted in slightly higher loading at midspan. The lower rotor losses near the walls for the unslotted rotor with vortex generators are also shown in the loss parameters vs diffusion factor distributions presented in figure 62. As shown in figure 62a, the addition of the rotor inlet vortex generators to the stage comprised of unslotted rotor 4 and slotted stator 4 reduced the unslotted rotor tip minimum loss parameter to a value consistent with the predicted values. The predicted values included an assumed improvement in losses due to the anticipated reduction in secondary flow from the addition of slots and vortex generators. Although the hub loss parameter values (figure 62c) for the unslotted rotor with inlet vortex generators are above the data from References 6 through 8, the addition of the hub vortex generators resulted in a reduction in the unslotted rotor loss parameter values.

Comment on Stage Stall Flow Comparisons

The operating characteristics (pressure ratio-flow) for the four stage 4 configurations tested are compared for both the rotor and stage in figure 63. All three configurations tested resulted in stall flows that were lower than the unslotted rotor-unslotted stator configuration. These configurations are listed below:

1. Slotted Rotor 4 - Slotted Stator 4

2. Slotted Rotor 4 - Slotted Stator 4 With Vortex Generators Ahead of the Rotor

3. Unslotted Rotor 4 - Slotted Stator 4 With Vortex Generators Ahead of the Rotor and Between the Rotor and Stator.

It might be concluded that slotted stator 4, which was common to all three configurations, was responsible for the increased stall range. As shown previously in figures 50 and 51, the hub and tip region losses near stall and the tip deviation angles for the slotted stator were lower than those for the unslotted stator, and the slotted stator tip was operated to higher incidence angles and loading than the unslotted stator. Furthermore, the addition of vortex generators ahead of the slotted rotor reduced losses and loading in the wall regions but they did not appreciably change the stage stall flow. Inspection of the hub and tip region losses and deviation angles for the slotted stator behind the unslotted rotor, shown in figures 64 and 65, indicates that the only apparent benefit from the stator slots for this configuration was a reduction in the average level of the hub and tip region deviation angles. The wall region loss levels of the slotted stator behind the unslotted rotor are actually the same or higher than those for the unslotted stator tested behind the unslotted rotor. Since these results do not support the conclusion that the stator slots reduced the stator losses and thereby increased the stage operating range, the respective operating ranges and loss levels are attributed to the difference between slotted and unslotted rotor exit flow profiles (figure 46).

Although the stall flow for the stage comprised of the unslotted rotor and slotted stator with vortex generators ahead of the rotor and between the rotor and stator was approximately the same as the stall flow for the slotted stage both with and without vortex generators at design equivalent rotor speed, the stall flow for this stage was appreciably lower at 70% design equivalent rotor speed. However, as previously stated, the loss of approximately one-third of the stator inlet vortex generators precluded their evaluation, and, since the stage was not tested without the stator inlet vortex generators, the individual effects of the rotor inlet vortex generators, stator slots, and stator inlet vortex generators on operating range cannot be separated.

Effect of Rotor Tip and Stator Hub and Tip Boundary Layer Bleed on Performance

Overall and blade element performance data were recorded with the control valves in the rotor and stator boundary layer bleed lines closed for three data points at design equivalent rotor speed for slotted stage 4 and two data points at design equivalent rotor speed for the stage 4 configurations with vortex generators. Stall transient measurements were also obtained at design equivalent rotor speed with the control valves in the boundary layer bleed lines closed for slotted stage 4 and the stage 4 configurations with vortex generators while operating these configurations into and out of stall to define the stall points. Although the control valves were closed, some leakage flow was present (approximately 0.2% and 0.4% of the inlet flow for the rotor and stator, respectively); therefore, these data points are referred to as "reduced bleed flow points". The influence of wall boundary layer bleed flow on performance was not evaluated for either unslotted stage 4 or unslotted stage 5.

The effect of reducing the boundary layer bleed flow on the rotor and stage performance of slotted stage 4 is shown in figures 66 and 67. The results

are also typical of the results obtained with the stage 4 configurations with vortex generators. Reducing the wall boundary layer bleed flow in the rotor and stator reduced the rotor and stage pressure ratio and efficiency and changed the pressure ratio-flow characteristic at constant rotor speed. The cause of this result is believed to be a redistribution of the flow brought about by increased secondary flow and higher losses in the rotor tip region.

The effect of rotor tip bleed on the slotted rotor 4 blade element performance is shown in figures 68a through 68c for the hub, mean, and tip sections, respectively. Reducing the rotor tip bleed flow resulted in greater losses, deviation angles, and diffusion factors for the tip (figure 68c). These increases do not appear to be normal extensions of the blade element loss, deviation angle, and diffusion factor characteristics and are apparently associated with increased secondary flow. The increase in rotor tip losses with reduced bleed shown in figure 68c are consistent with the results previously discussed. The changes in the hub and midspan section performance are more subtle and are apparently due to the redistribution of the flow in the rotor associated with the higher rotor tip losses with reduced bleed flow.

The effect of the stator hub and tip bleed flow on the slotted stator 4 blade element performance is shown in figures 69a through 69c for the hub, mean, and tip sections, respectively. As shown in figure 69a, reducing the stator bleed produced a noticeable increase in loss coefficient at the stator hub. The changes to large positive incidence angles shown in figure 69c for the stator tip with reduced bleed flow and the associated loss increase are attributed to a general flow shift from the tip to the hub with reduced rotor and stator bleed flow. The effect of the reduced bleed flow on the stator inlet axial velocity and corresponding stator incidence angle distributions at the near stall flow condition is shown in figure 70.

SUMMARY OF RESULTS

An experimental investigation was conducted with a single-stage compressor to determine the extent that slots and vortex generators can be applied to reduce the losses in the wall regions and increase the efficiency and stable operating range of highly loaded compressor stages. A secondary objective of this program was to determine the effects of loading level and boundary layer suction on stage efficiency and operating range. In summary, the results of this investigation indicated that:

1. Slotting the rotor not only failed to provide the desired reduction in loss, but actually increased the hub and tip losses.

2. The effect of the stator slots on loss and operating range was inconclusive. When the slotted stator was tested with the slotted rotor the losses near the walls were generally lower than for the unslotted stator at the same or higher incidence angles. However, the slotted stator, when tested with the unslotted rotor and vortex generators, had the same or higher losses than the unslotted stator, with little or no change in operating range. The lower losses and higher incidence angles for the slotted stator, when tested with the slotted rotor, were apparently associated with a flow redistribution observed for this configuration.

3. Rotor inlet vortex generators can unload the blade end regions and thereby reduce the losses at high incidence angles.

4. There is an apparent limit to the amount of work input that will result in useful work output.

5. The selected work distribution may have a substantial effect on stage performance.

6. Reducing the boundary layer suction (i.e., bleed flow) in the rotor and stator resulted in lower rotor and stage pressure ratio and efficiency and changed the pressure ratio-flow characteristic at constant rotor speed.

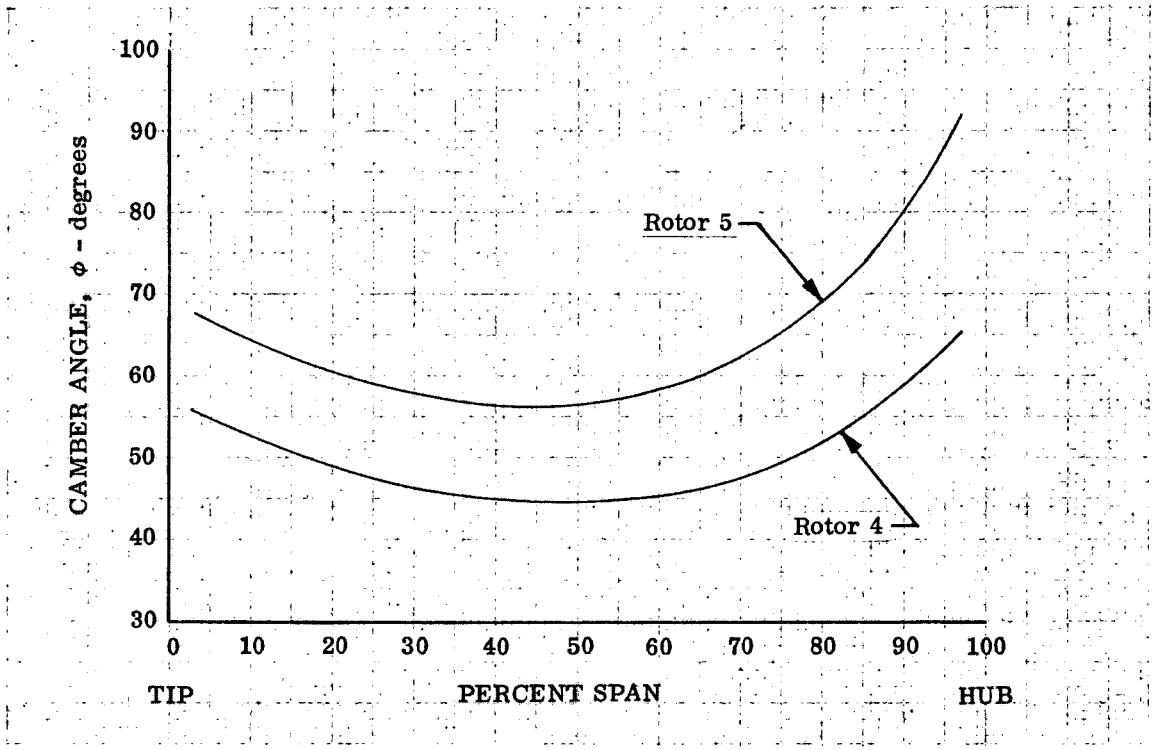

Figure 1. Rotor Camber Angle Distributions DF 89713

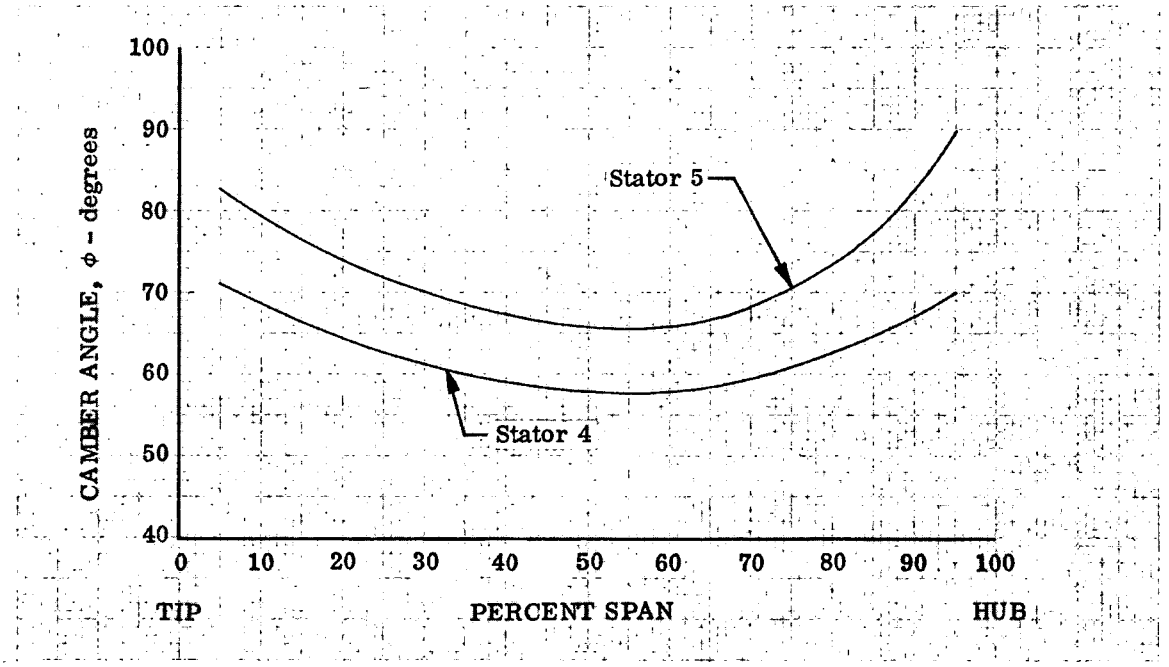

Figure 2. Stator Camber Angle Distributions DF 89714

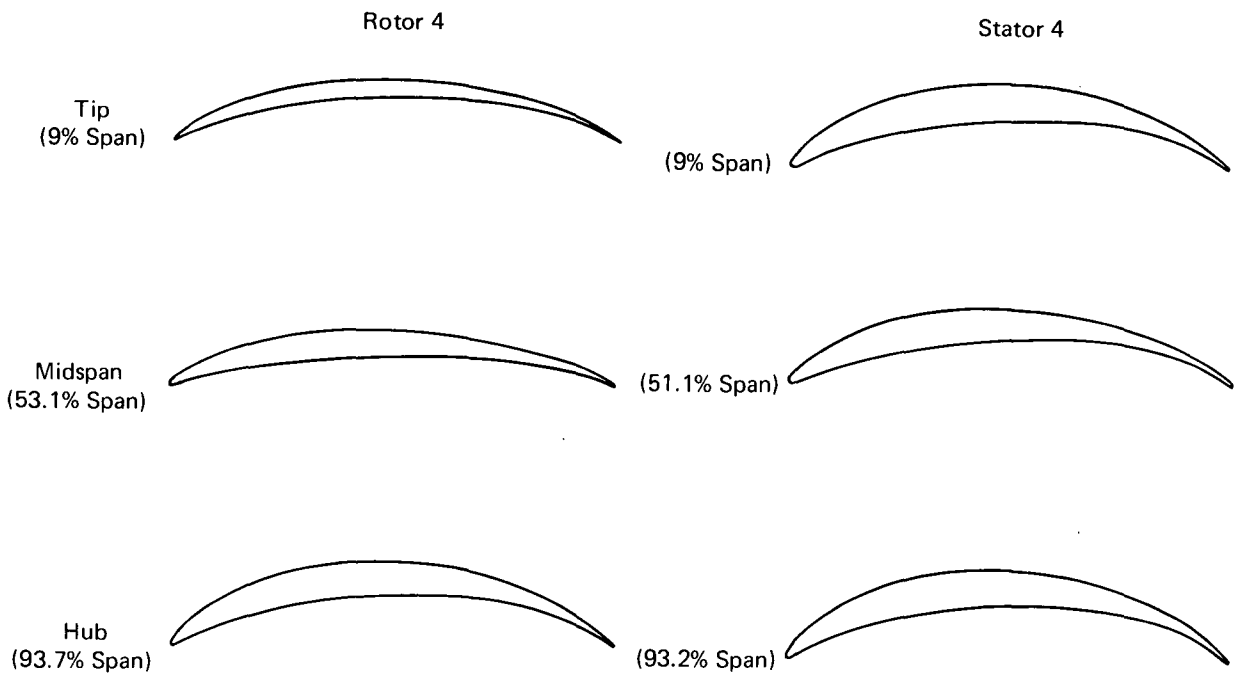

Figure 3. Stator 4 Blading Section Geometry

FD 38123A

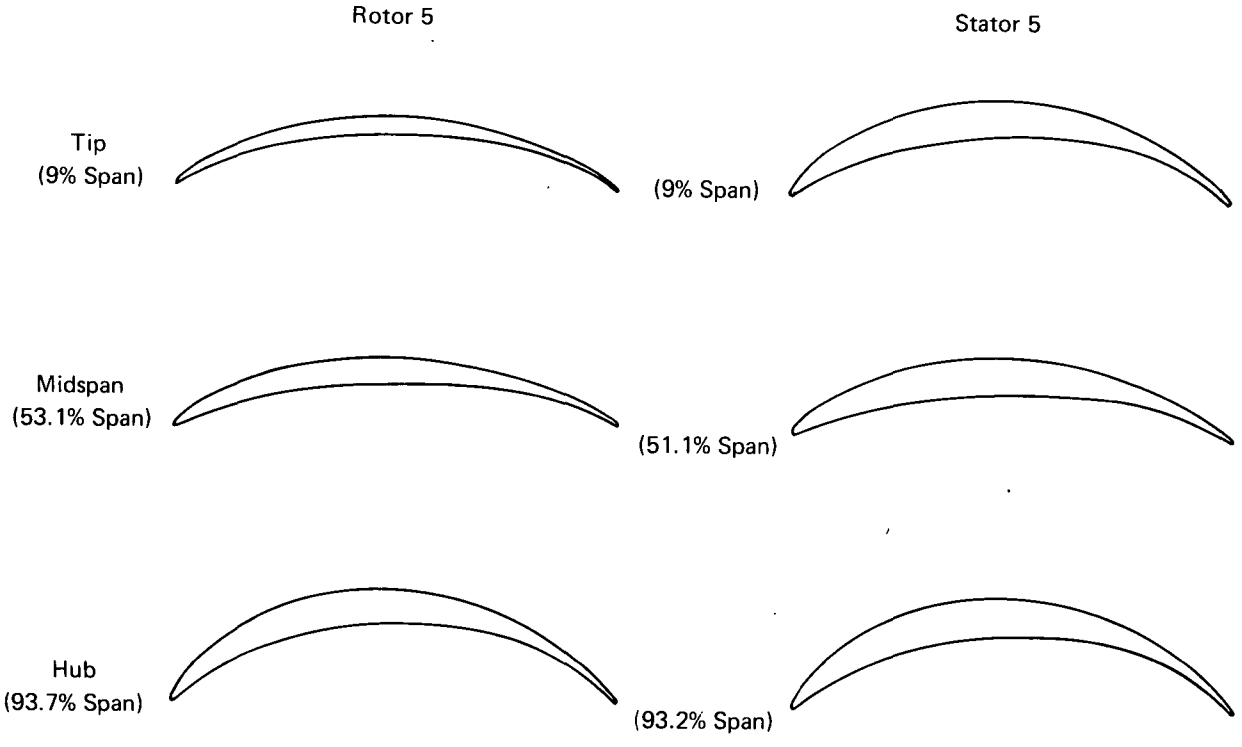

Figure 4. Stage 5 Blading Section Geometry

FD 38122A

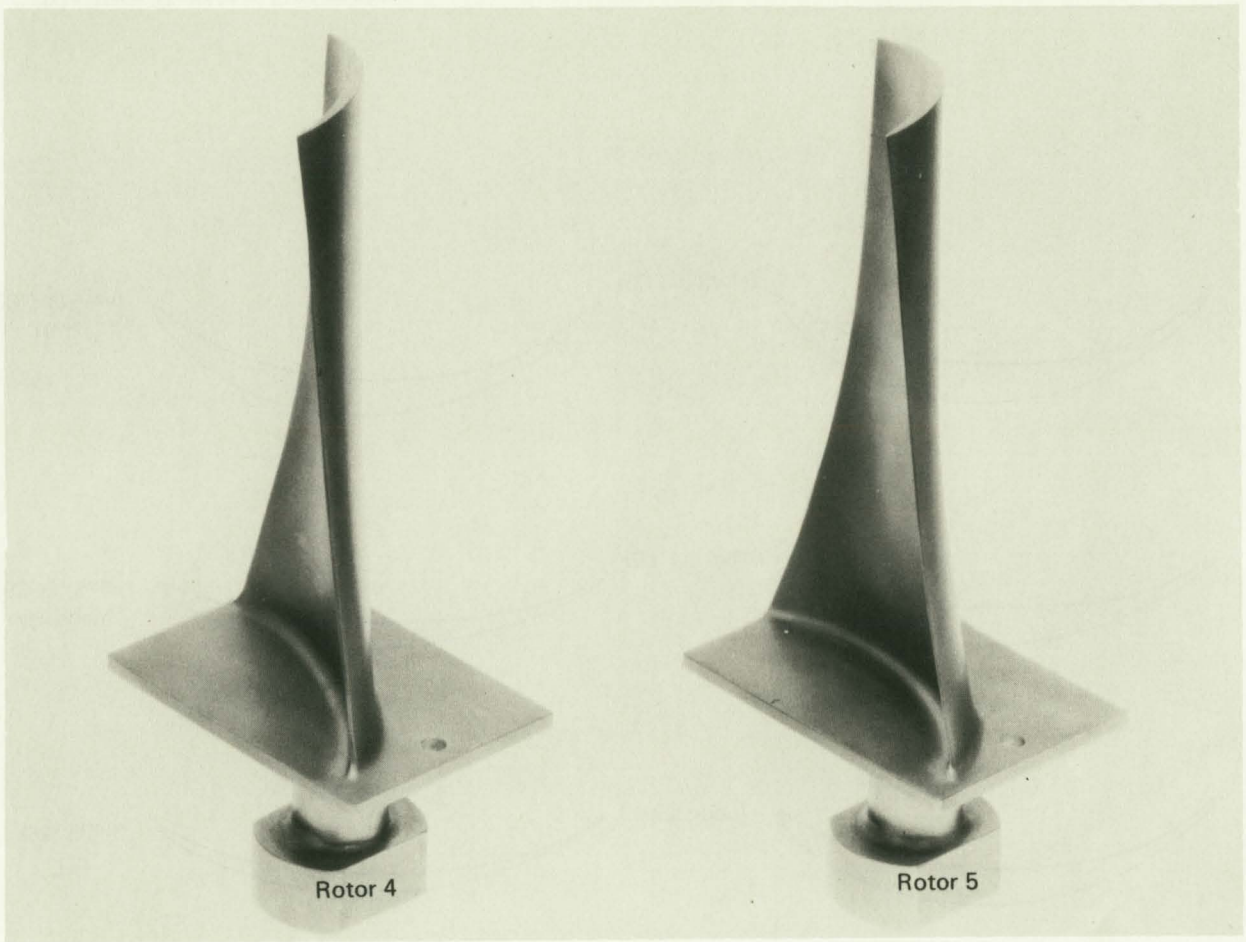

Figure 5. Rotor 4 and 5 Blading

FE 77064A

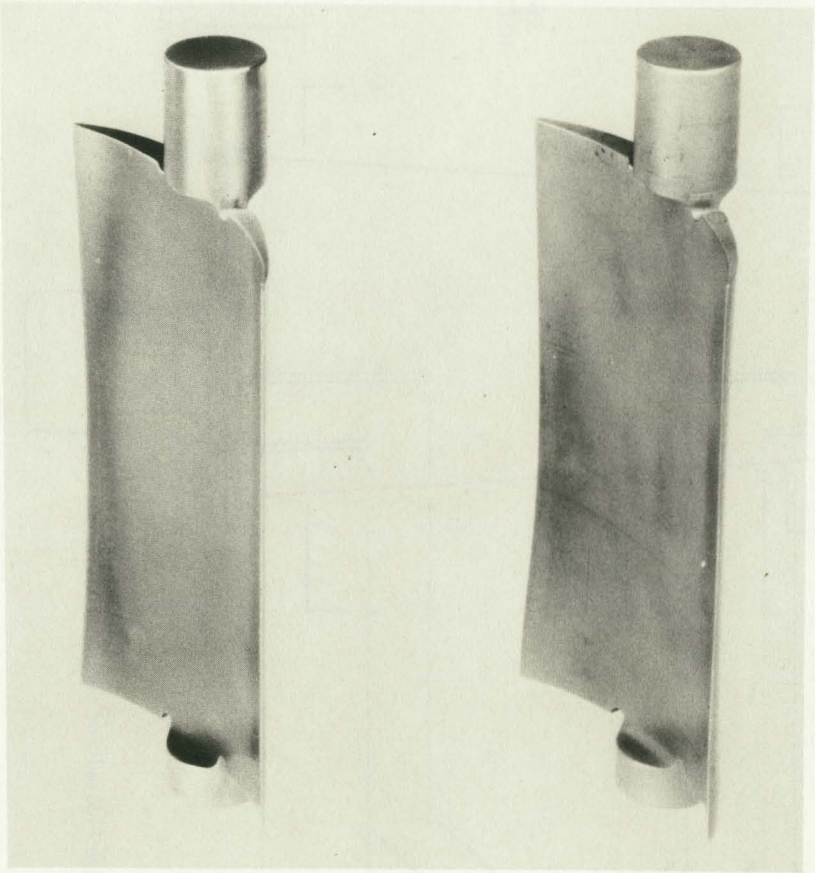

Stator 4 Stator 5

Figure 6. Stator 4 and 5 Blading

FE 79517A

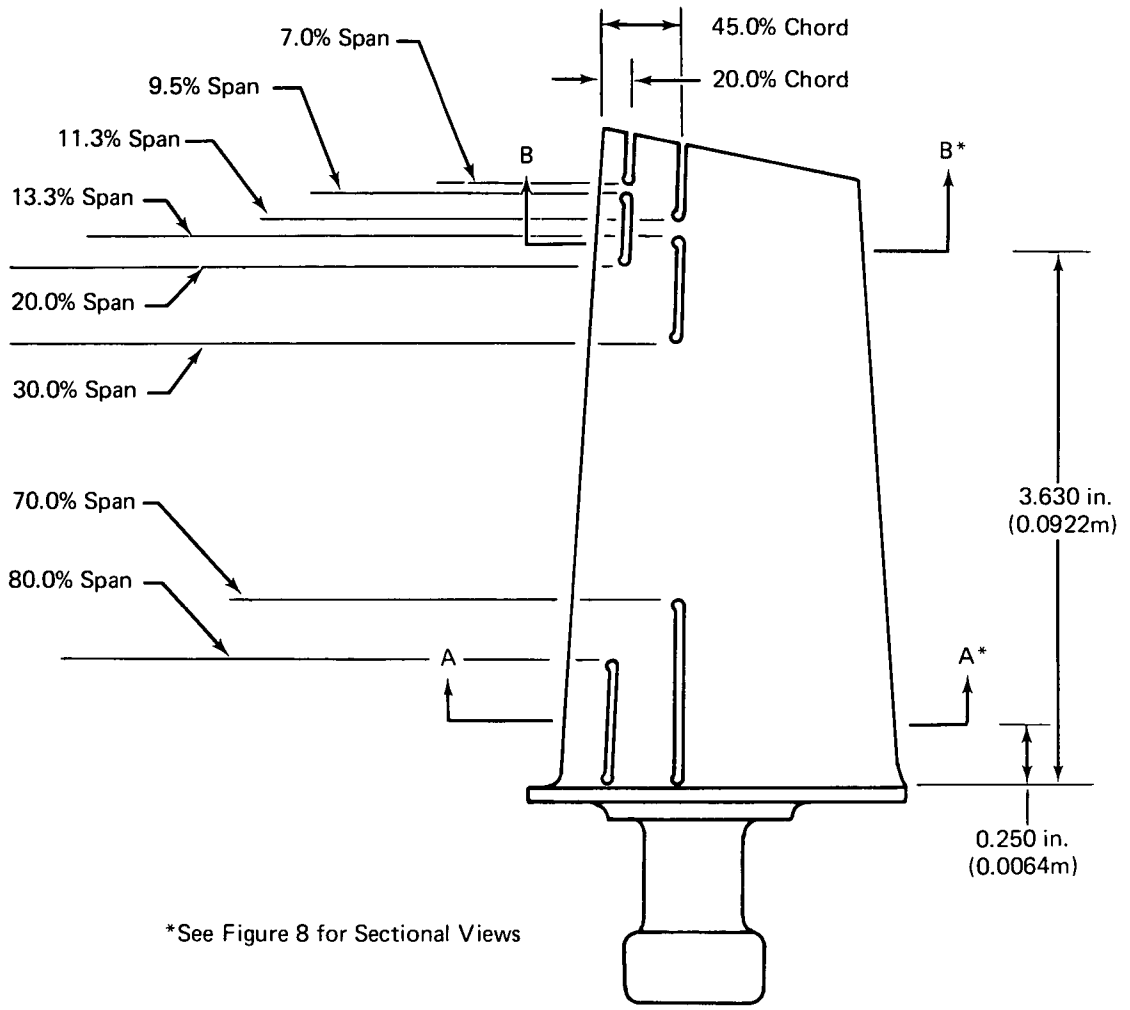

Figure 7. Rotor 4 Slot Locations on Suction Surface FD 38121A

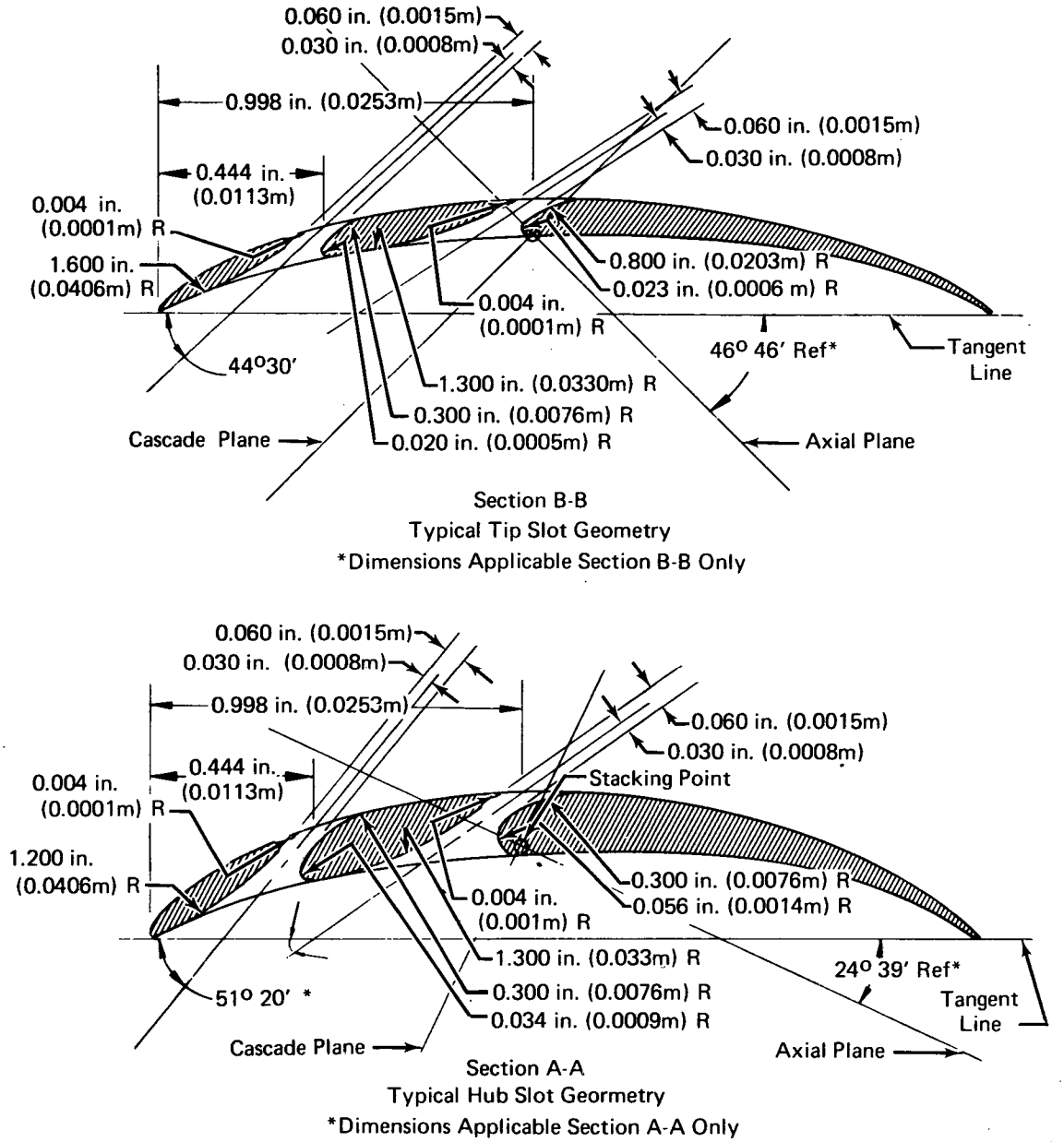

Figure 8. Rotor 4 Slot Configuration FD 38124A

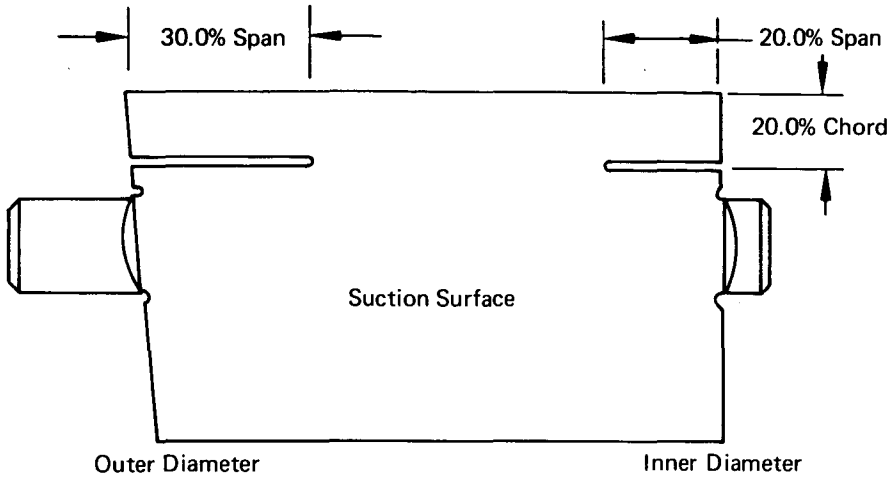

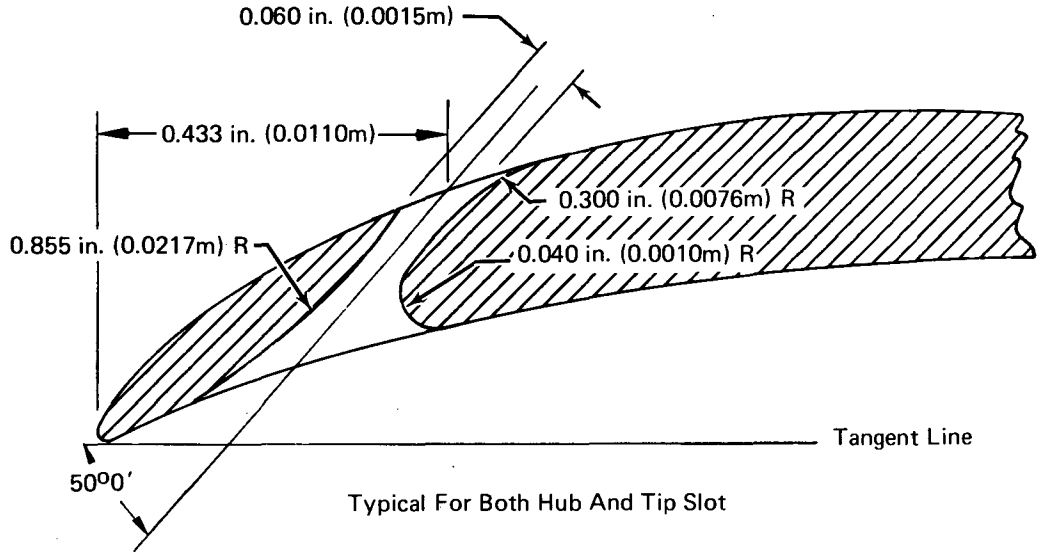

Figure 9. Stator 4 Slot Configuration FD 38120B

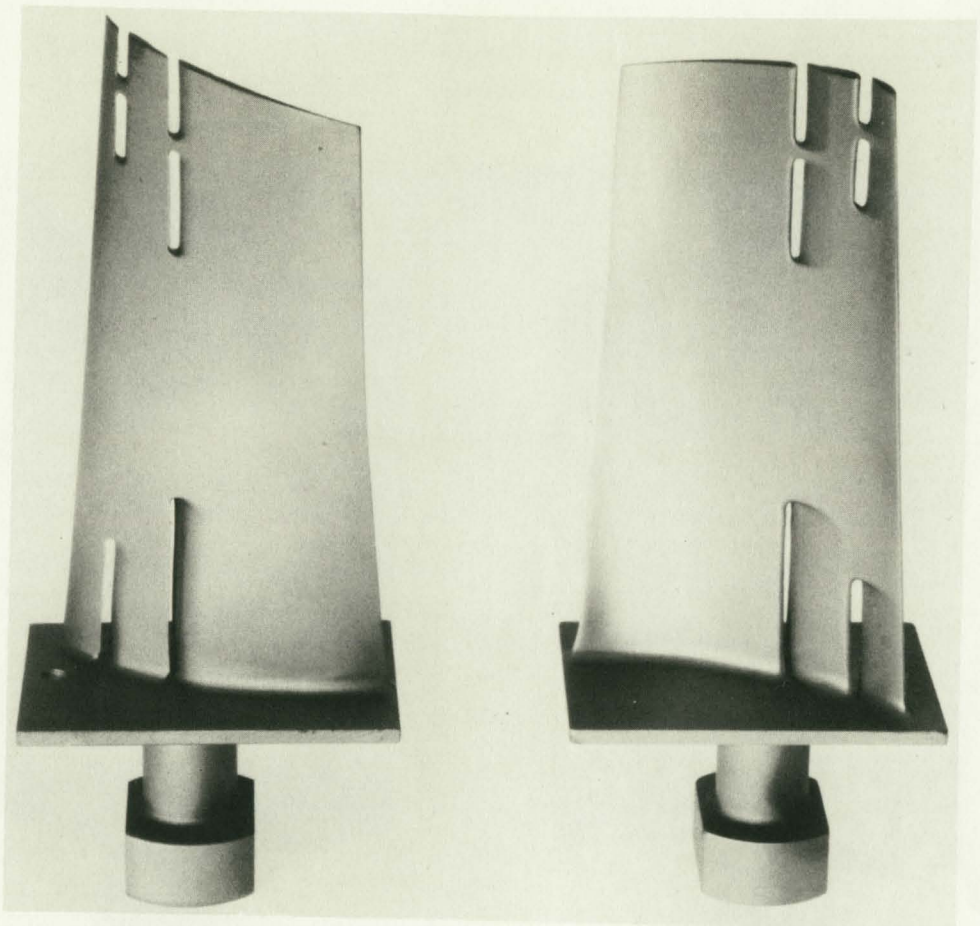

Suction Surface

Pressure Surface

Figure 10. Slotted Rotor 4

FE 84319A

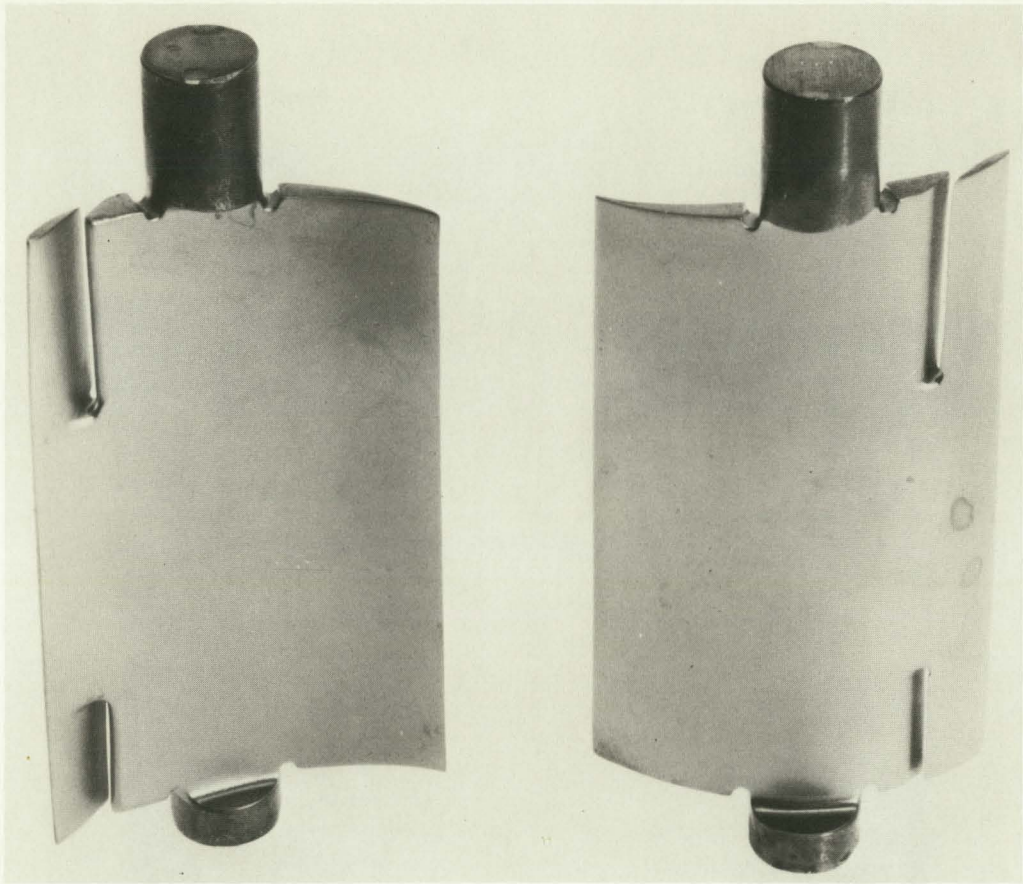

Pressure Surface

Suction Surface

Figure 11. Slotted Stator 4

FE 84317A

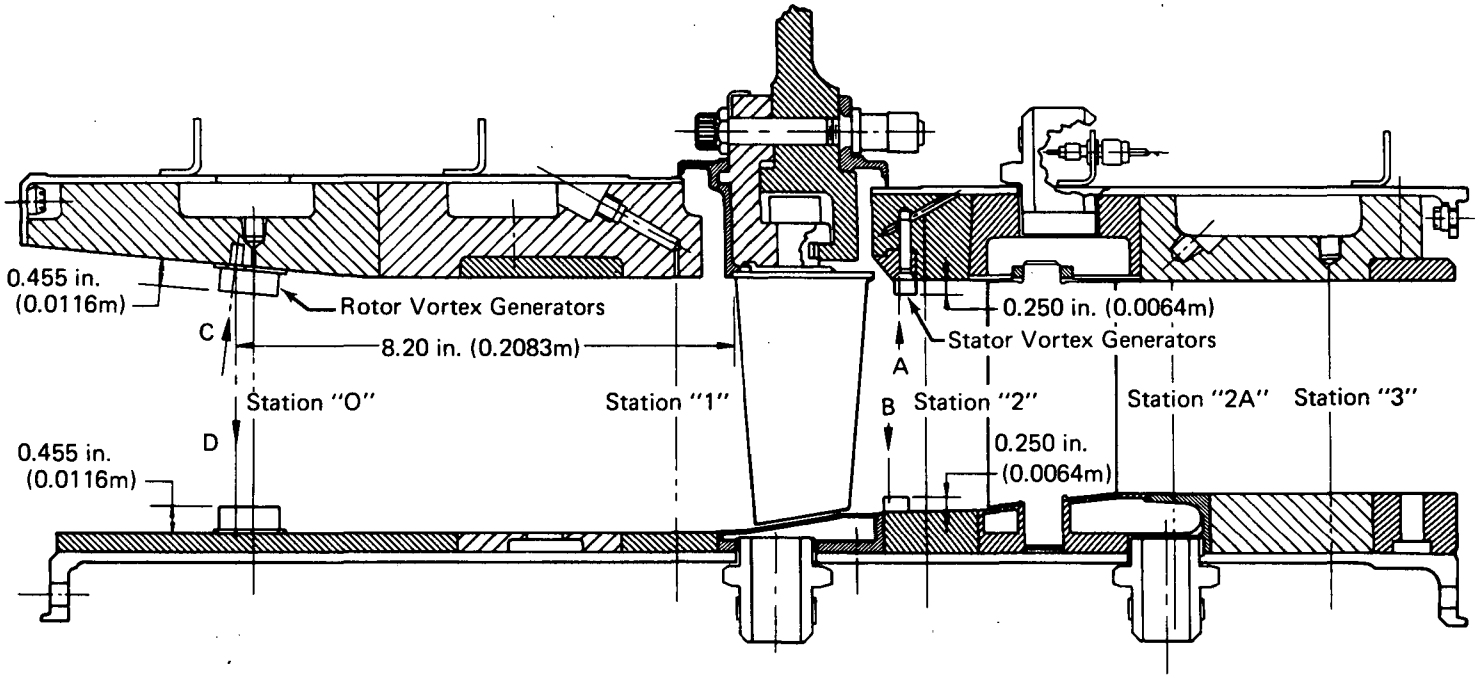

Figure 12. Vortex Generator Locations

FD 38119B

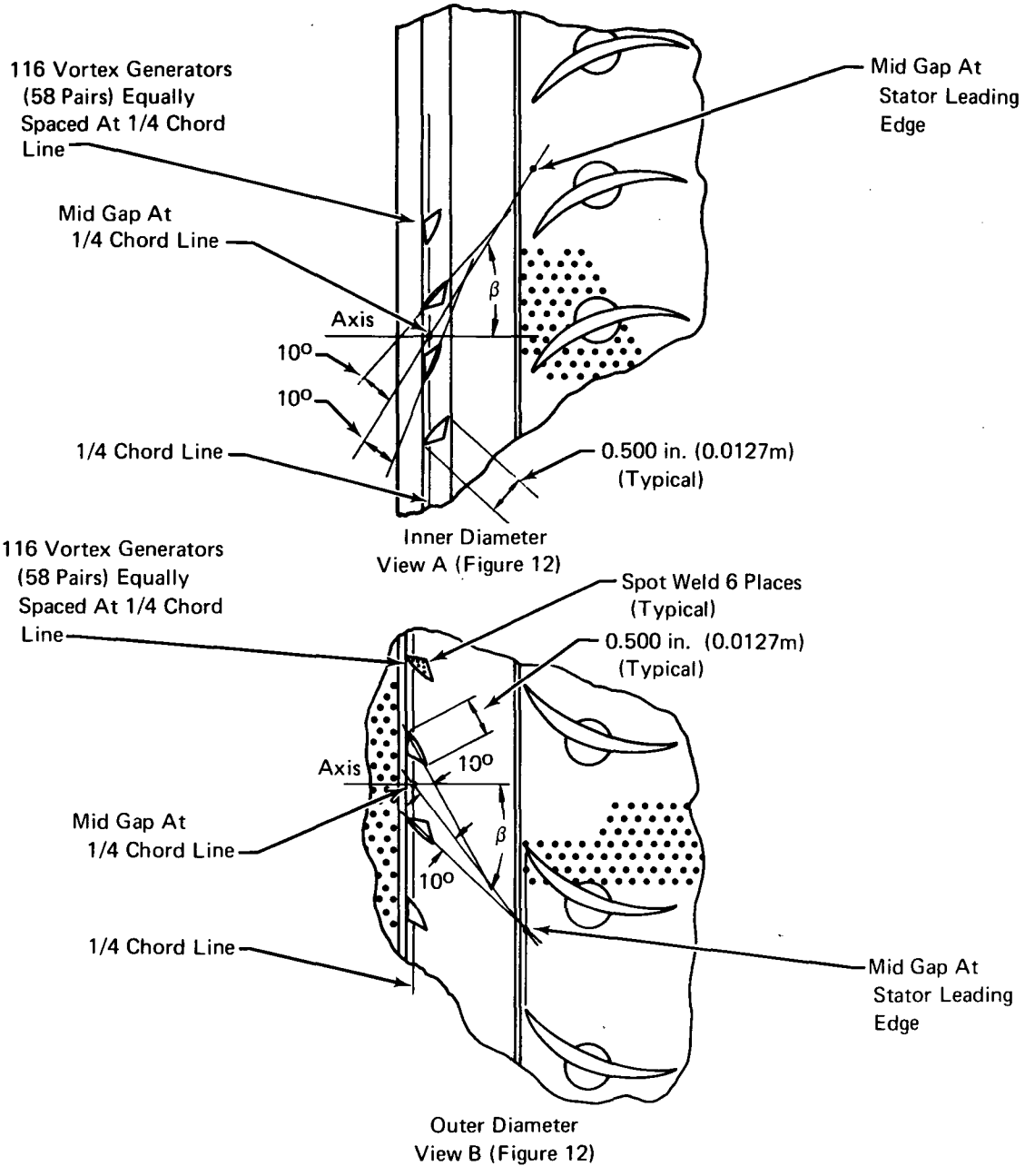

Figure 13. Stator Vortex Generator Design FD 38117B

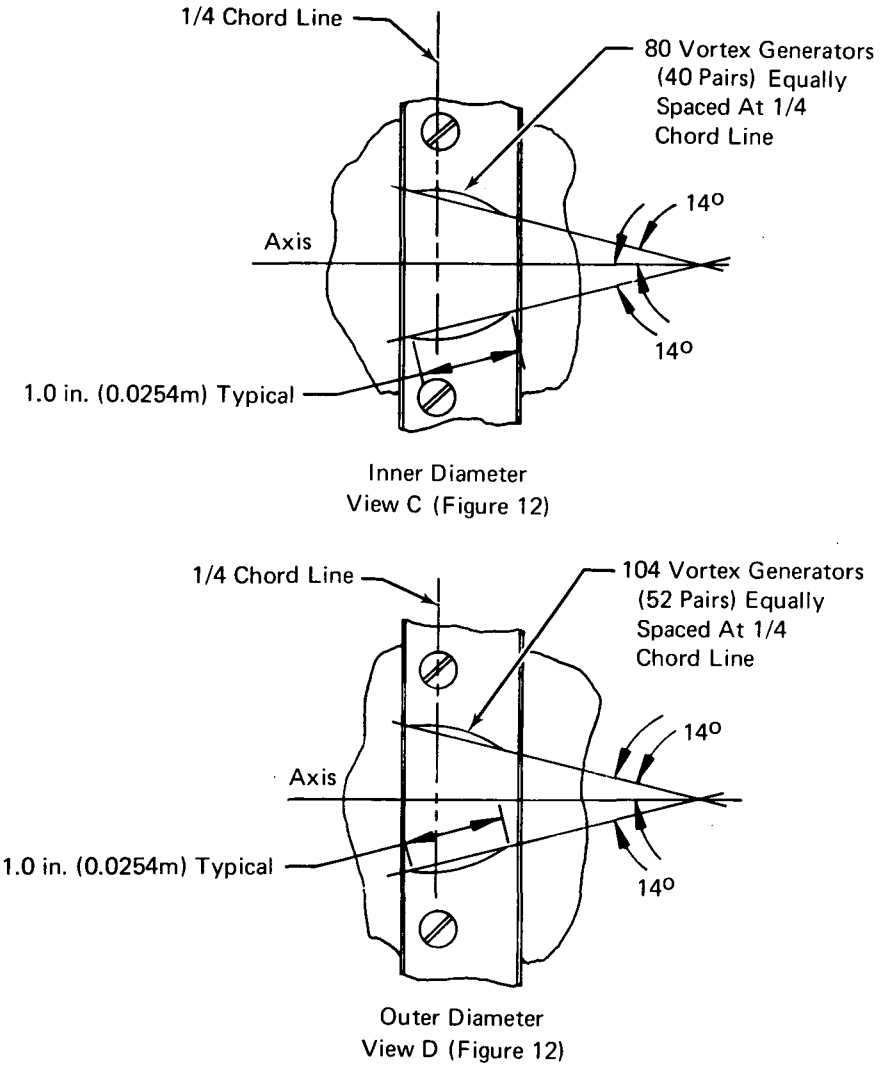

Figure 14. Rotor Vortex Generator Design FD 38118B

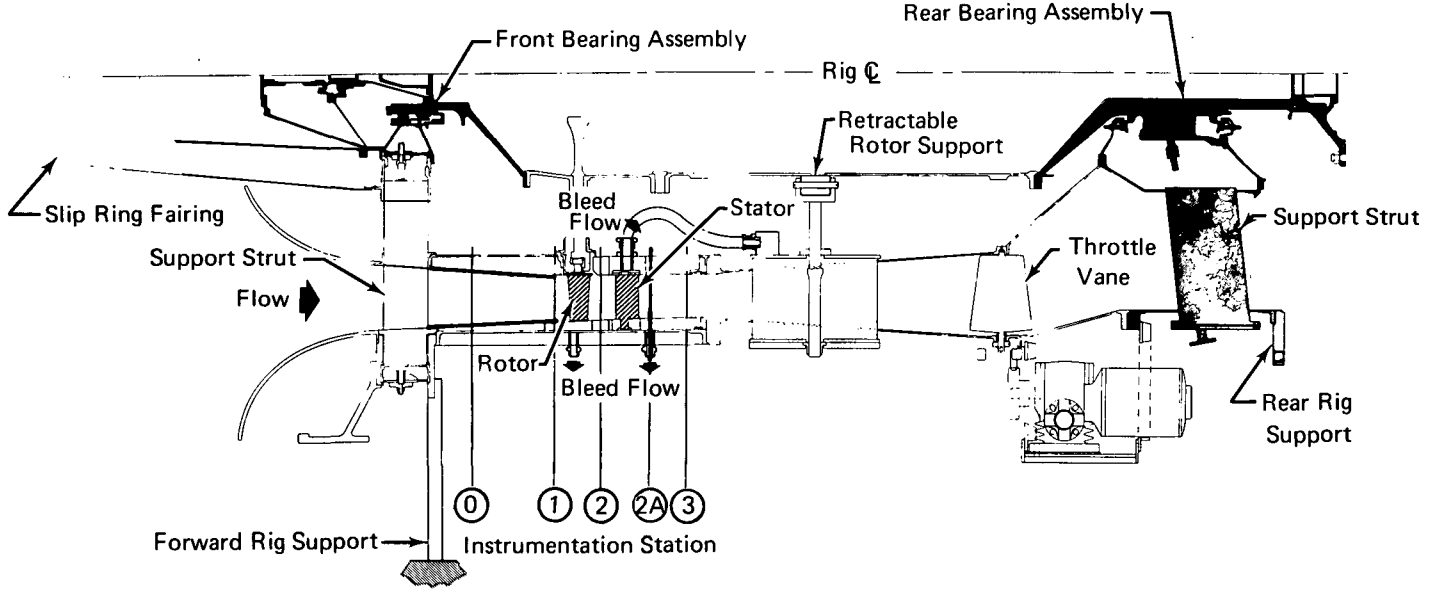

Figure 15. Single-Stage Compressor Rig

FD 14681C

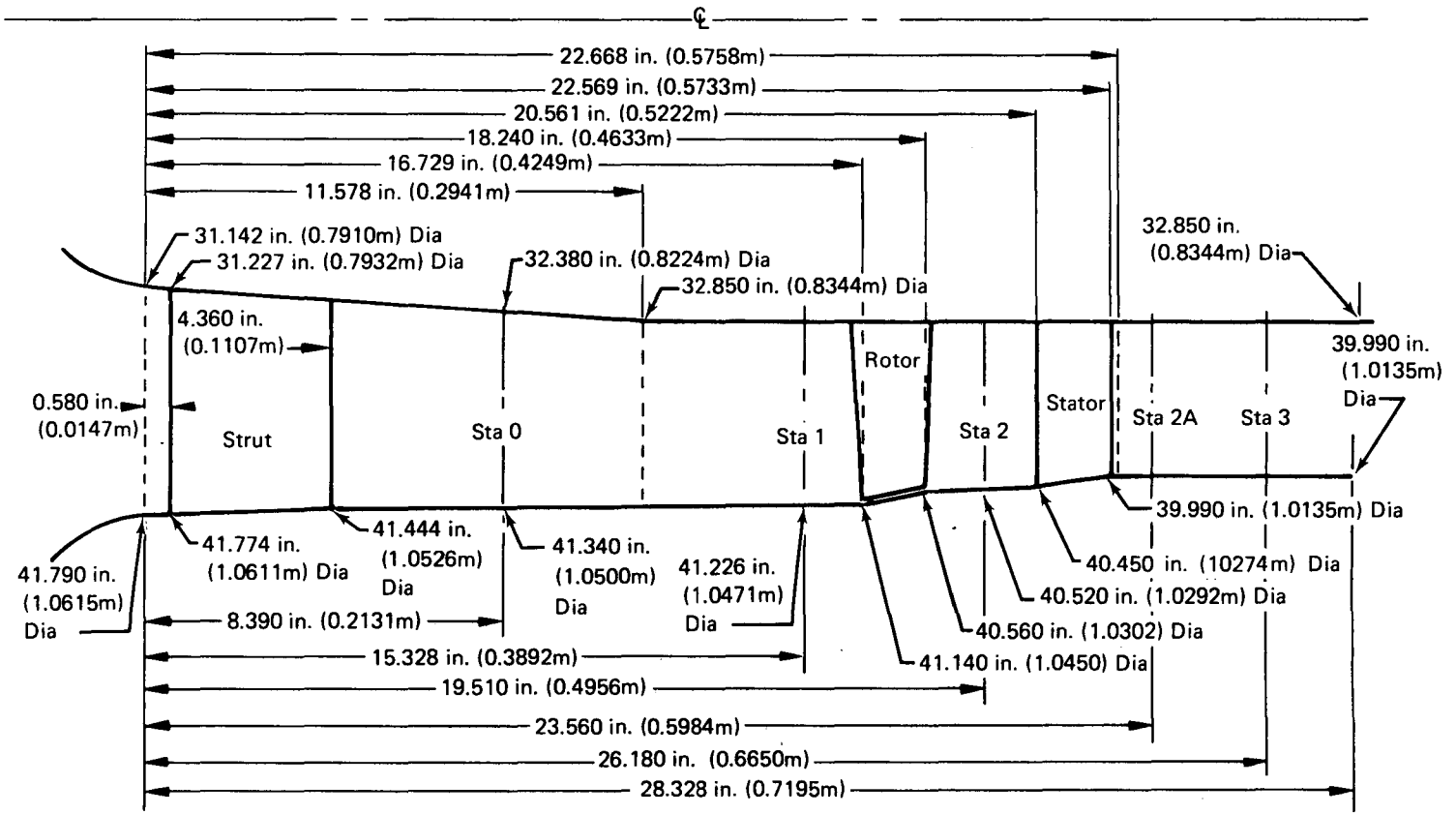

Figure 16. Flowpath Dimensions

FD 34364B

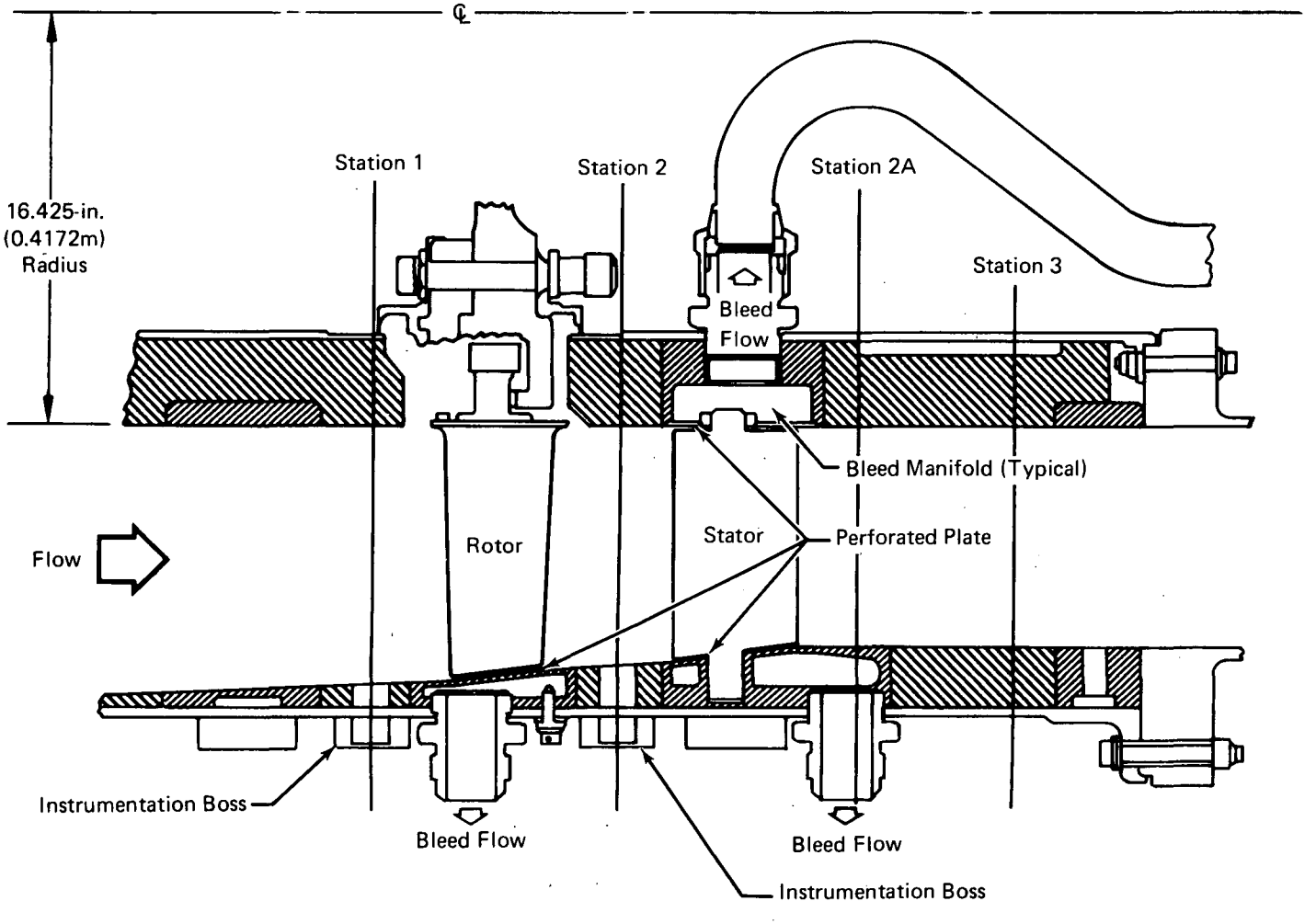

Figure 17. Boundary Layer Bleed System

FD 34363A

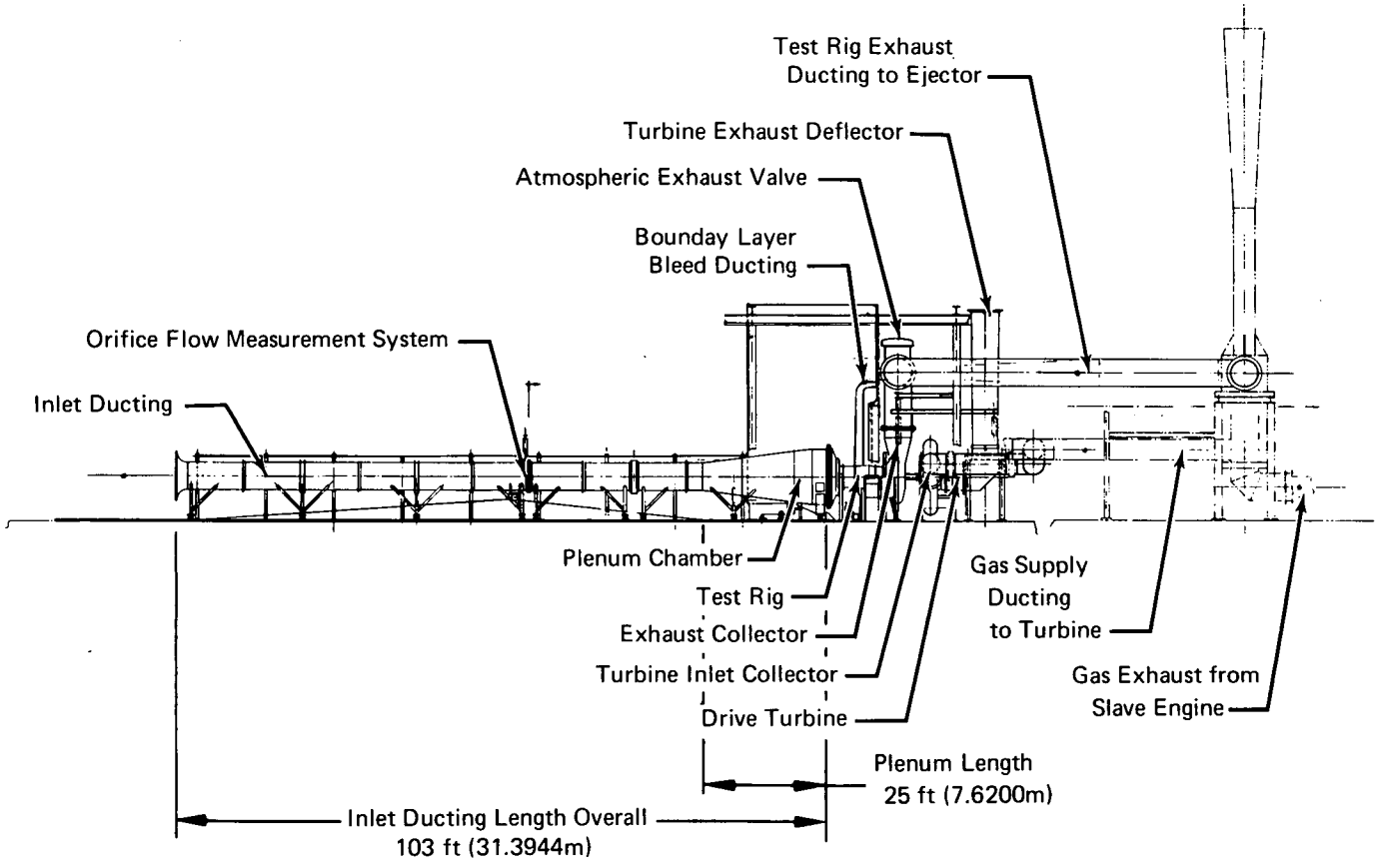

Figure 18. Compressor Research Facility

FD 10891J

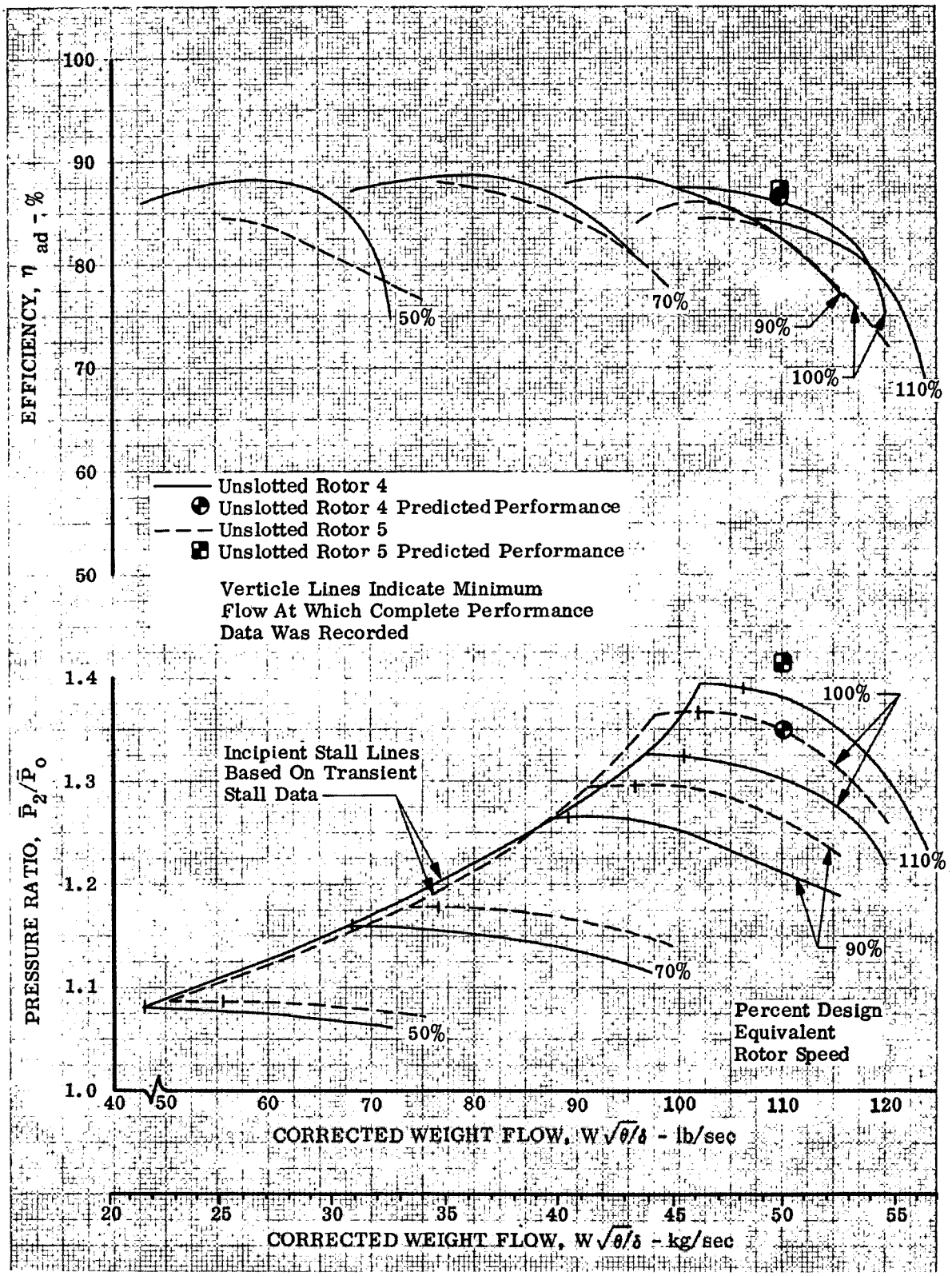

Figure 19. Overall Performance - Unslotted Rotors 4 and 5 DF 89715

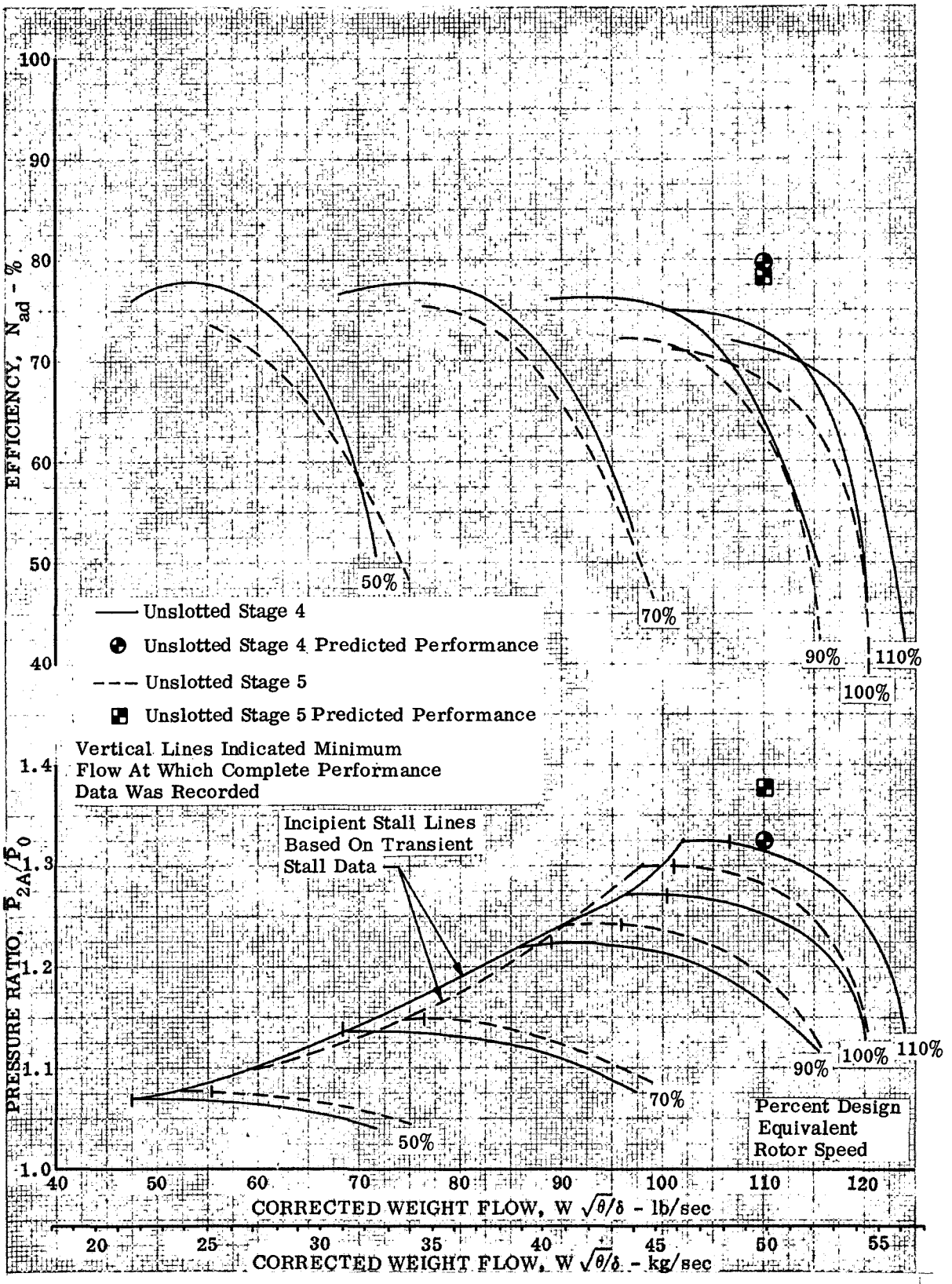

Figure 20. Overall Performance - Unslotted Stages 4 and 5 DF 89716

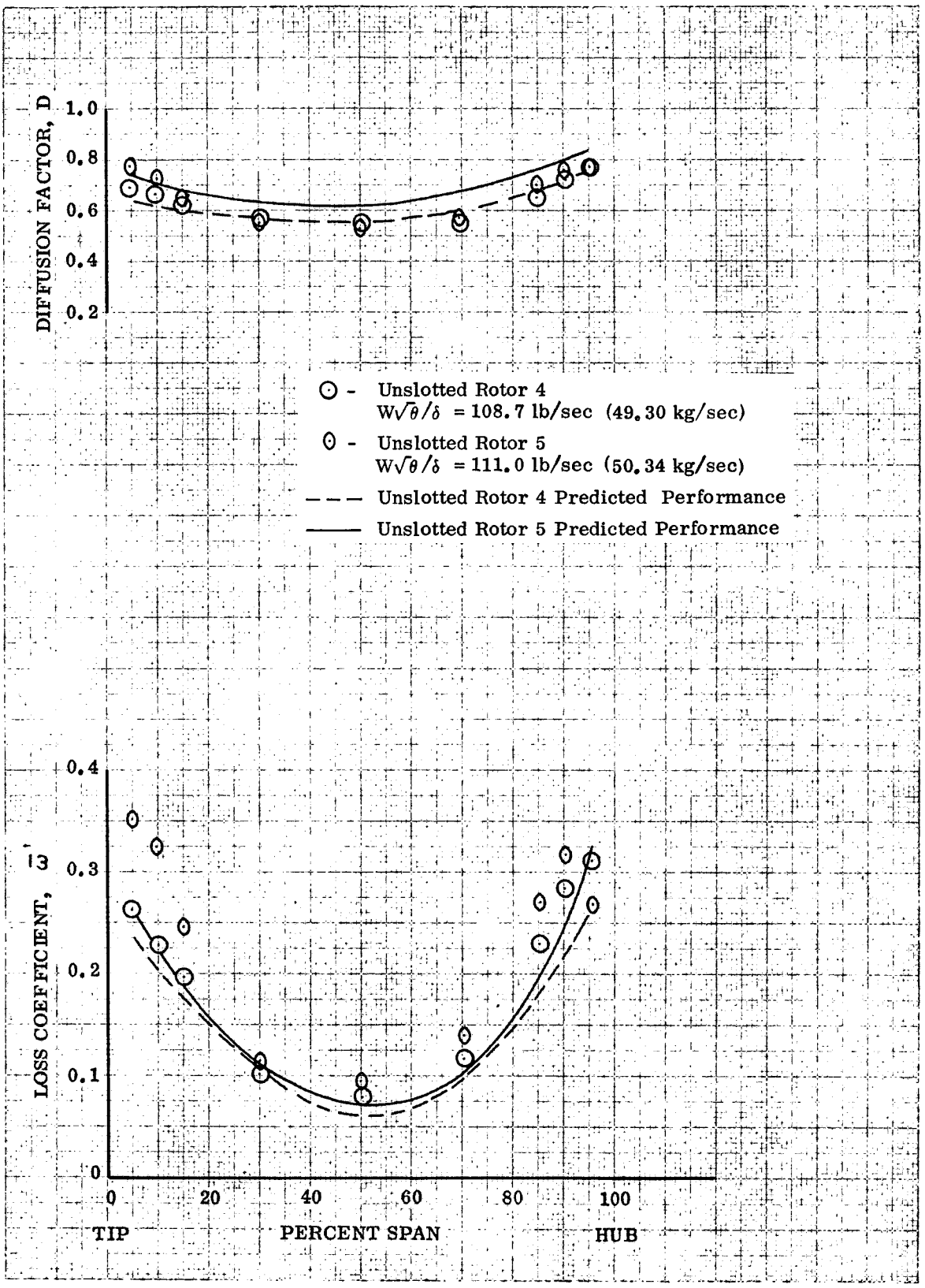

Figure 21. Blade Element Performance, Unslotted Rotors 4 and 5 at Design Eqivalent Rotor Speed and Near Design Corrected Flow

DF 89717

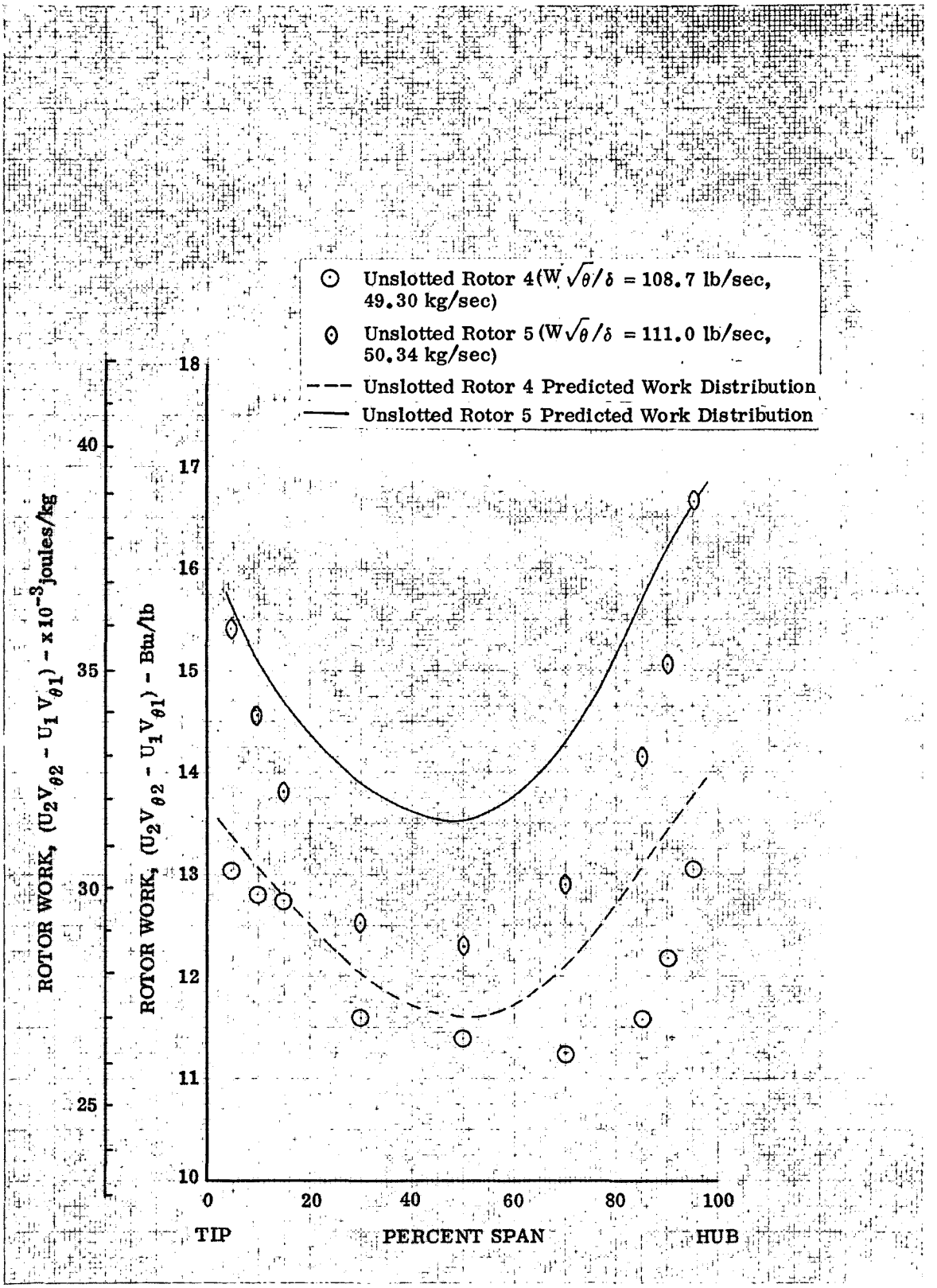

Figure 22. Radial Work Distributions for Unslotted Rotors 4 and 5 at Design Equivalent Rotor Speed and Near Design Corrected Flow

DF 89718

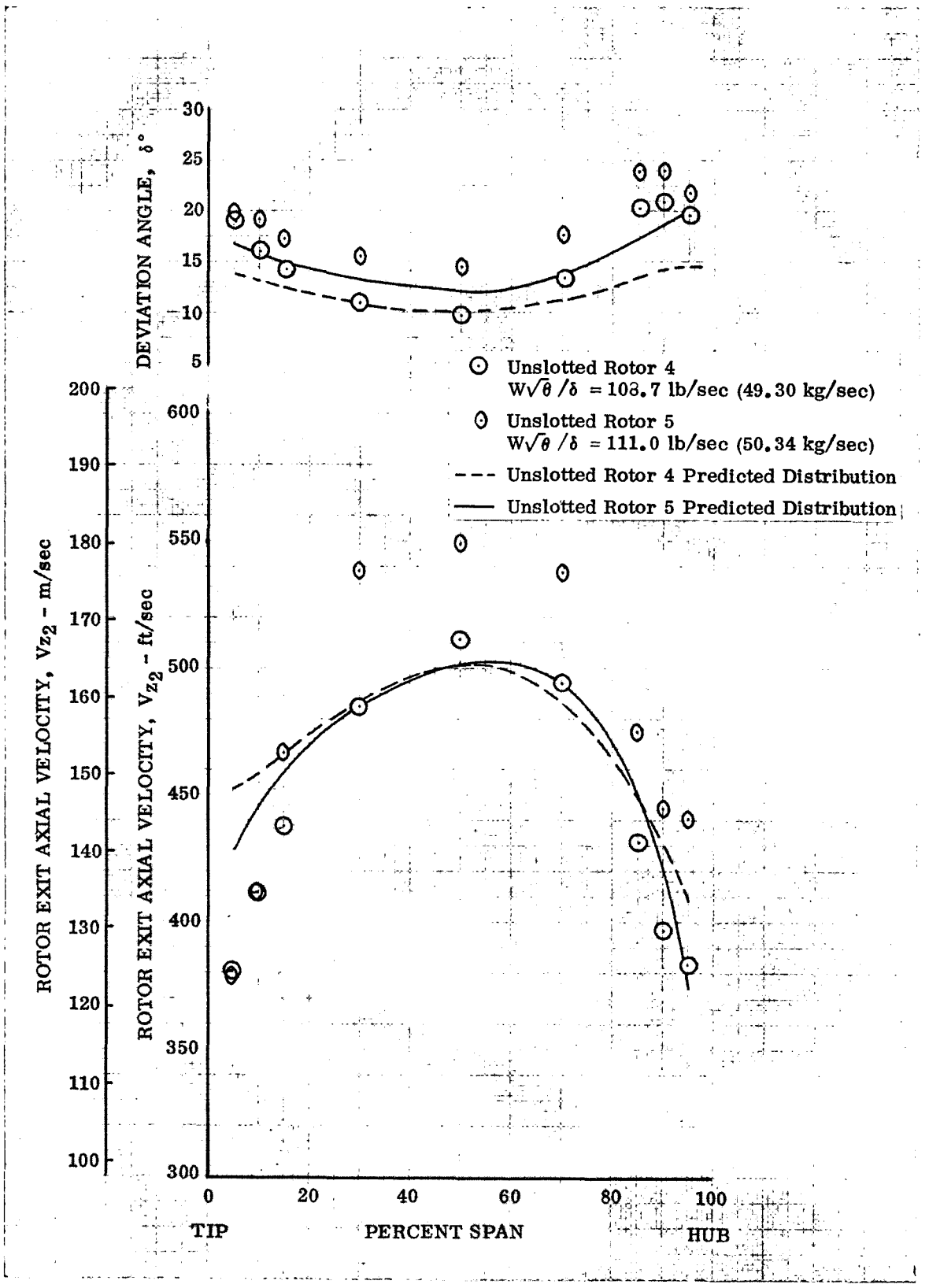

Figure 23. Comparison of Rotor Exit Axial Velocity and Deviation Angle Distributions for Unslotted Rotors 4 and 5 at Design Equivalent Speed and Near Design Corrected Flow

DF 89719

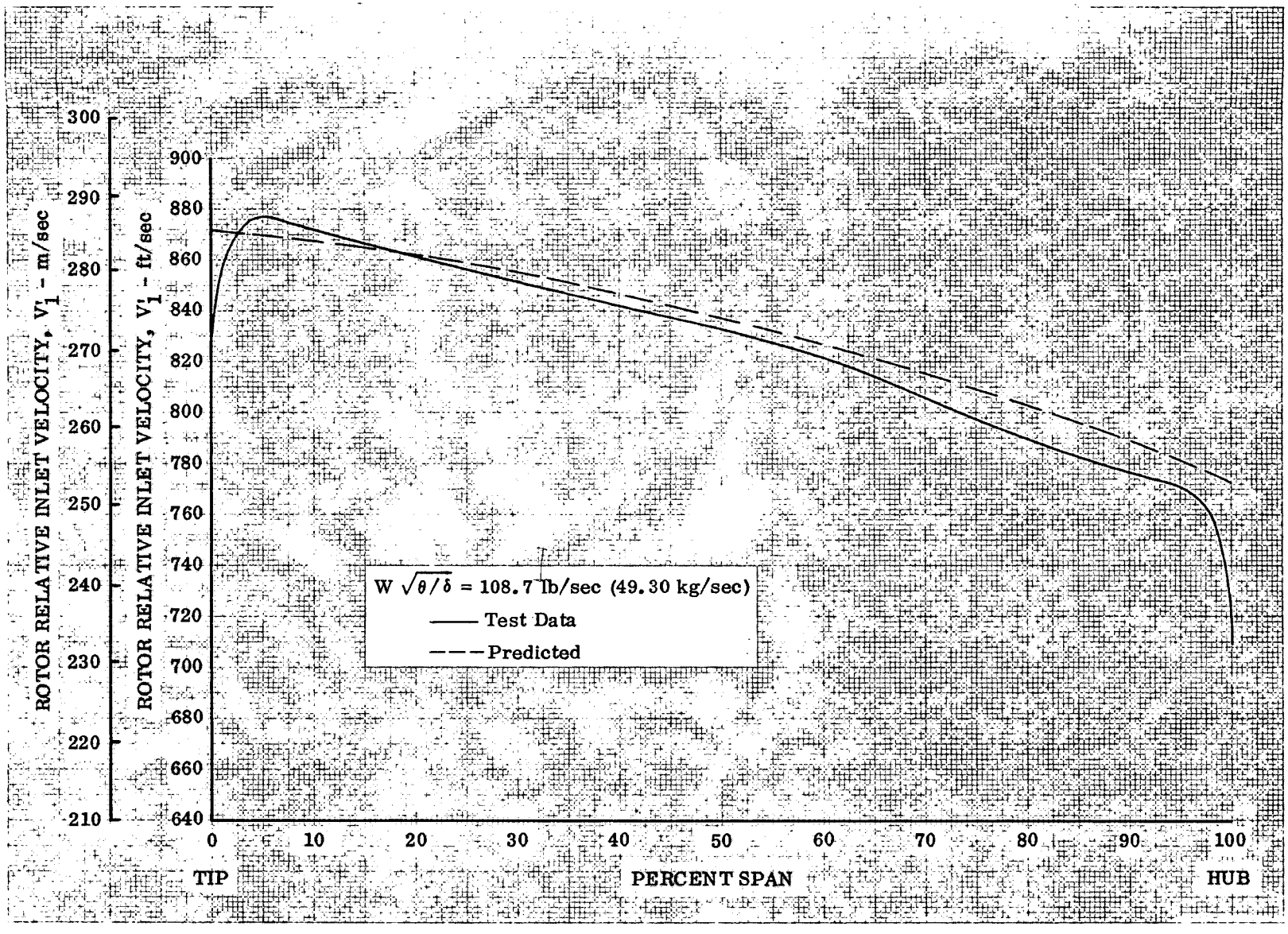

Figure 24. Unslotted Rotor 4 Relative Inlet Velocity Distribution at Design Equivalent Rotor Speed and Near Design Corrected Flow

DF 89720

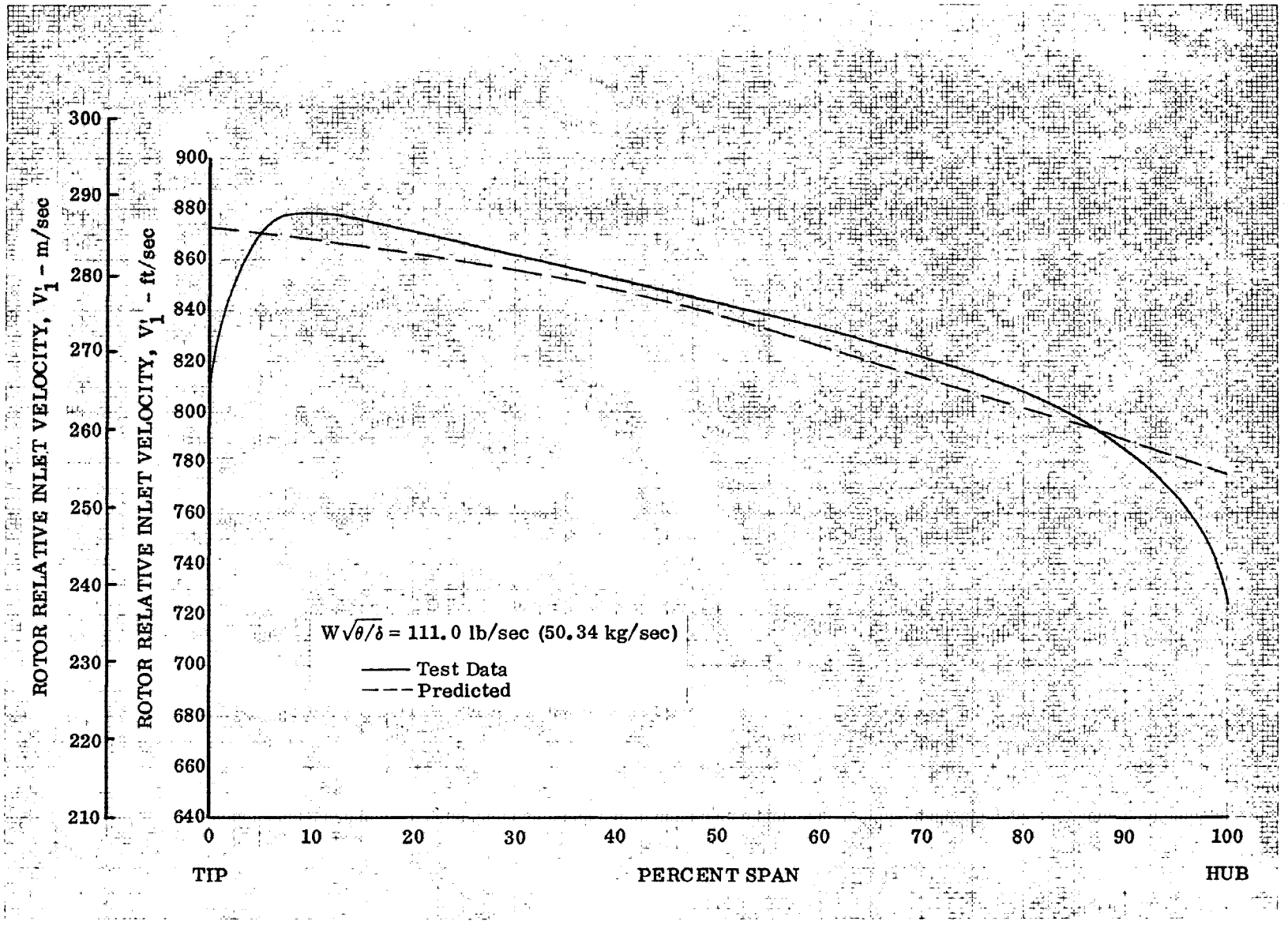

Figure 25. Unslotted Rotor 5 Relative Inlet Velocity Distribution at Design Equivalent Rotor Speed and Near Design Corrected Flow

DF 89721

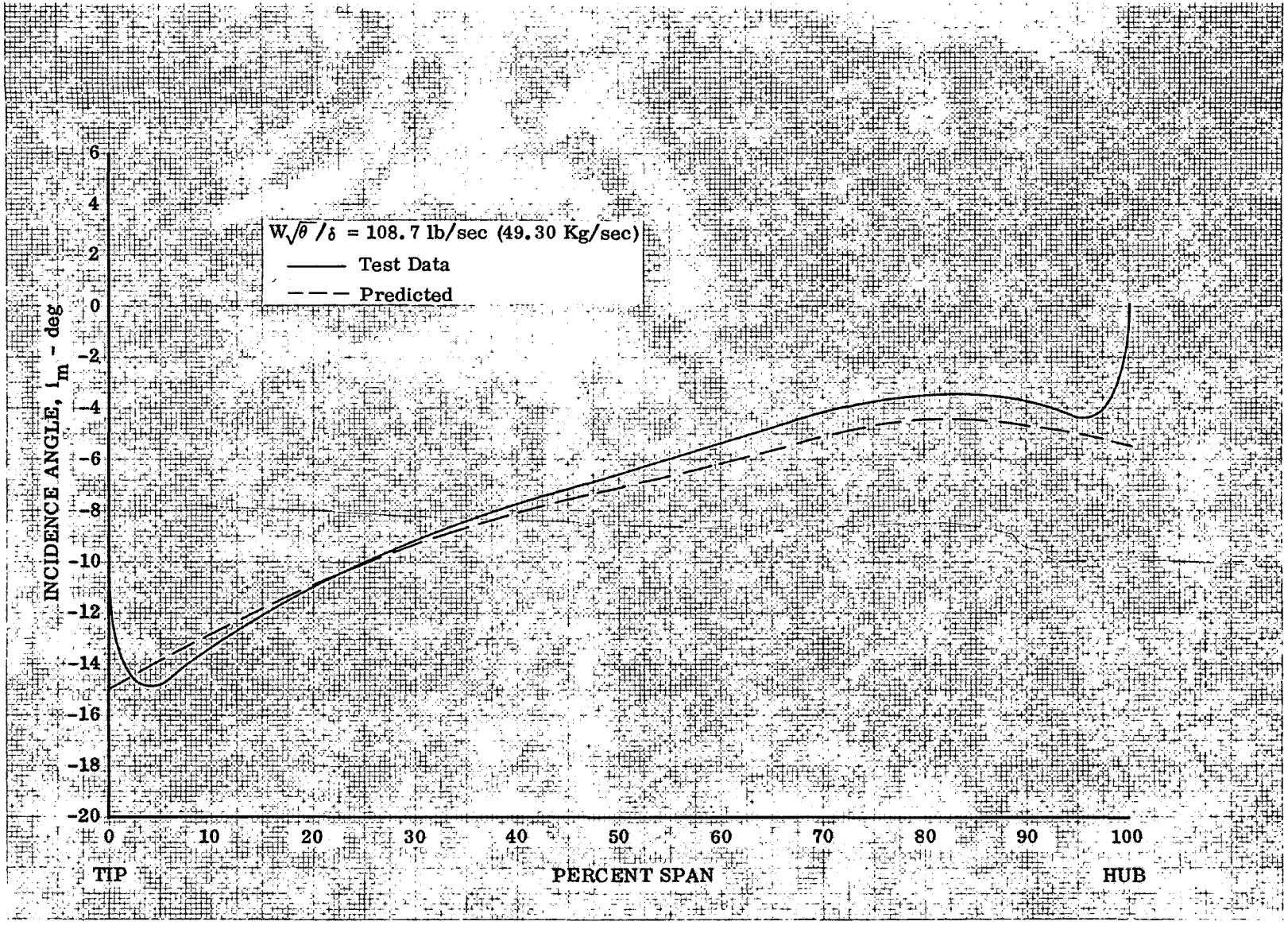

Figure 26. Unslotted Rotor 4 Incidence Angle Distribution at Design Equivalent Rotor Speed and Near Design Corrected Weight Flow

DF 89722

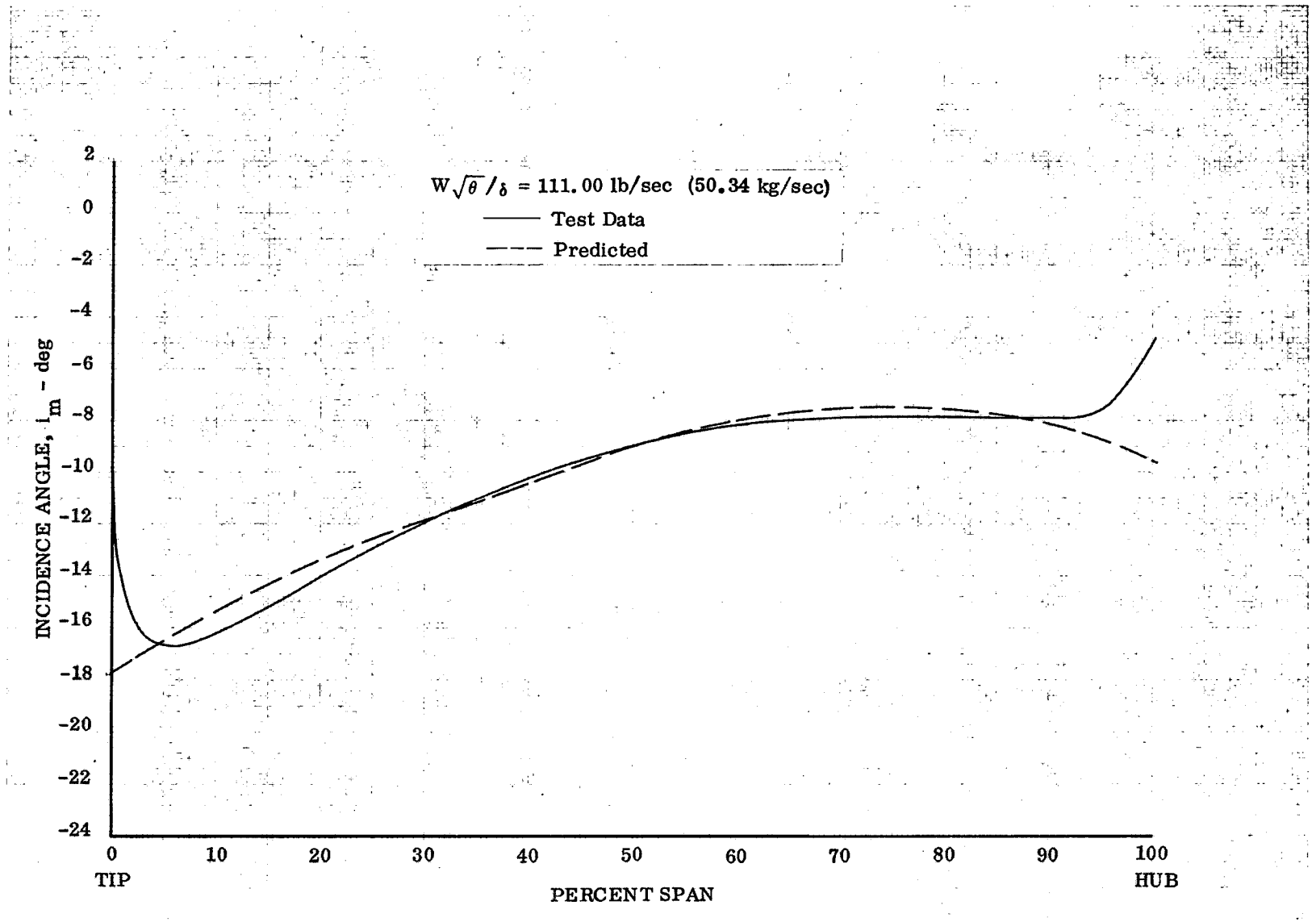

Figure 27. Unslotted Rotor 5 Incidence Angle Distribution Near Design Corrected Flow and Design Equivalent Rotor Speed

DF 89723

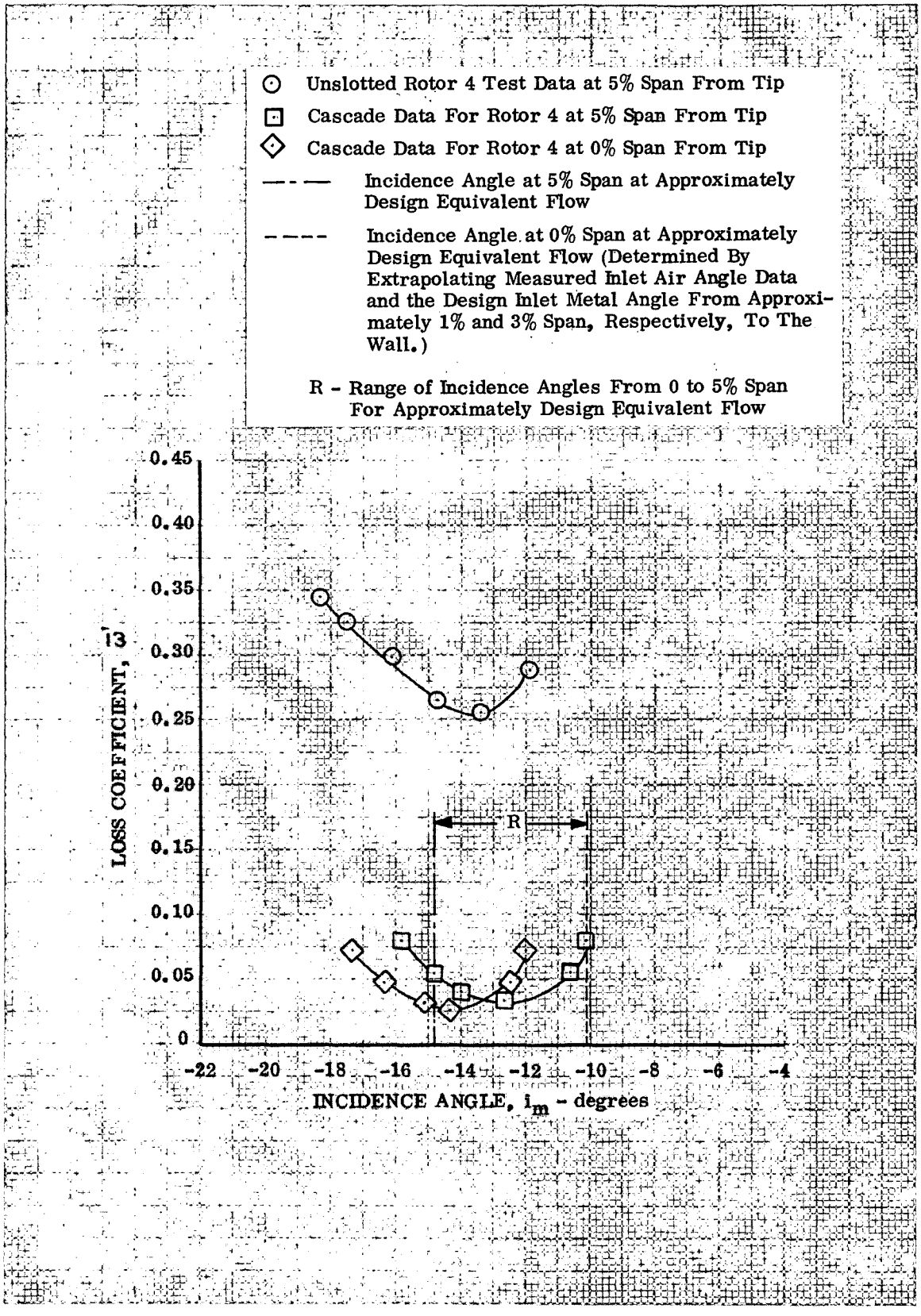

Figure 28. Unslotted Rotor 4 Tip Loss Coefficient vs Incidence Angle at Design Equivalent Rotor Speed DF 89724

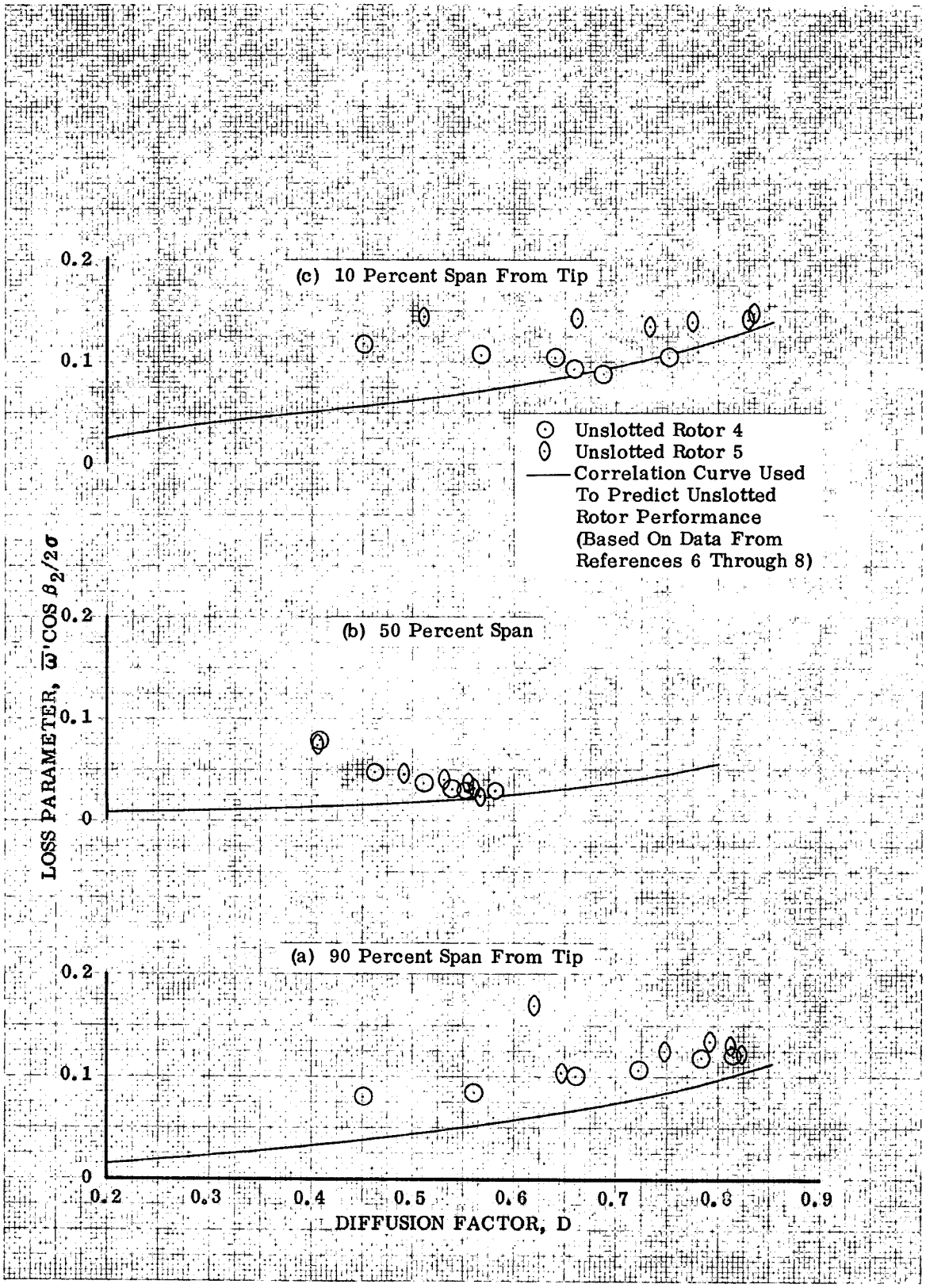

Figure 29 a - c. Comparison of Loss Parameter Distributions for Unslotted Rotors 4 and 5 DF 89725

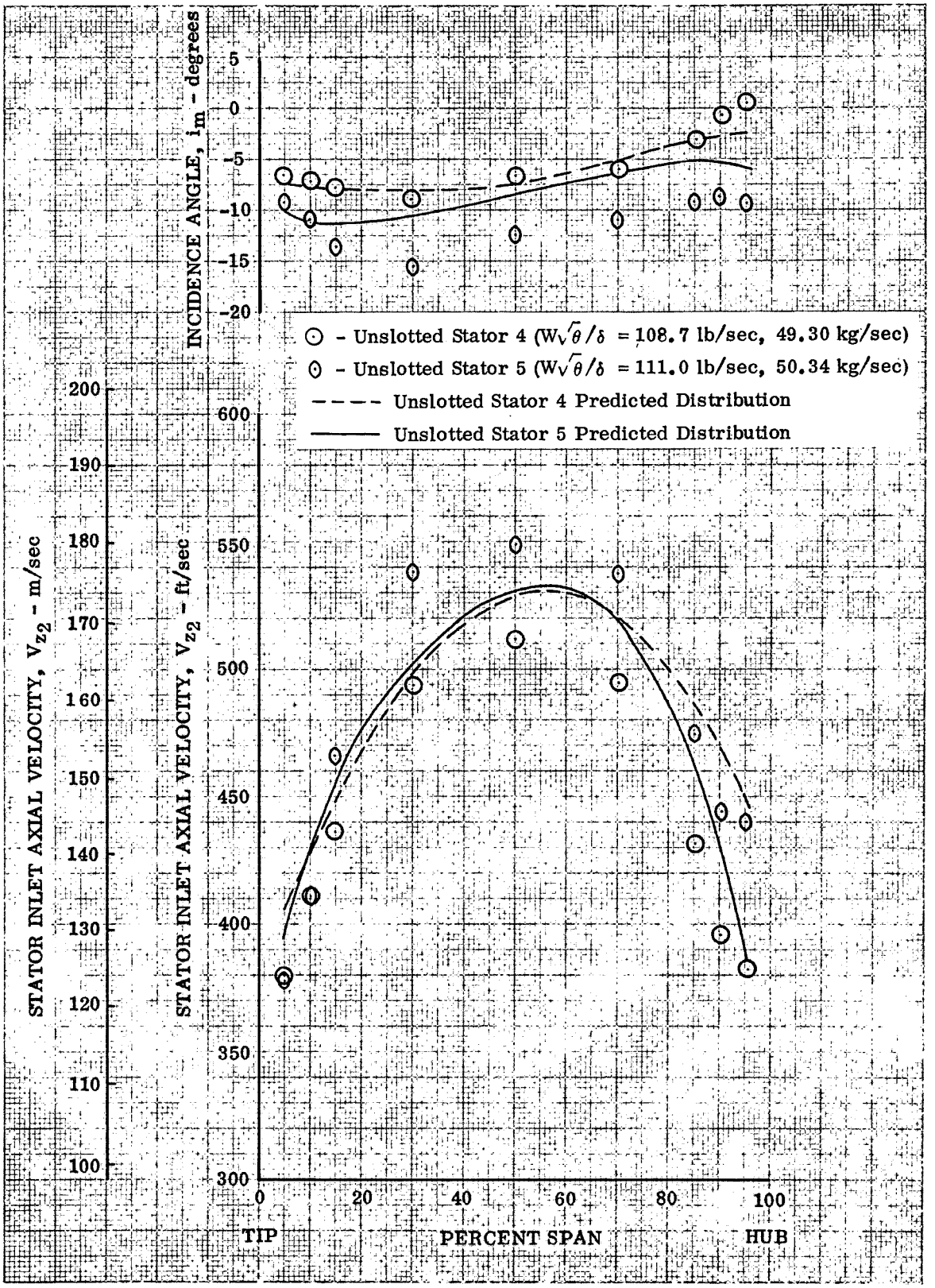

Figure 30. Comparison of Stator Inlet Axial Velocity and Incidence Angle Distributions for Unslotted Stators 4 and 5

DF 89726

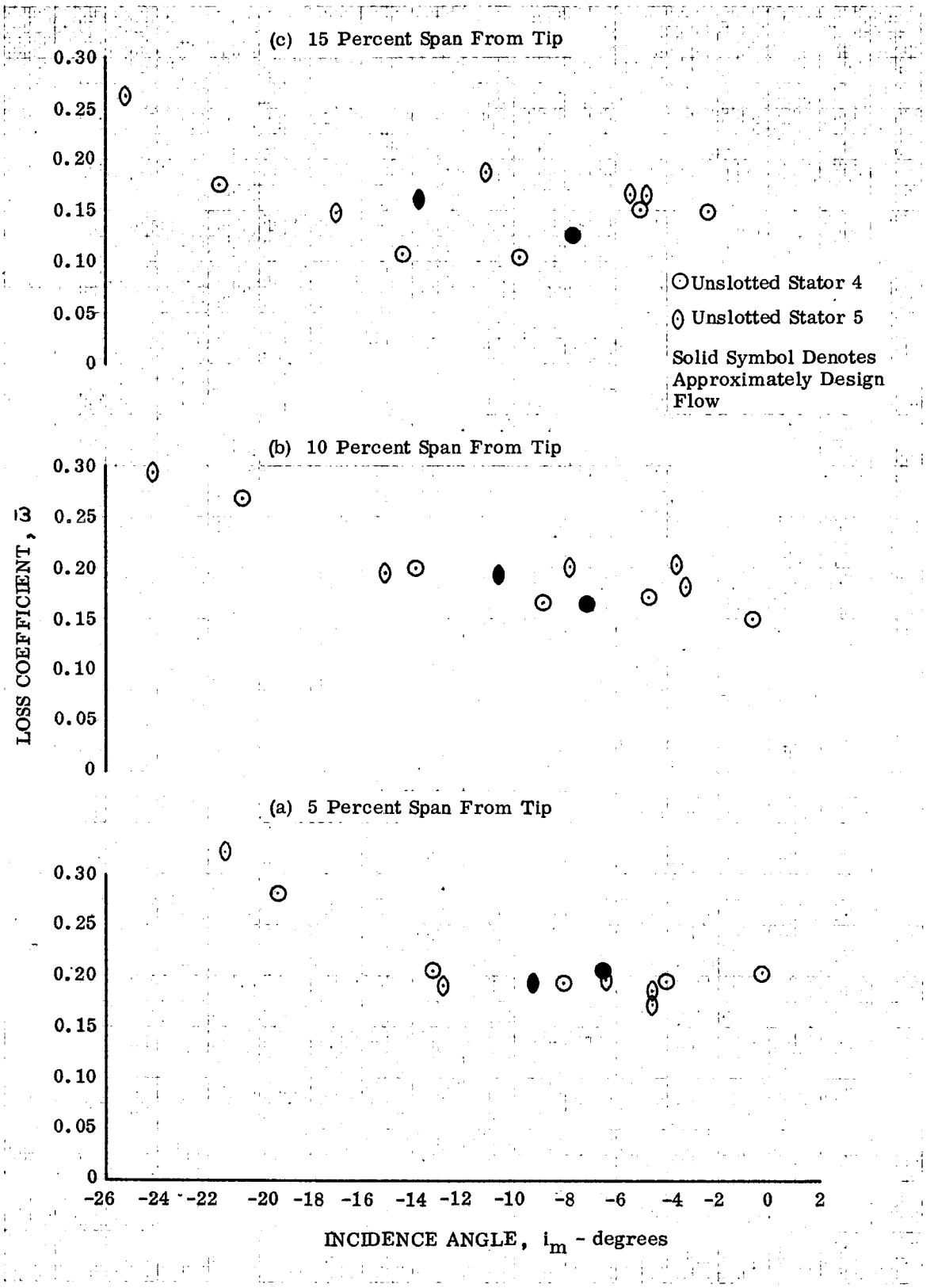

Figure 31 a - c. Stator Loss Coefficient for Design Equivalent Rotor Speed DF 89727

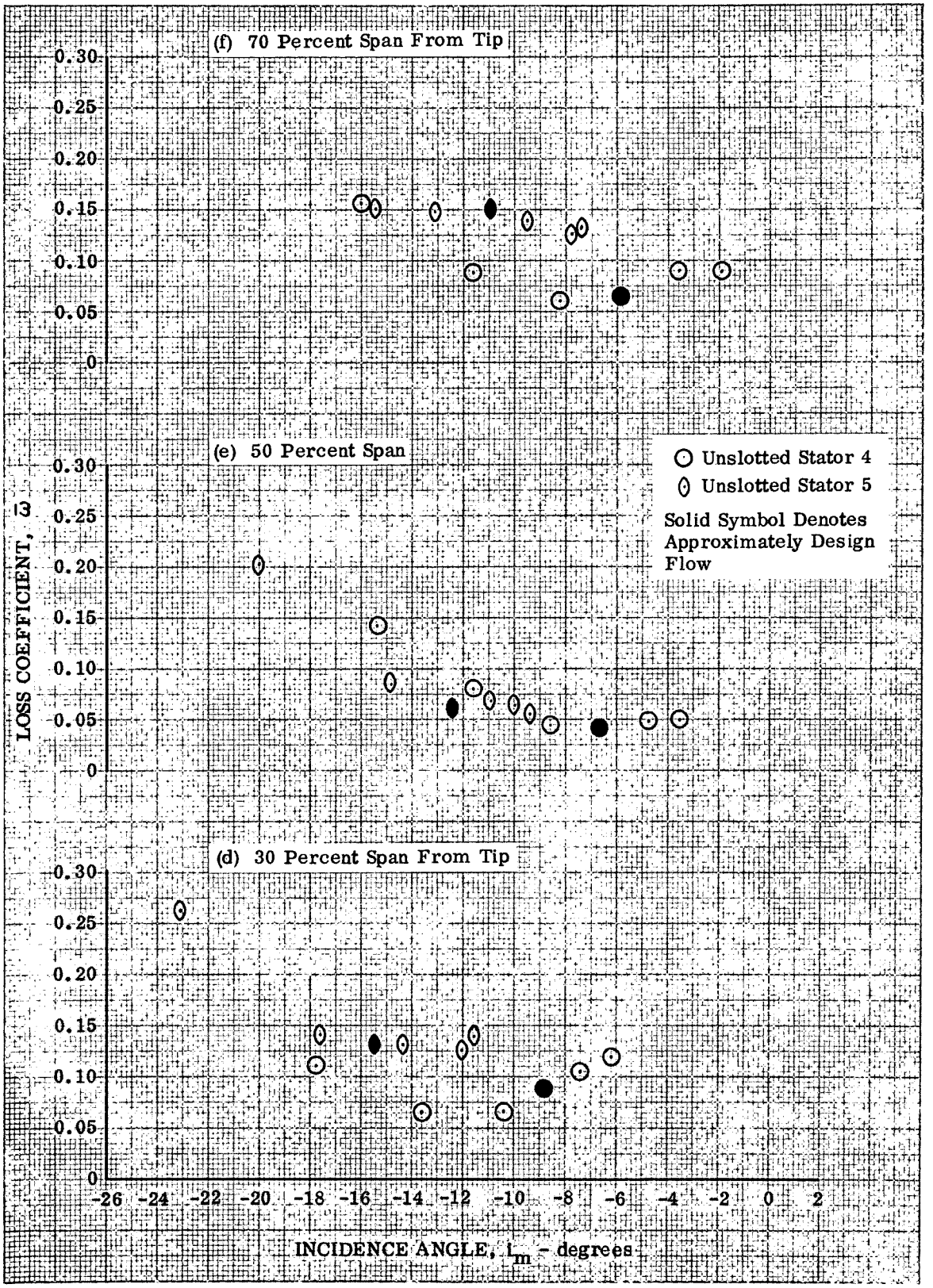

Figure 31 d - f. Stator Loss Coefficient for Design Equivalent Rotor Speed DF 89728

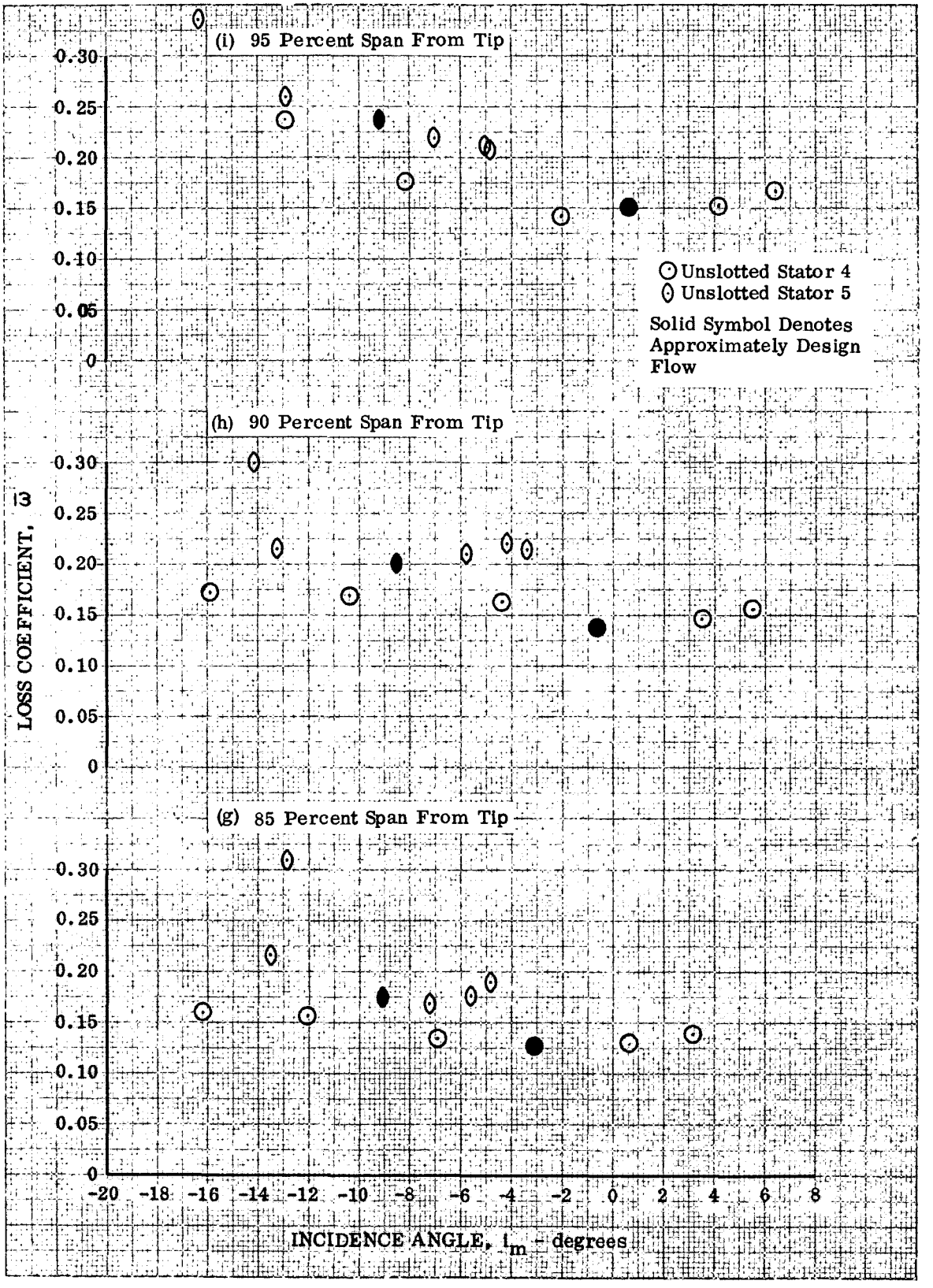

Figure 31 g - i. Stator Loss Coefficient for Design Equivalent Rotor Speed DF 89729

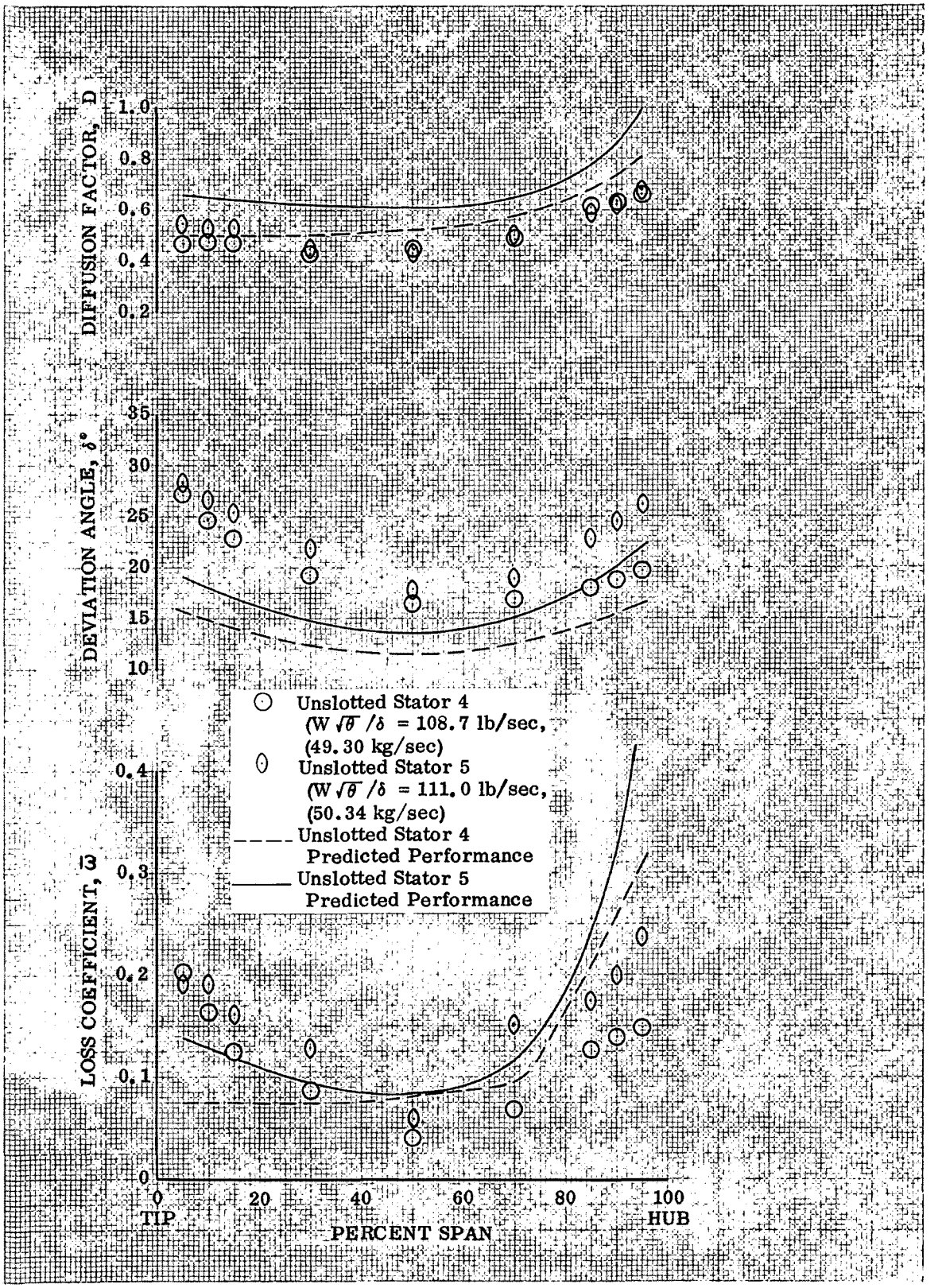

Figure 32. Blade Element Performance, Unslotted Stators 4 and 5 at Design Equivalent Rotor Speed and Near Design Corrected Flow

DF 89730

29

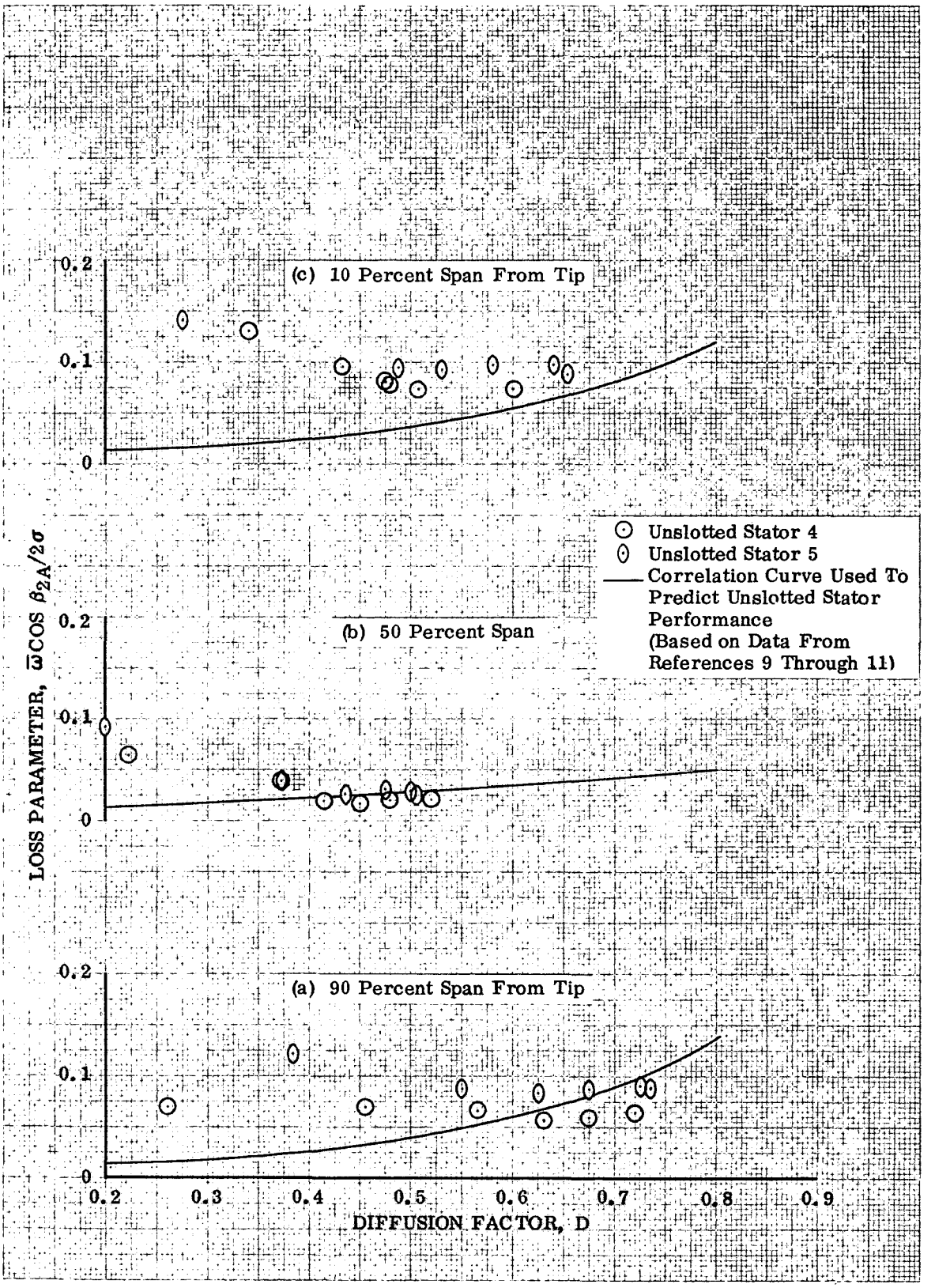

Figure 33 a - c. Comparison of Loss Parameter Distributions for Unslotted Stators 4 and 5 at Design Equivalent Rotor Speed

DF 89731

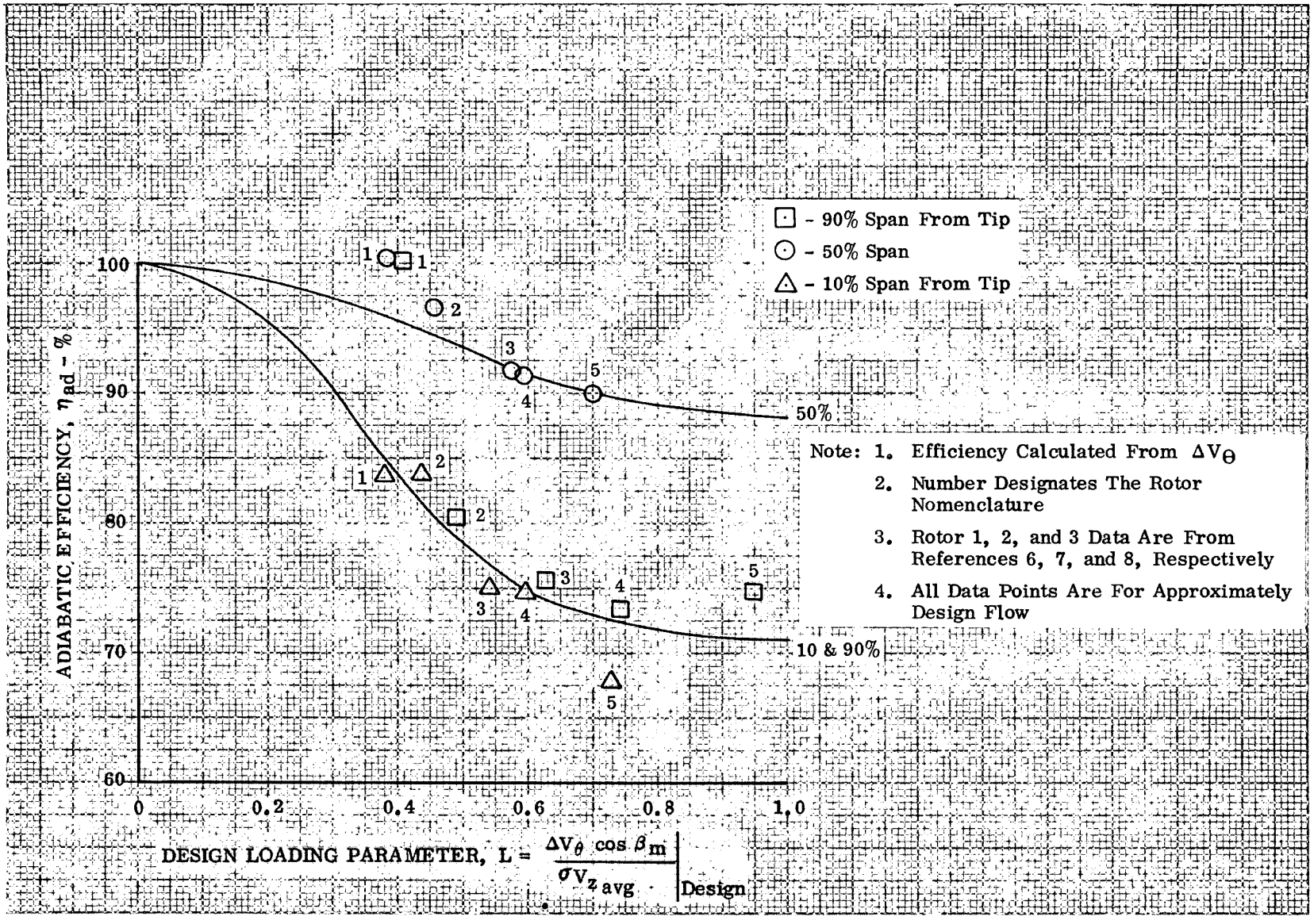

Figure 34. Rotor Adiabatic Efficiency vs Design Loading

DF 89732

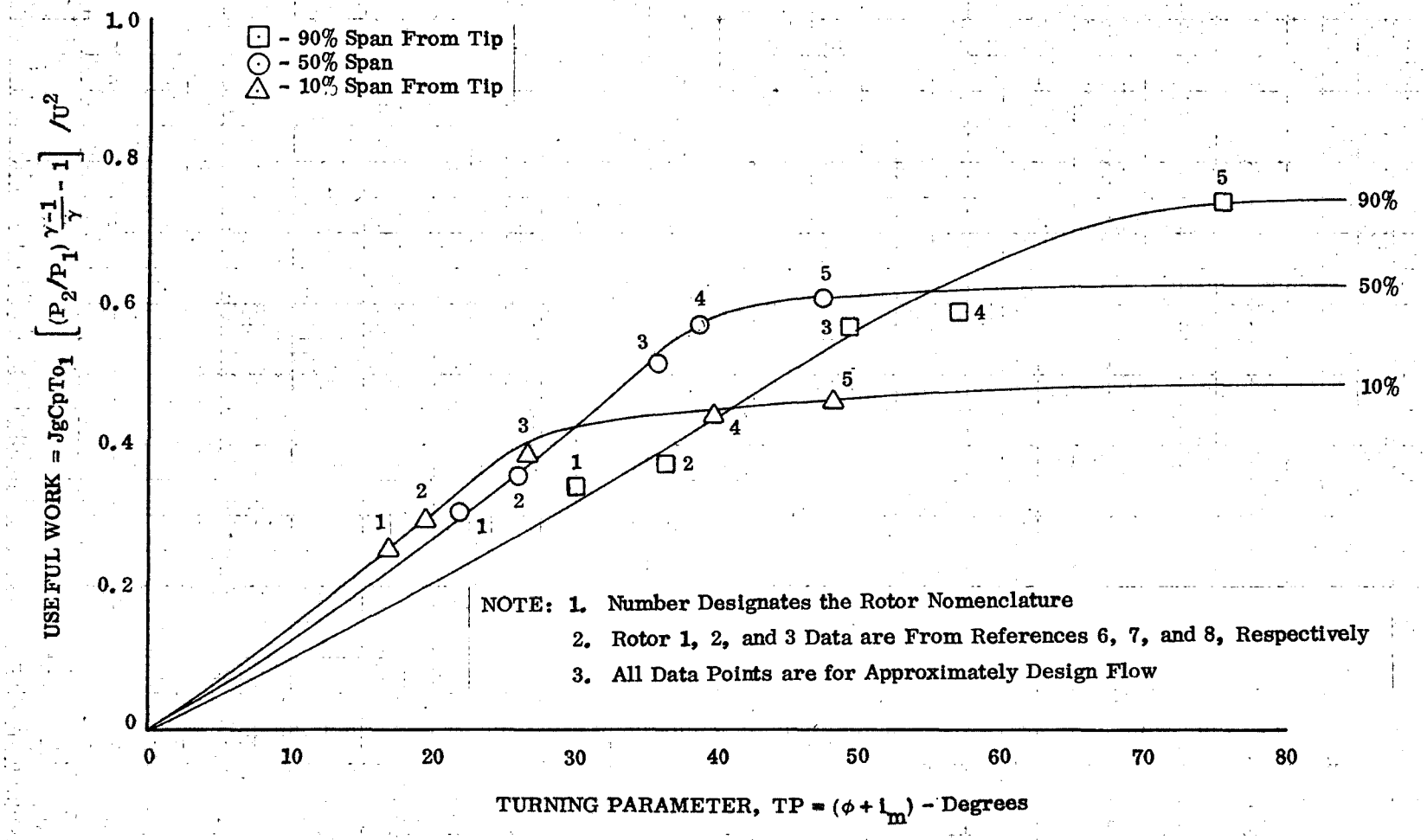

Figure 35. Useful Work vs Turning Parameter

DF 89733

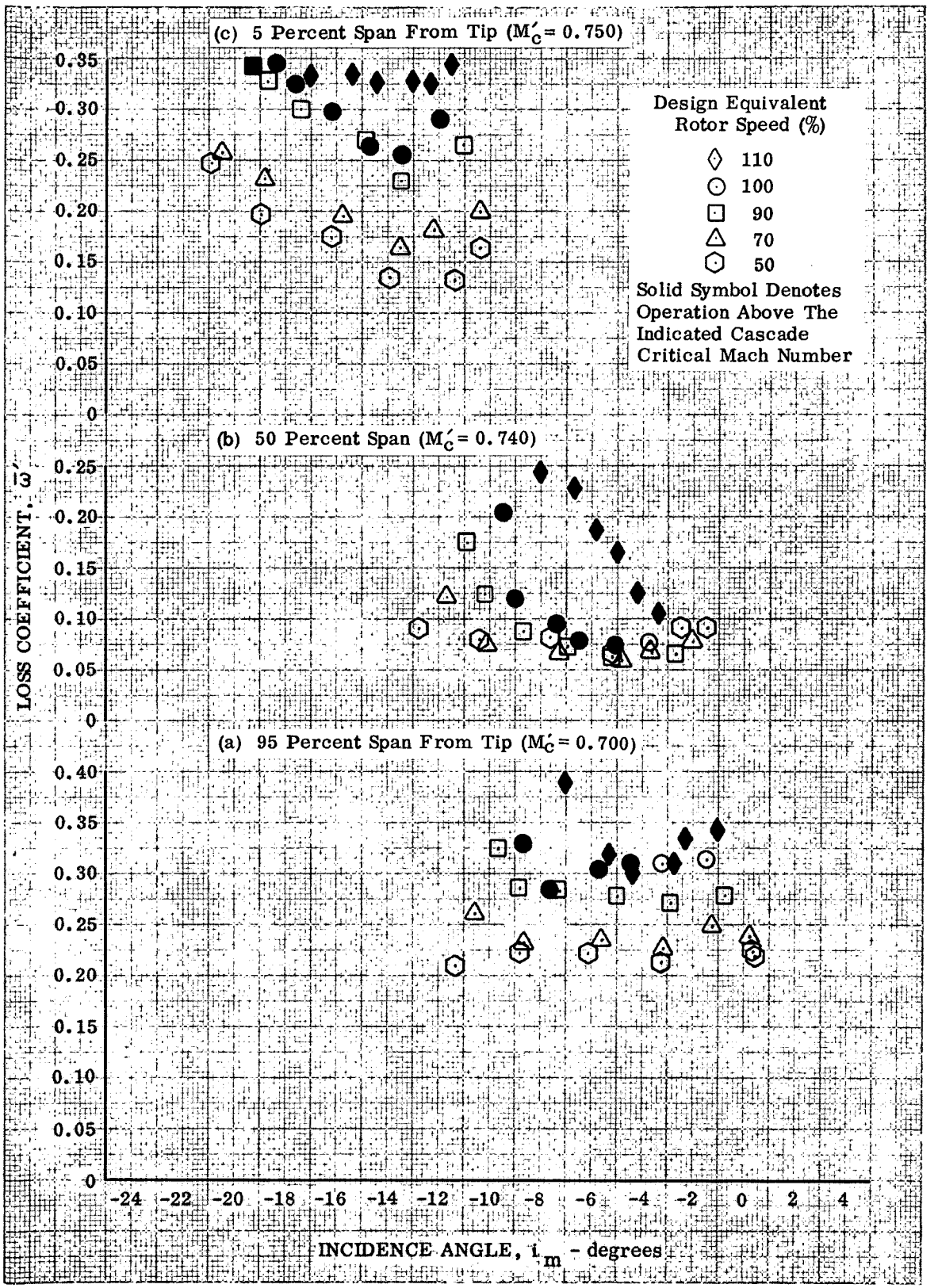

Figure 36 a - c. Unslotted Rotor 4 Loss Coefficient DF 89734

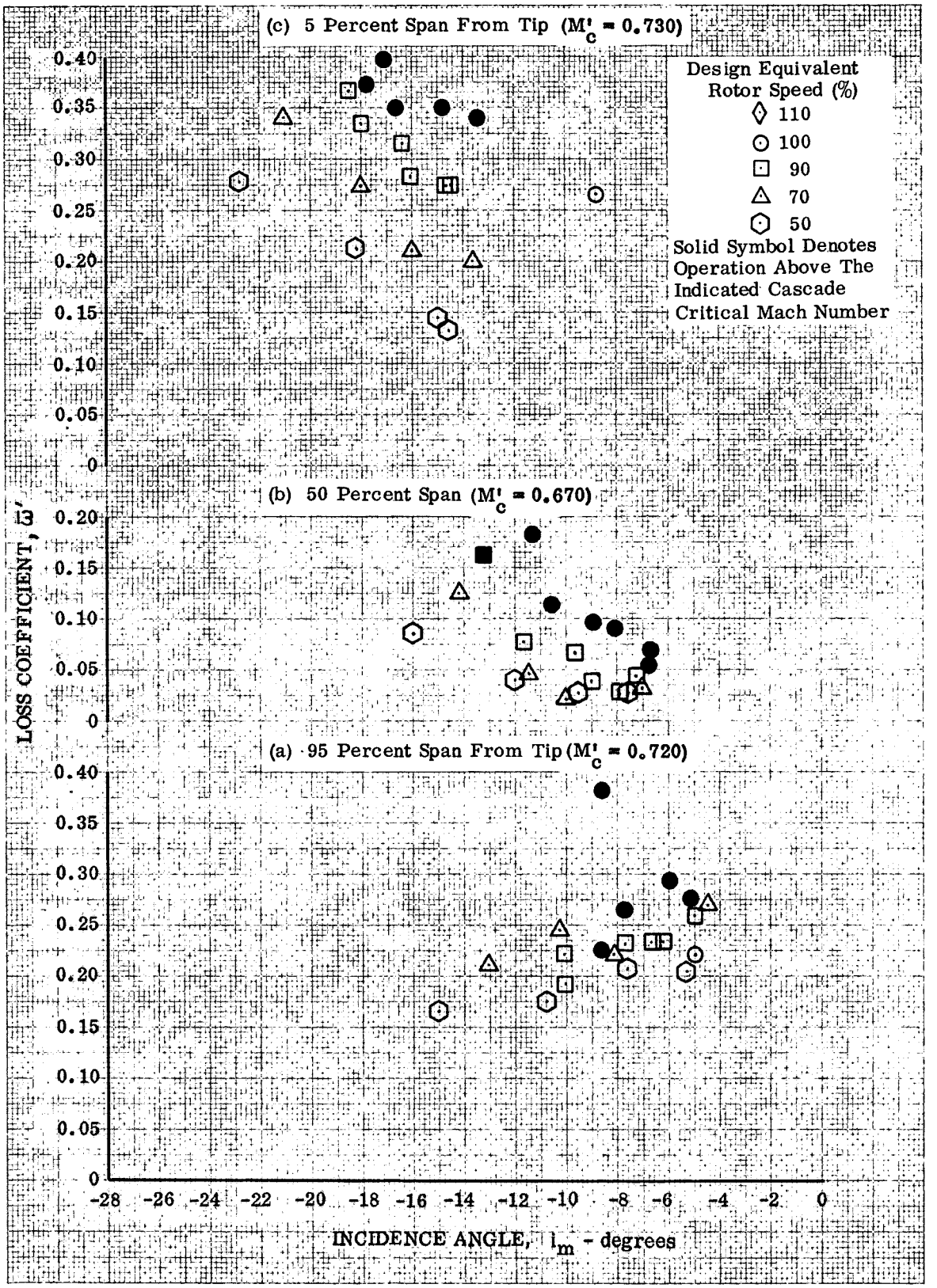

Figure 37 a - c. Unslotted Rotor 5 Loss Coefficient DF 89735

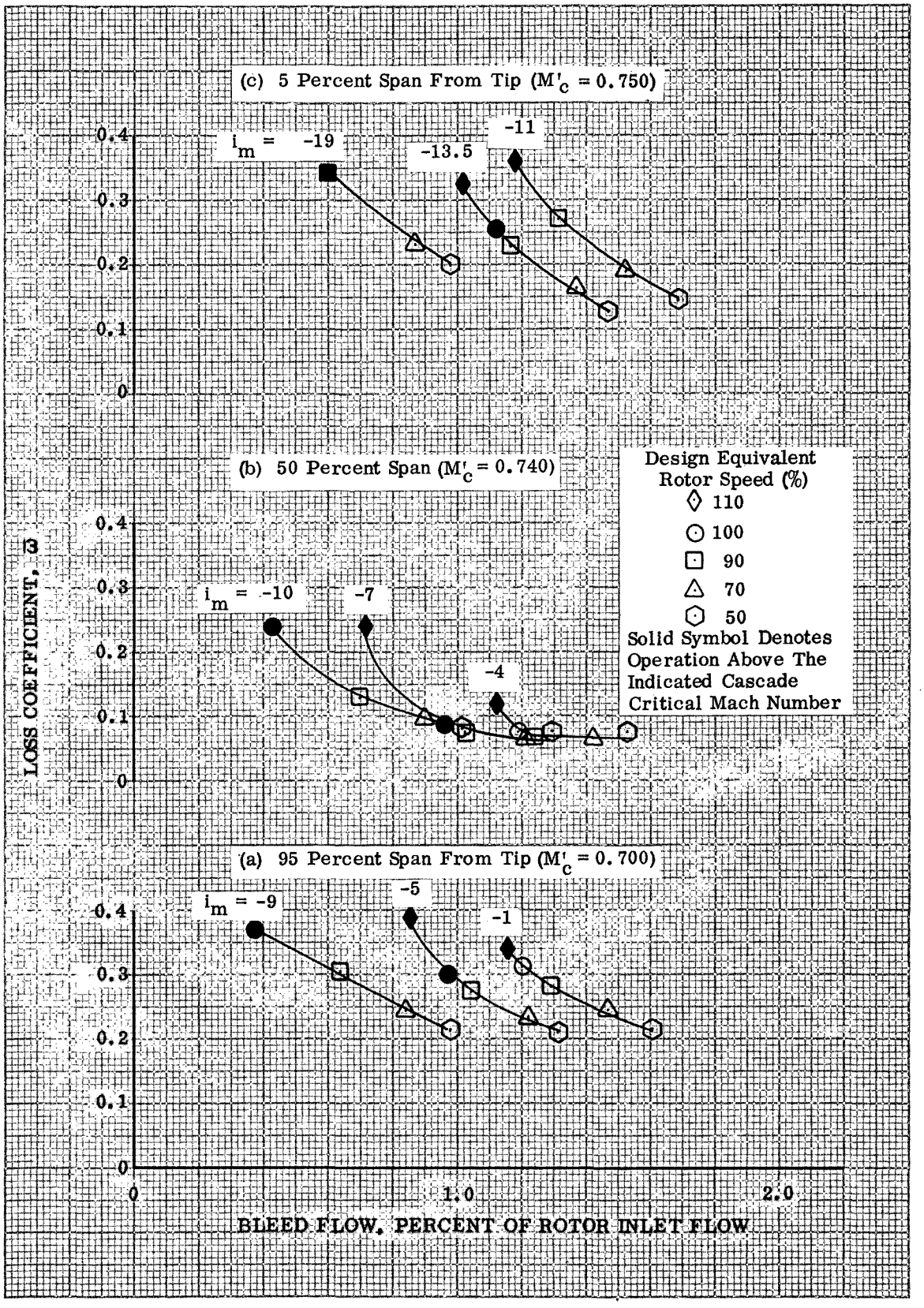

Figure 38 a - c. Variation in Unslotted Rotor 4 Loss Coefficient With Rotor Bleed Flow DF 89736

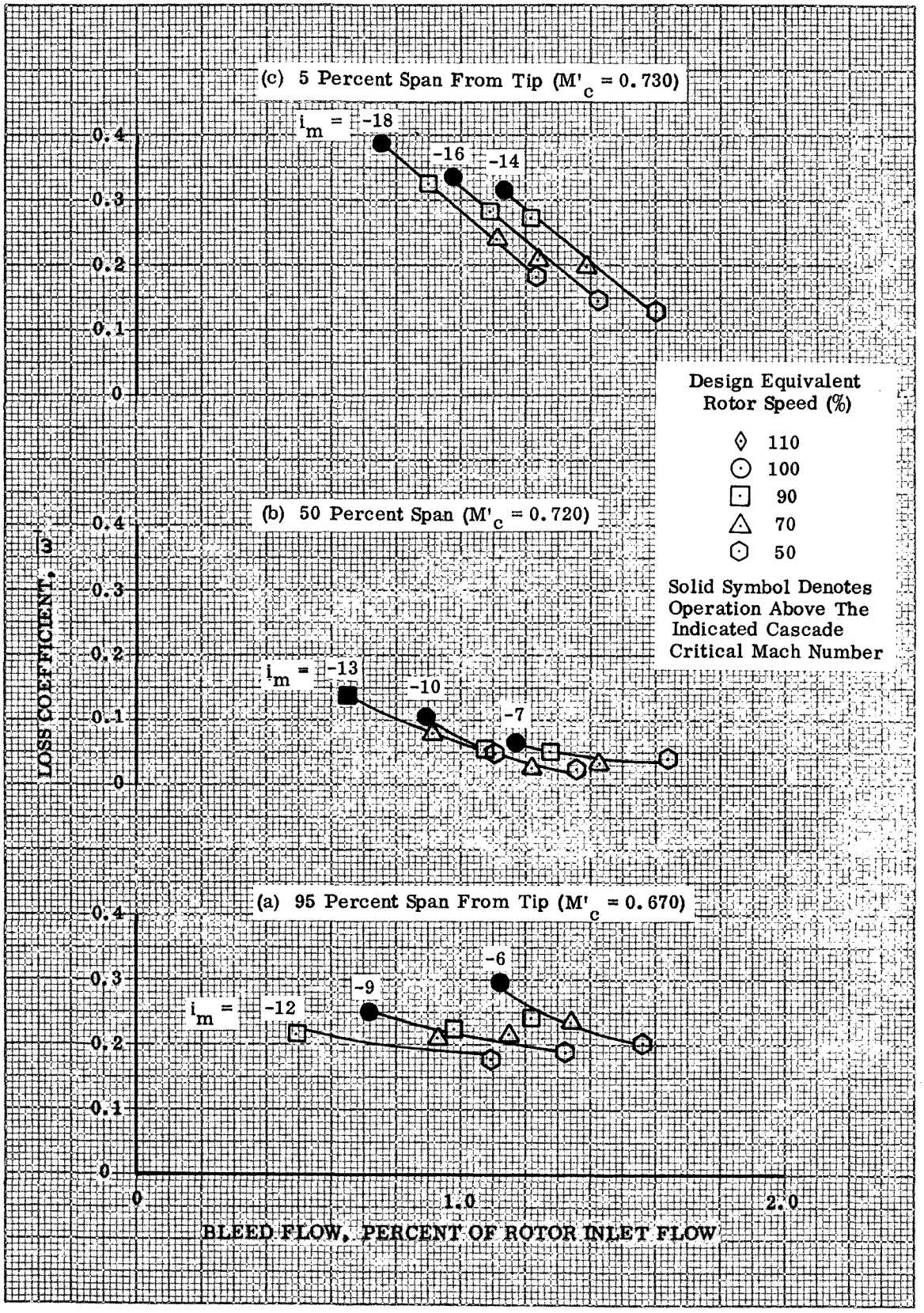

Figure 39 a - c. Variation in Unslotted Rotor 5 Loss Coefficient With Rotor Bleed Flow DF 89737

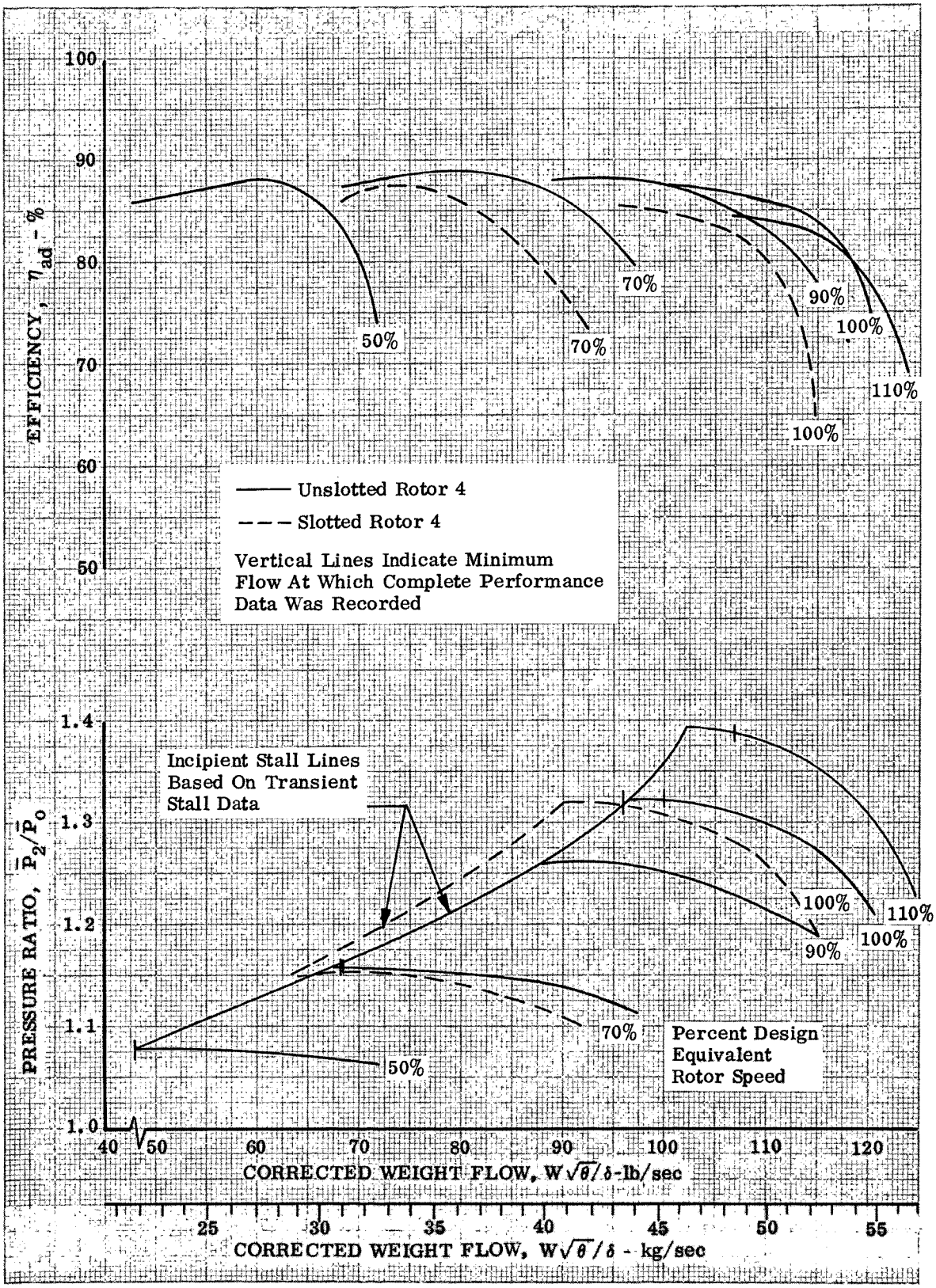

Figure 40. Comparison of Unslotted and Slotted Rotor 4 Overall Performance

DF 89738

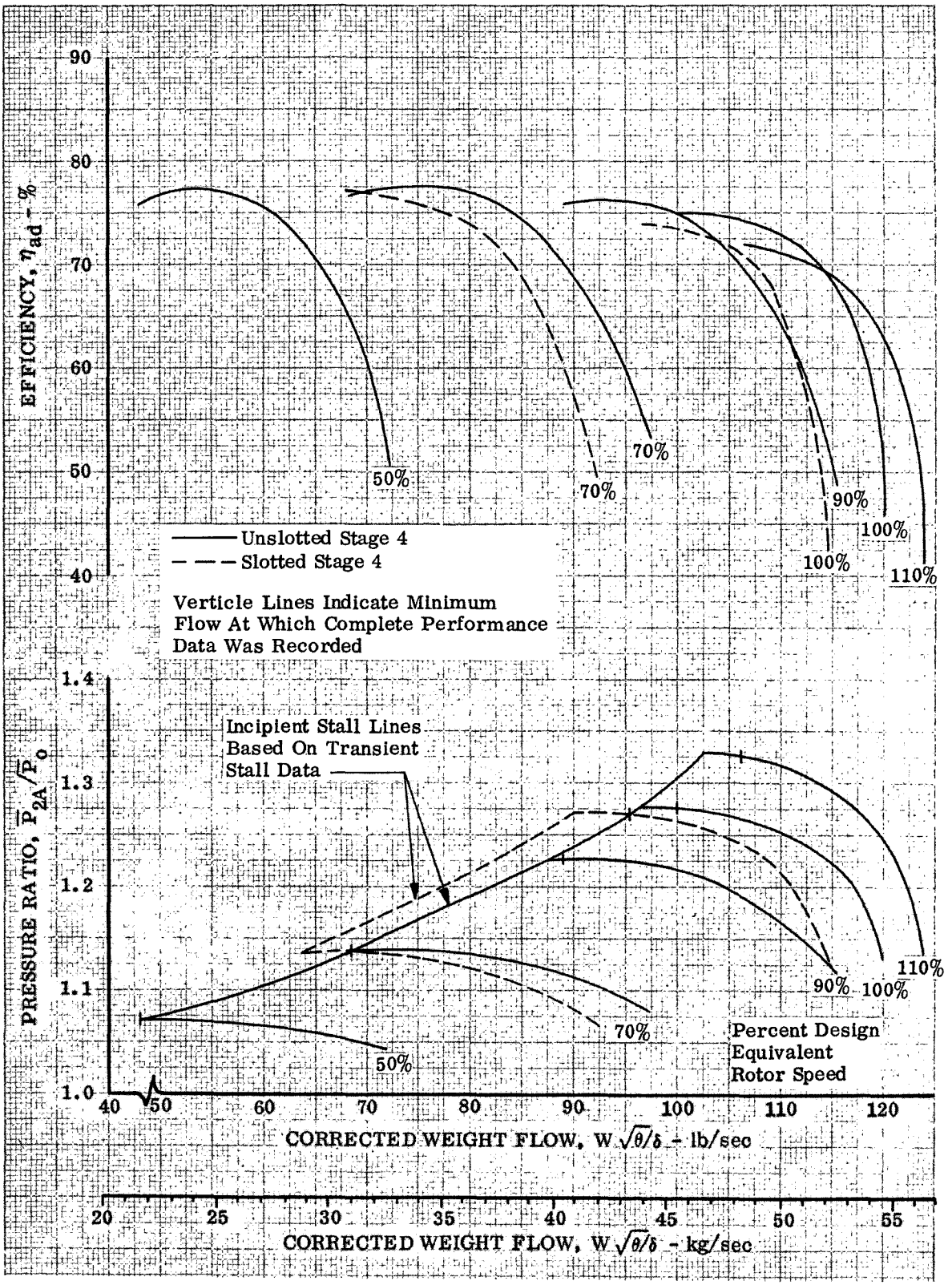

Figure 41. Comparison of Unslotted and Slotted Stage 4 Overall Performance

DF 89739

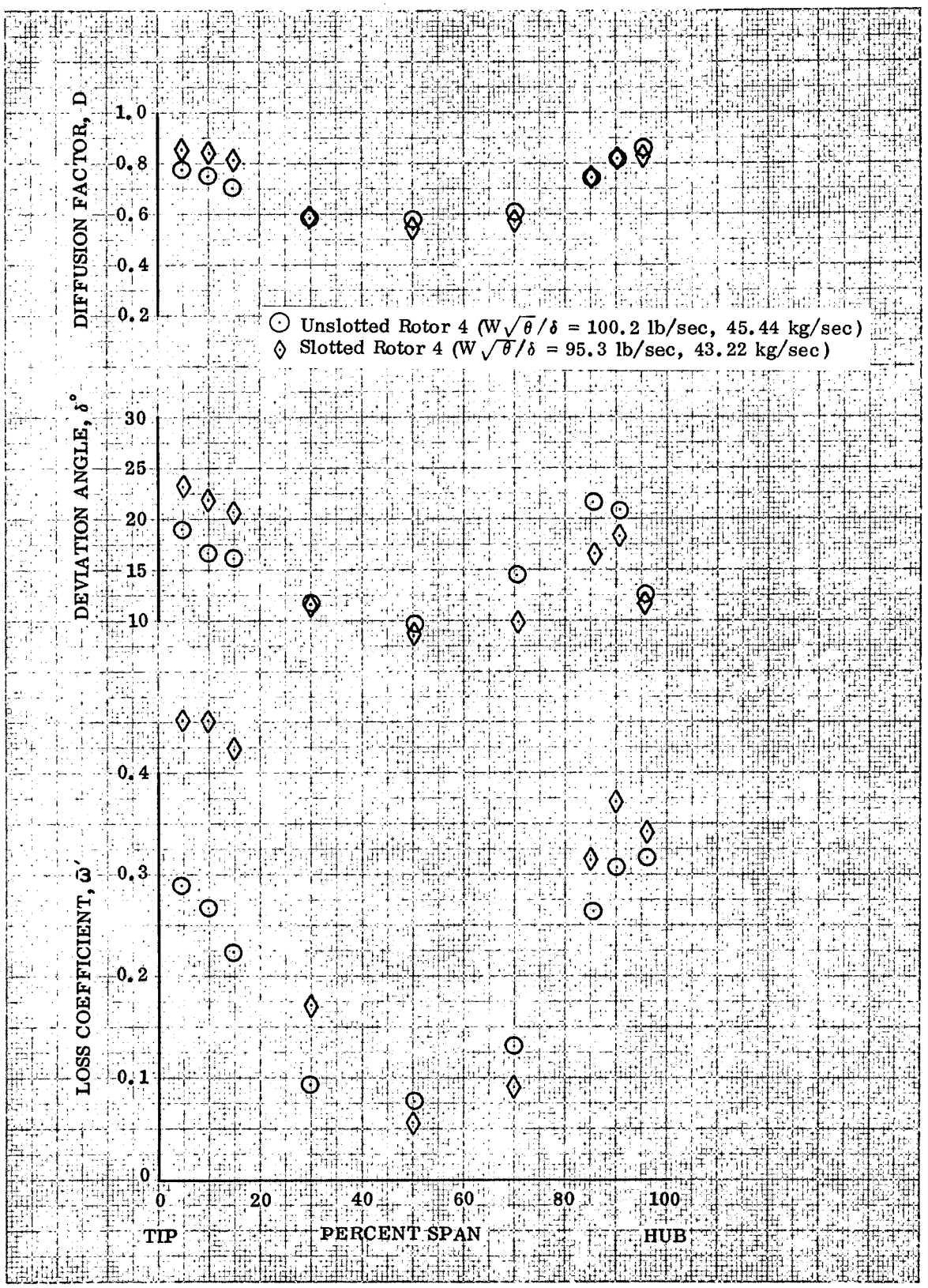

Figure 42. Blade Element Performance, Unslotted and Slotted Rotor 4 at Design Equivalent Rotor Speed and Near Stall Corrected Flow

DF 89740

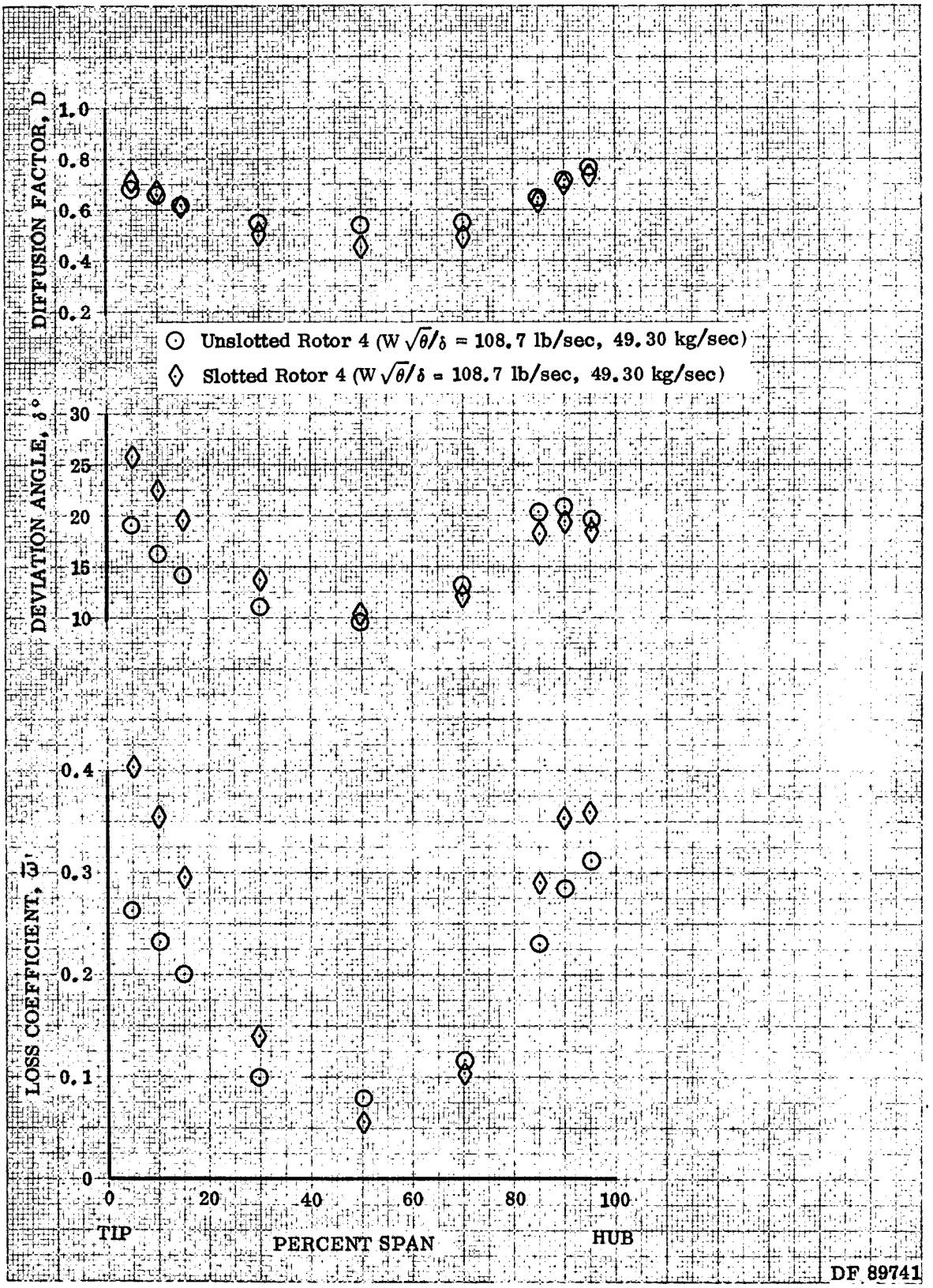

Figure 43. Blade Element Performance, Unslotted and Slotted Rotor 4 at Design Equivalent Rotor Speed and Near Design Corrected Flow DF 89741

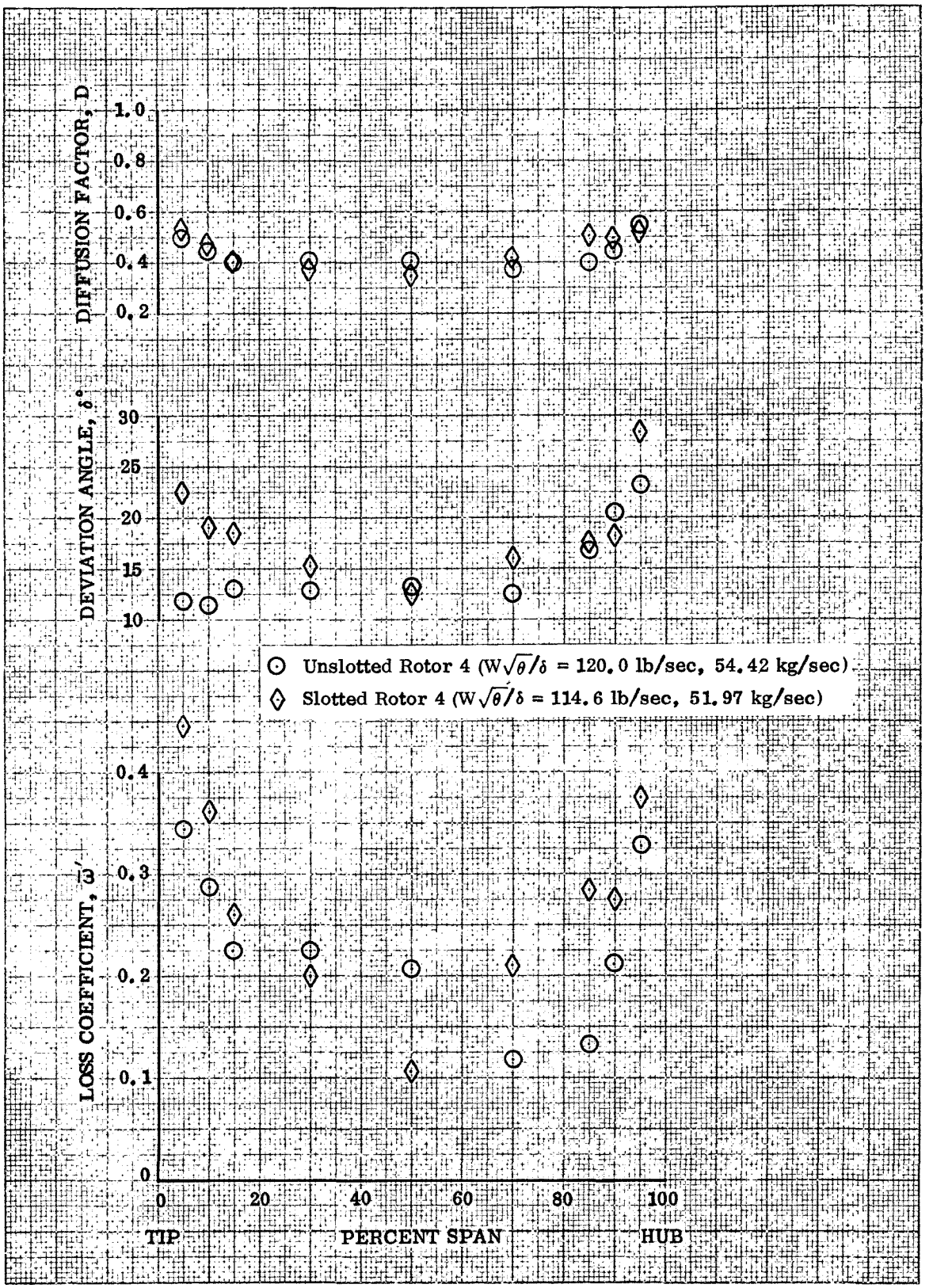

Figure 44. Blade Element Performance, Unslotted and Slotted Rotor 4 at Design Equivalent Rotor Speed and Maximum Corrected Flow

DF 89742

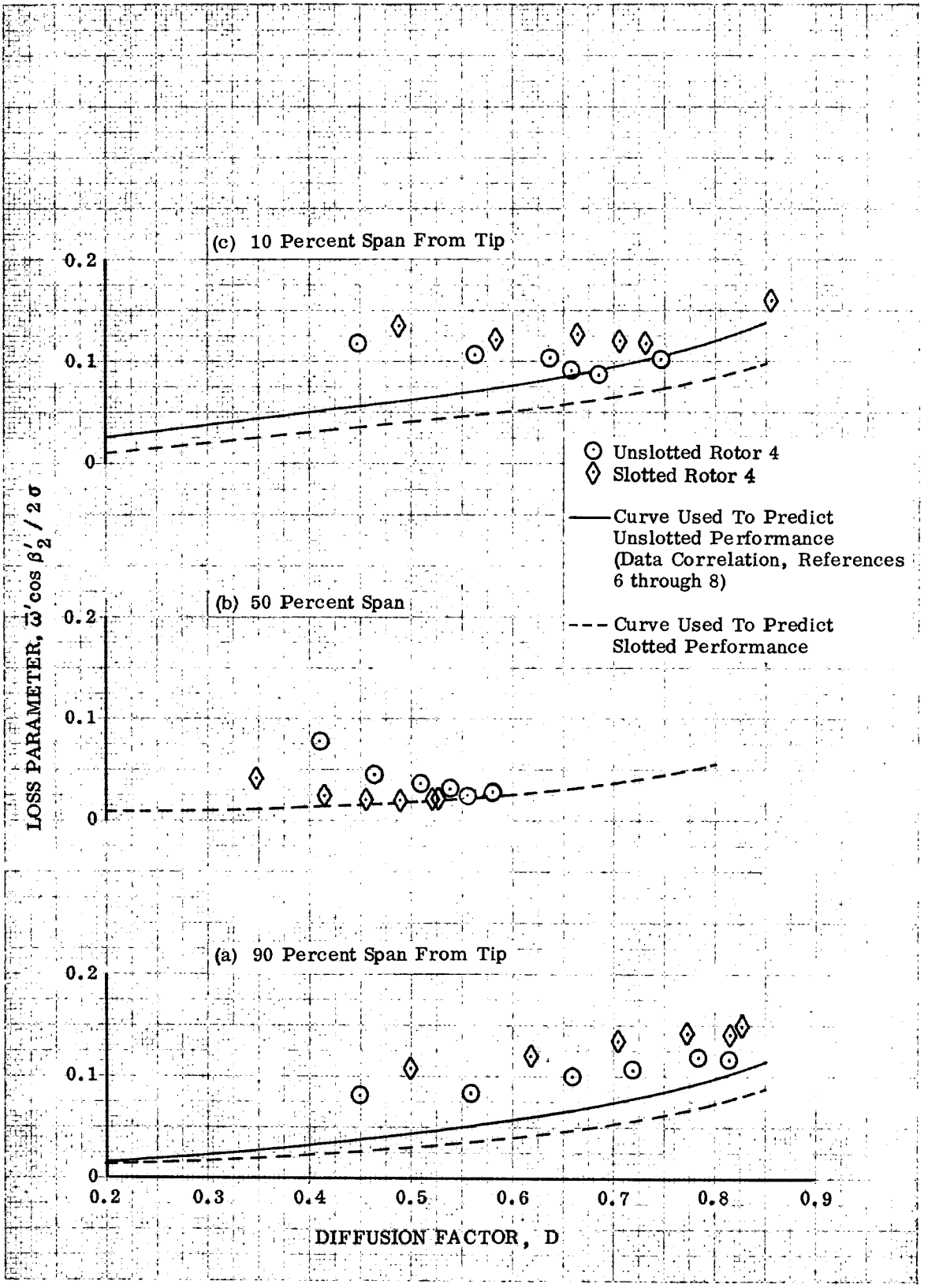

Figure 45 a - c. Loss Parameter Distributions for Unslotted and Slotted Rotor 4 at Design Equivalent Rotor Speed DF 89743

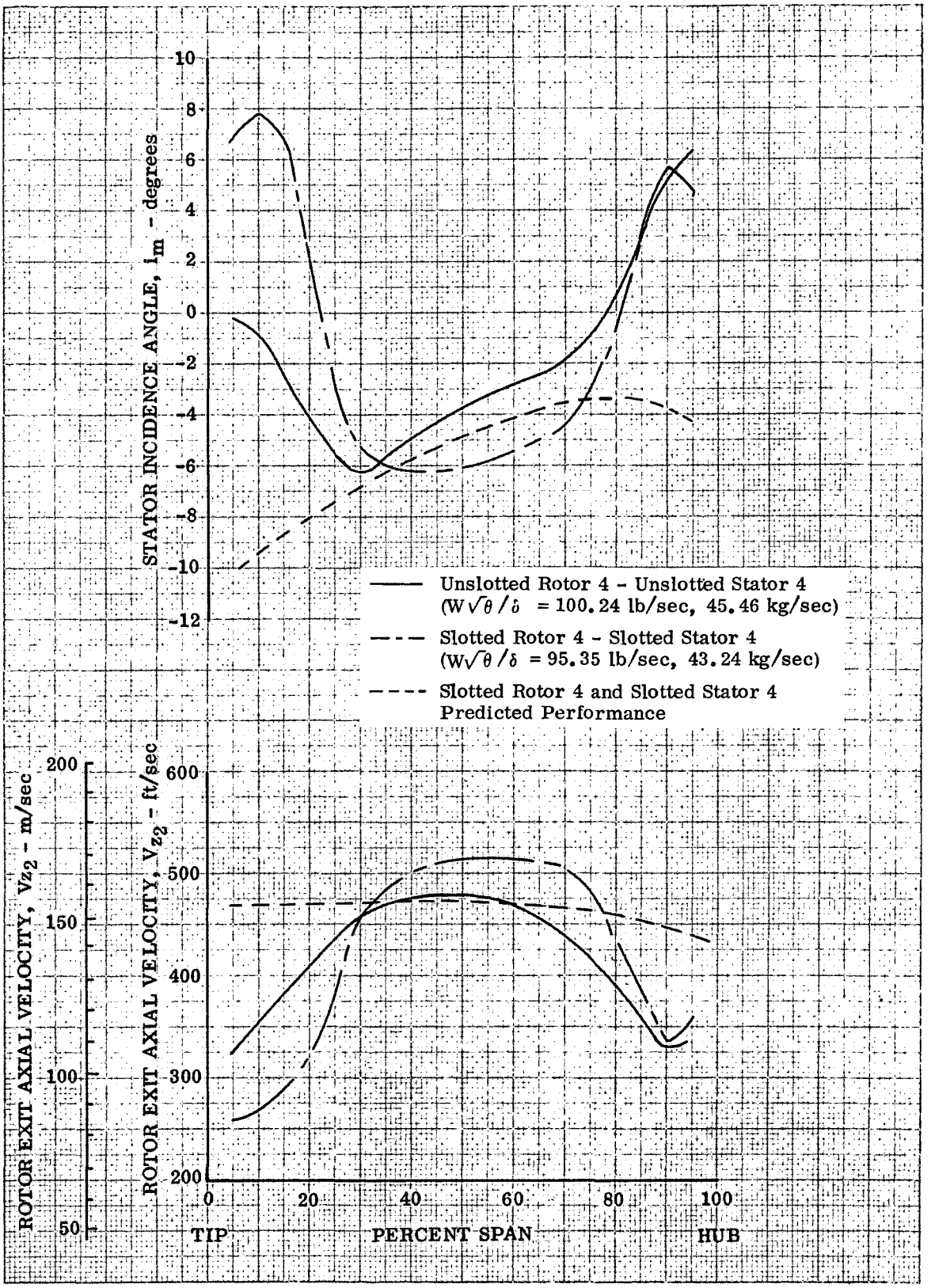

Figure 46. Comparison of Rotor Exit Axial Velocity and Stator Incidence Angle Distributions for Unslotted and Slotted Stator 4 at Design Equivalent Rotor Speed and Near Stall Corrected Flow

DF 89744

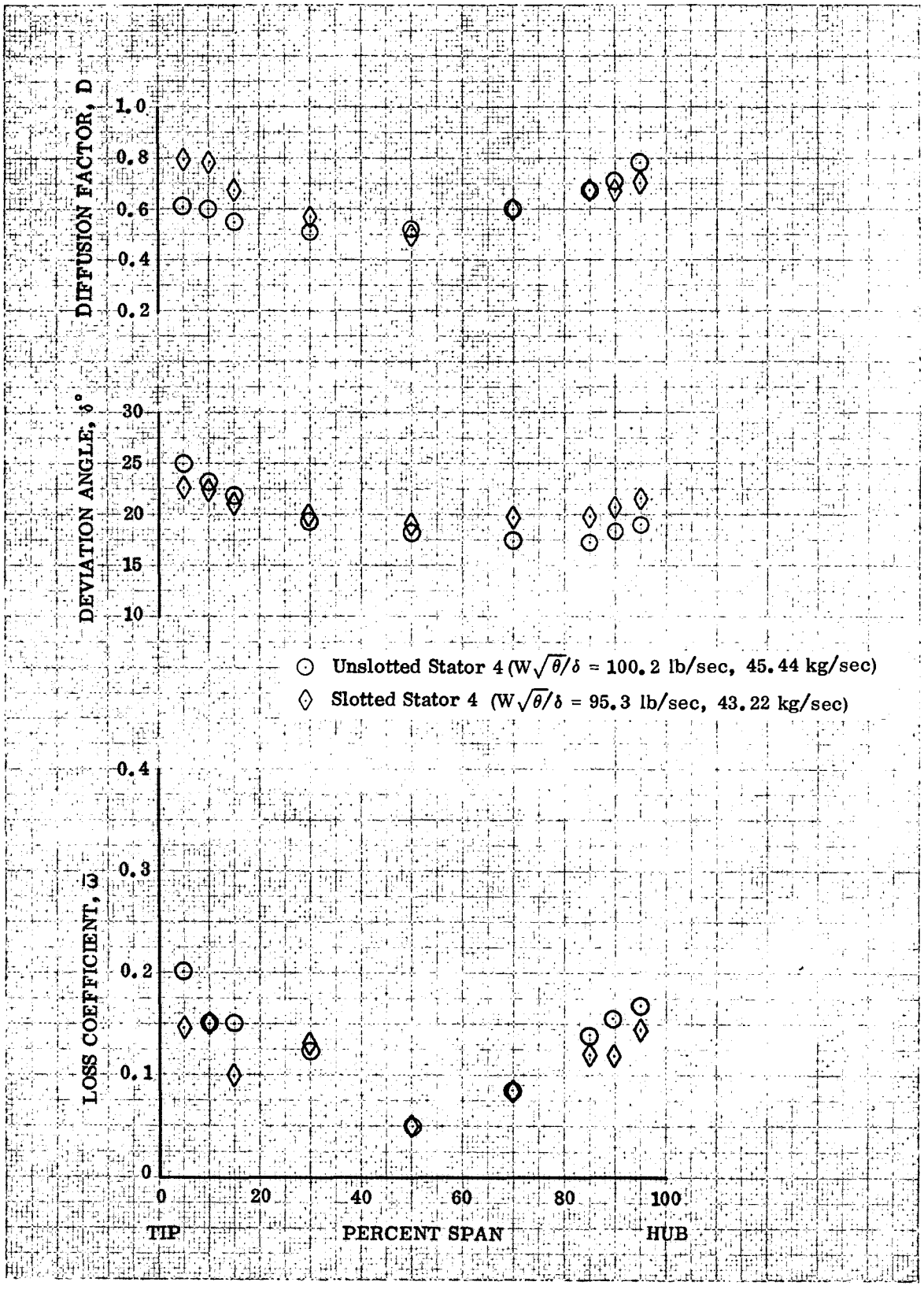

Figure 47. Blade Element Performance, Unslotted and Slotted Stator 4 at Design Equivalent Rotor Speed and Near Stall Corrected Flow

DF 89745

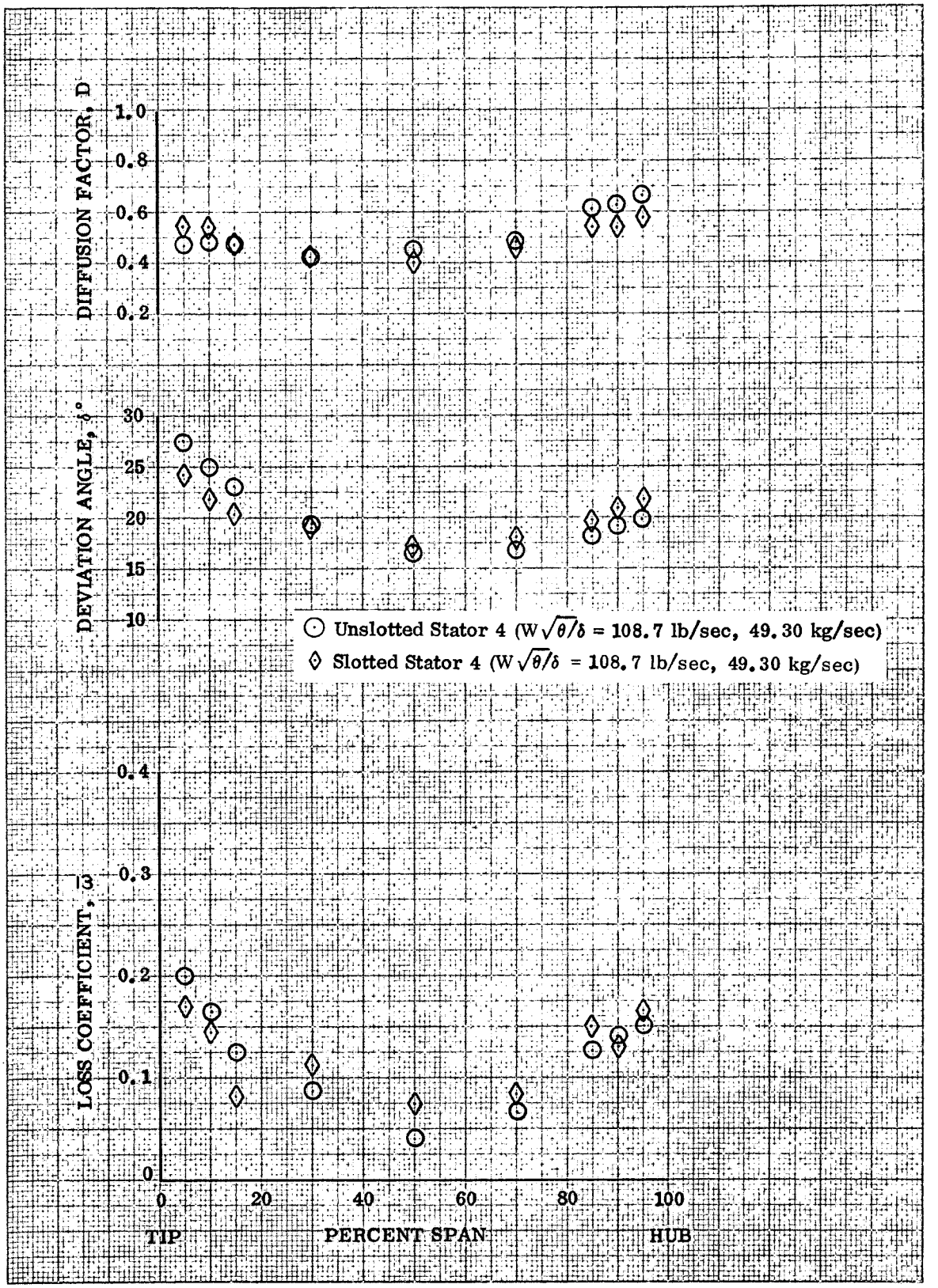

Figure 48. Blade Element Performance, Unslotted and Slotted Stator 4 at Design Equivalent Rotor Speed and Near Design Corrected Flow

DF 89746

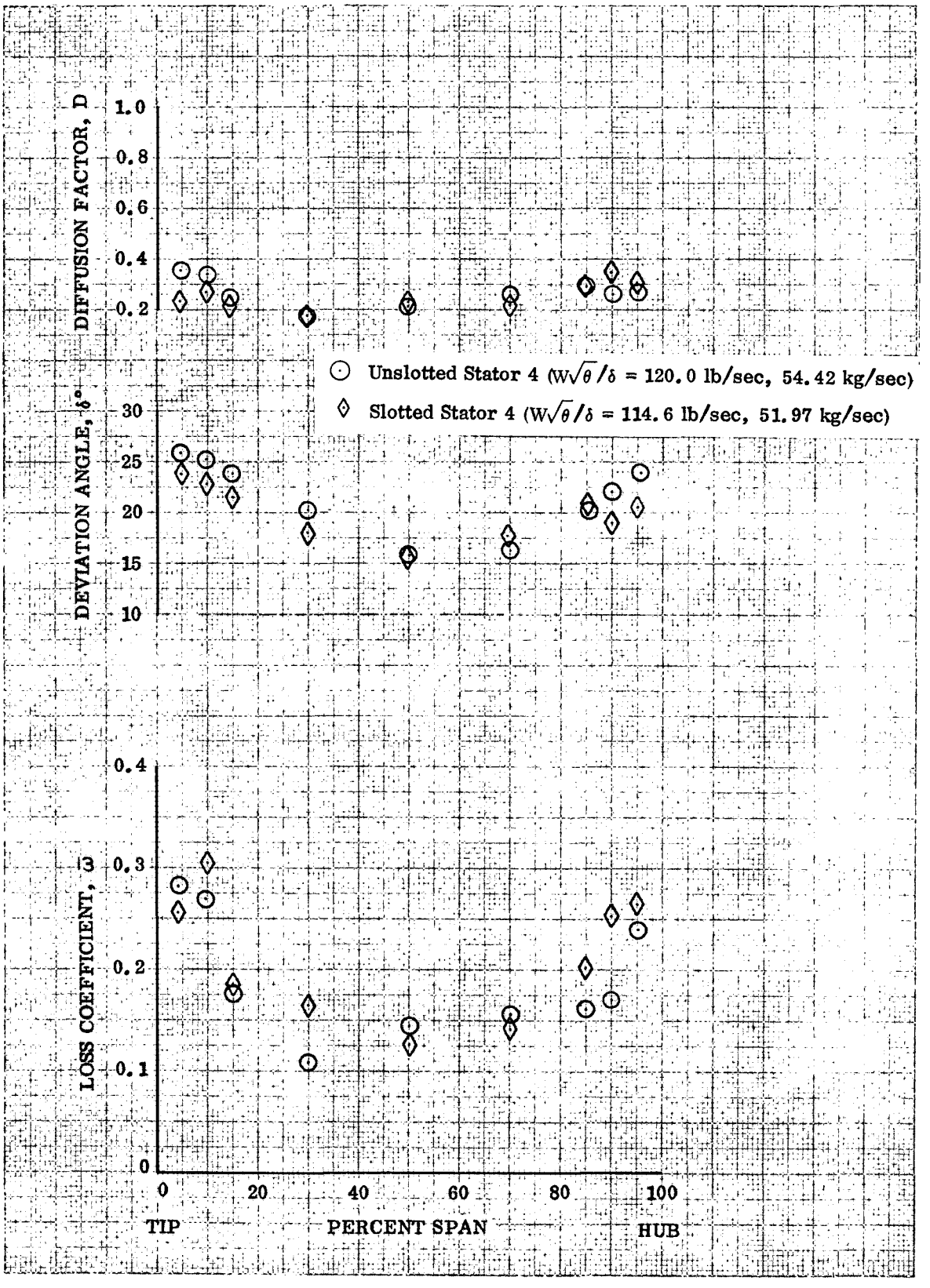

Figure 49. Blade Element Performance, Unslotted and Slotted Stator 4 at Design Equivalent Rotor Speed and Maximum Corrected Flow DF 89747

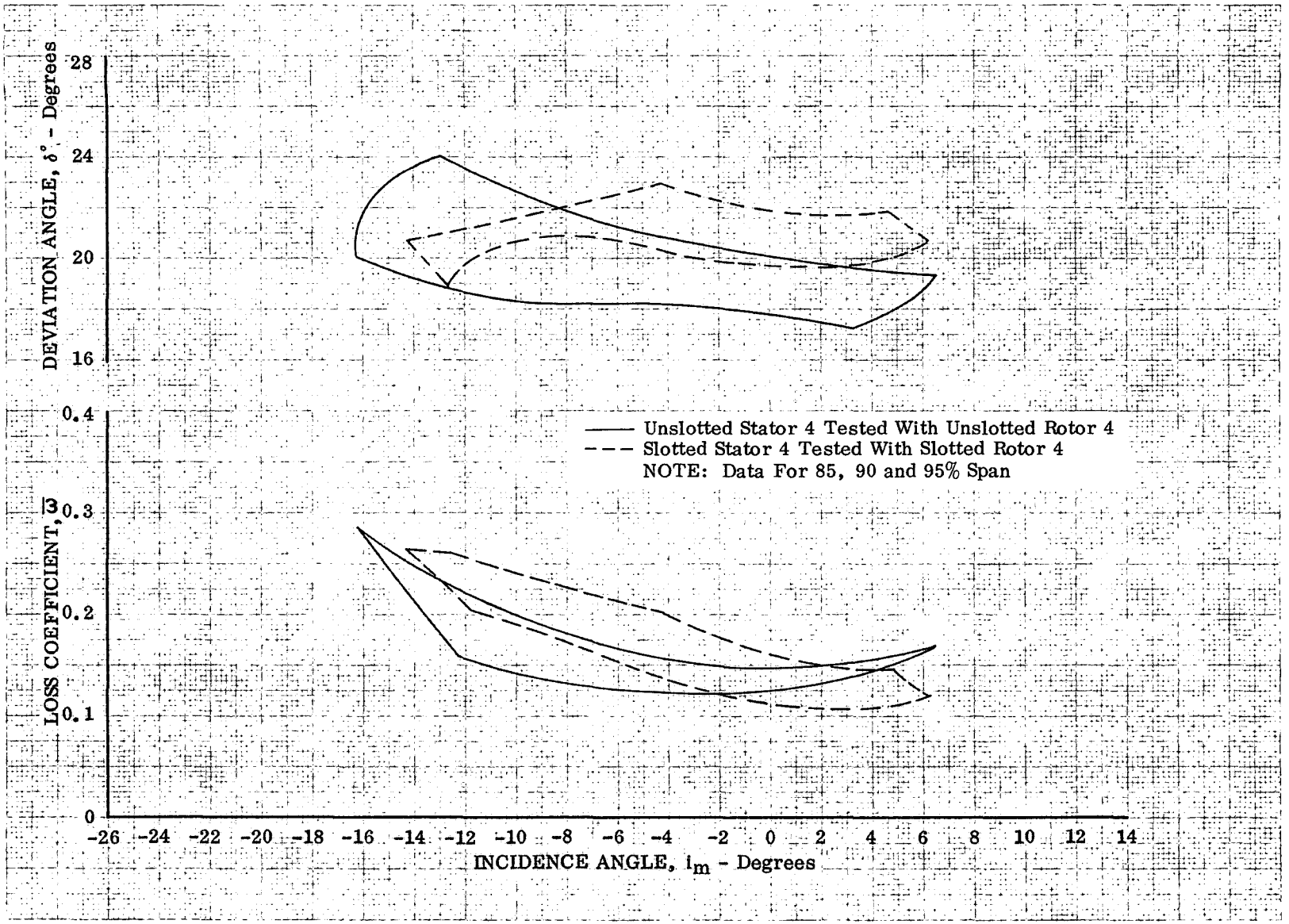

Figure 50. Comparison of the Ranges of the Loss Coefficient and Deviation Angle Data for the Hub of Unslotted and Slotted Stator 4 at Design Equivalent Rotor Speed

DF 89748

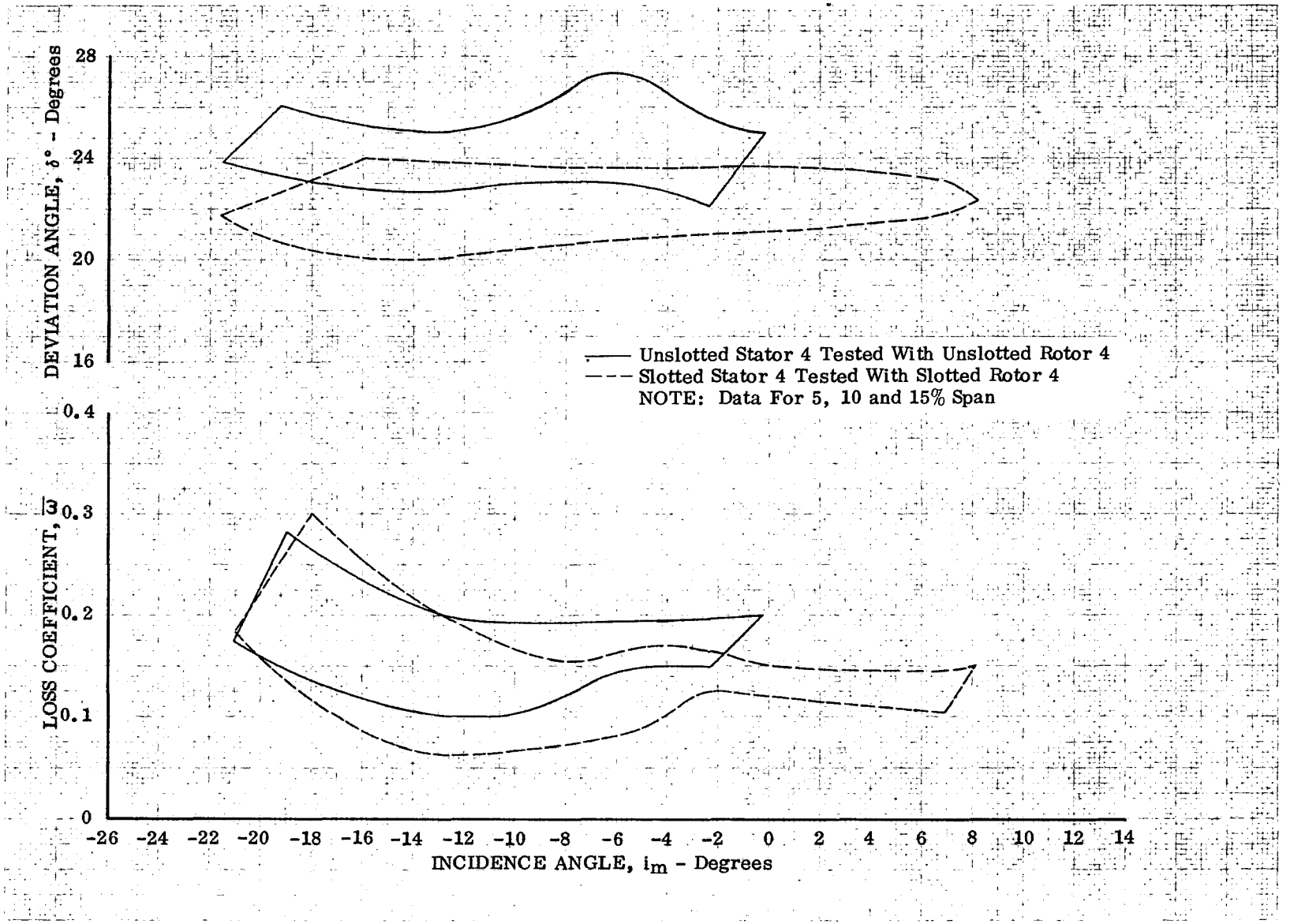

Figure 51. Comparison of the Ranges of the Loss Coefficient and Deviation Angle Data for the Tip of Unslotted and Slotted Stator 4 at Design Equivalent Rotor Speed

DF 89749

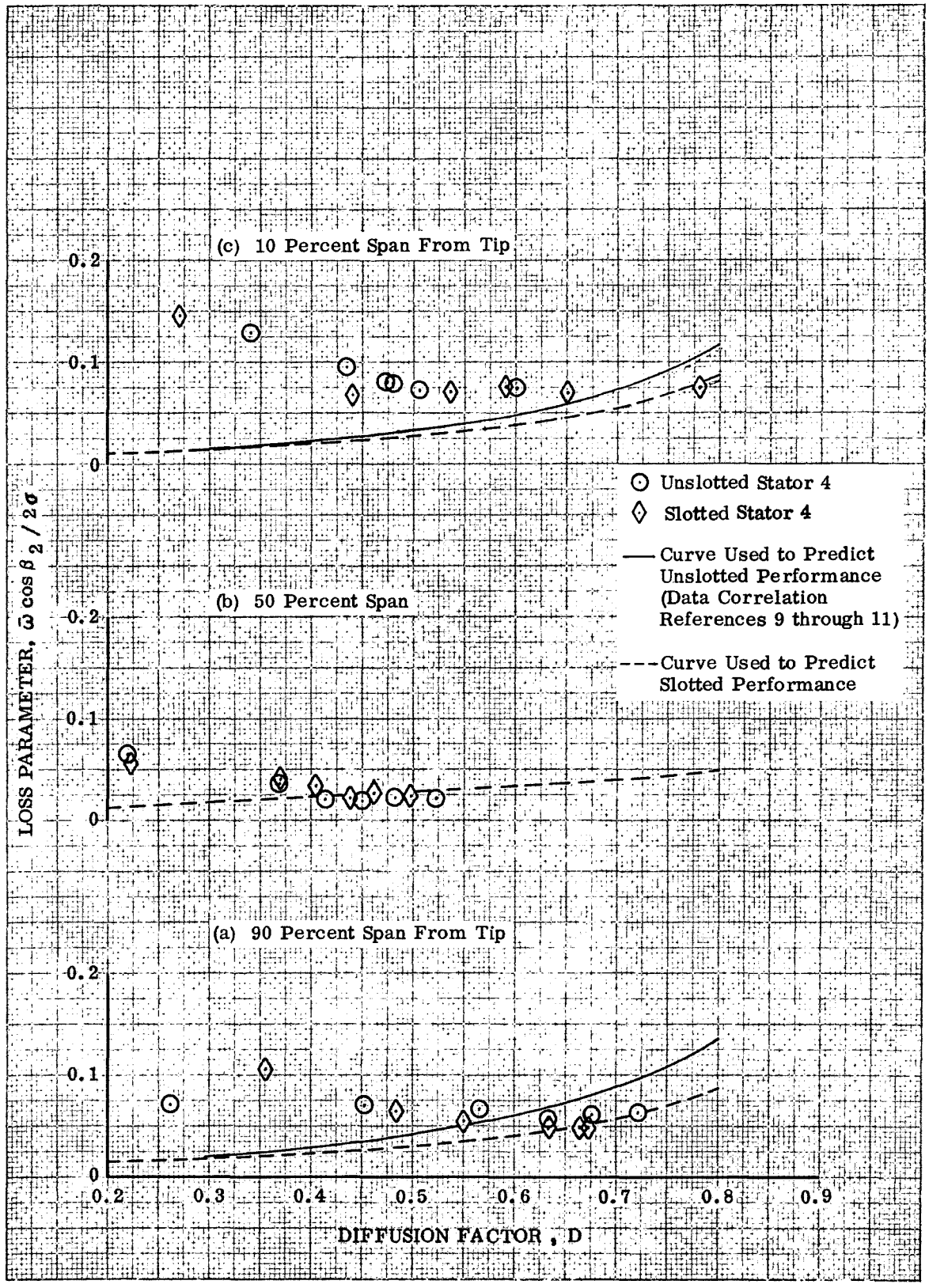

Figure 52 a - c. Loss Parameter Distributions for Unslotted and Slotted Stator 4 at Design Equivalent Rotor Speed

DF 89750

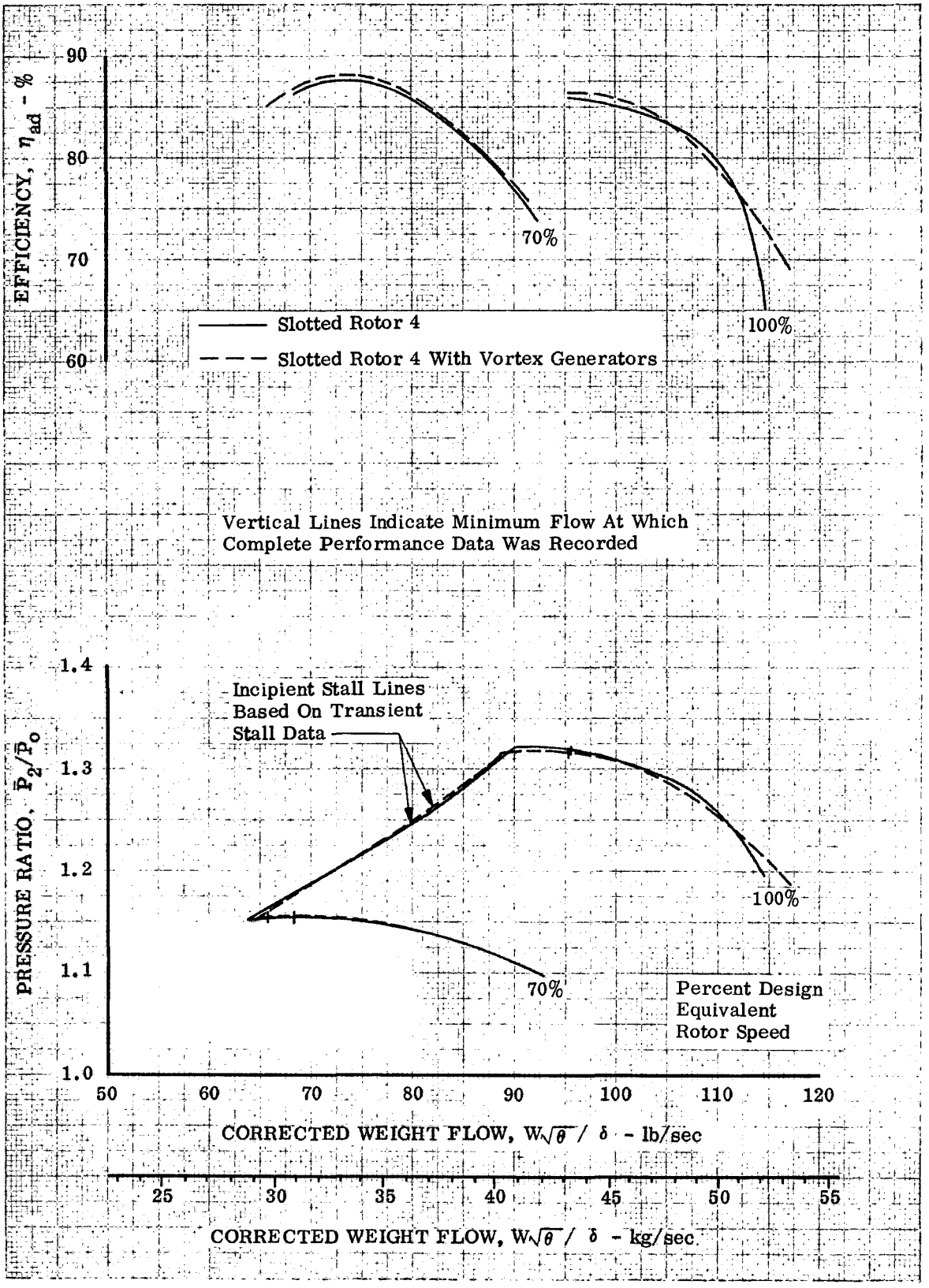

Figure 53. Comparison of Slotted Rotor 4 Overall Performance With and Without Vortex Generators DF 89751

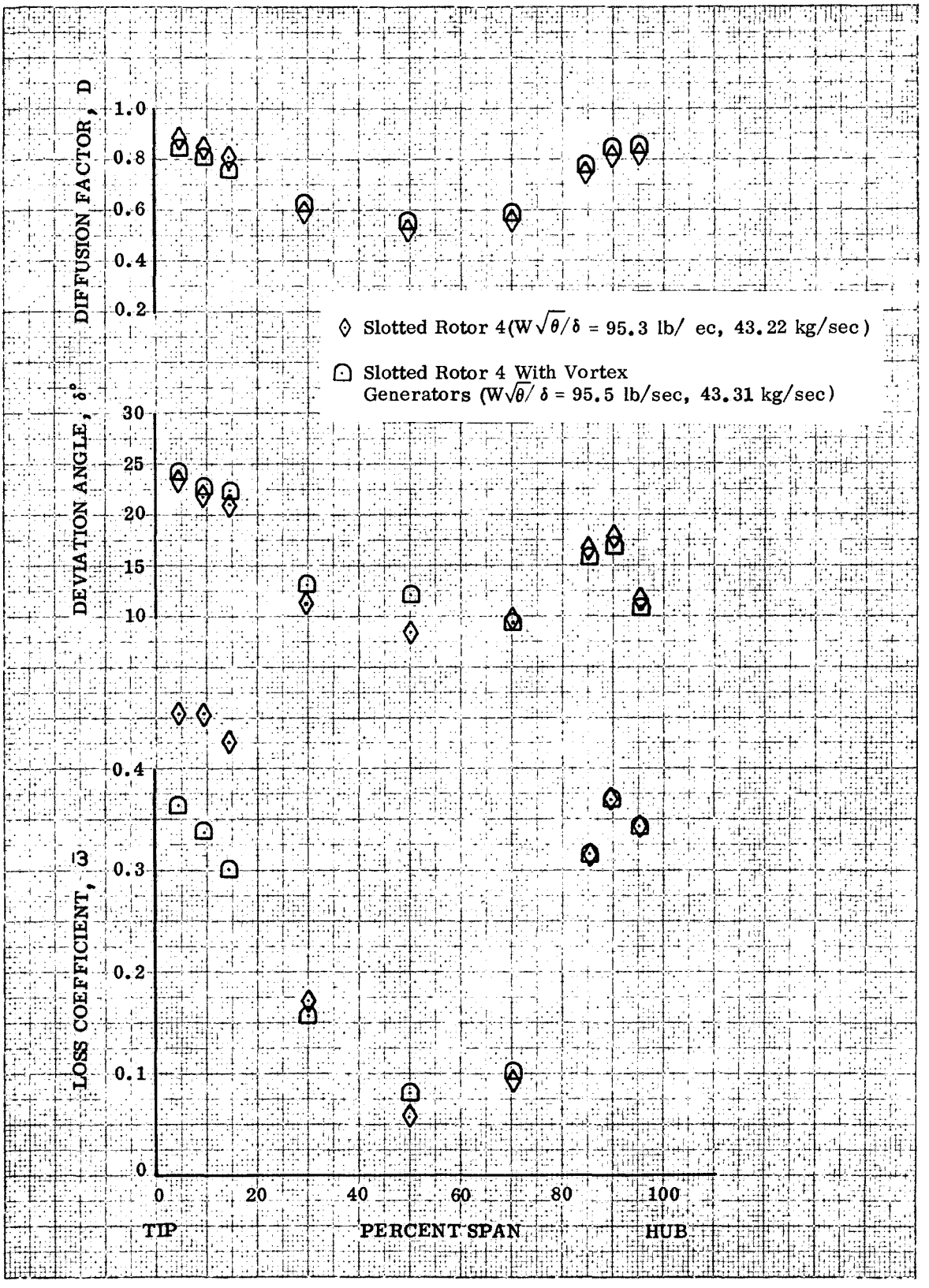

Figure 54. Blade Element Performance for Slotted Rotor 4 With and Without Vortex Generators at Design Equivalent Rotor Speed and Near Stall Corrected Flow

DF 89752

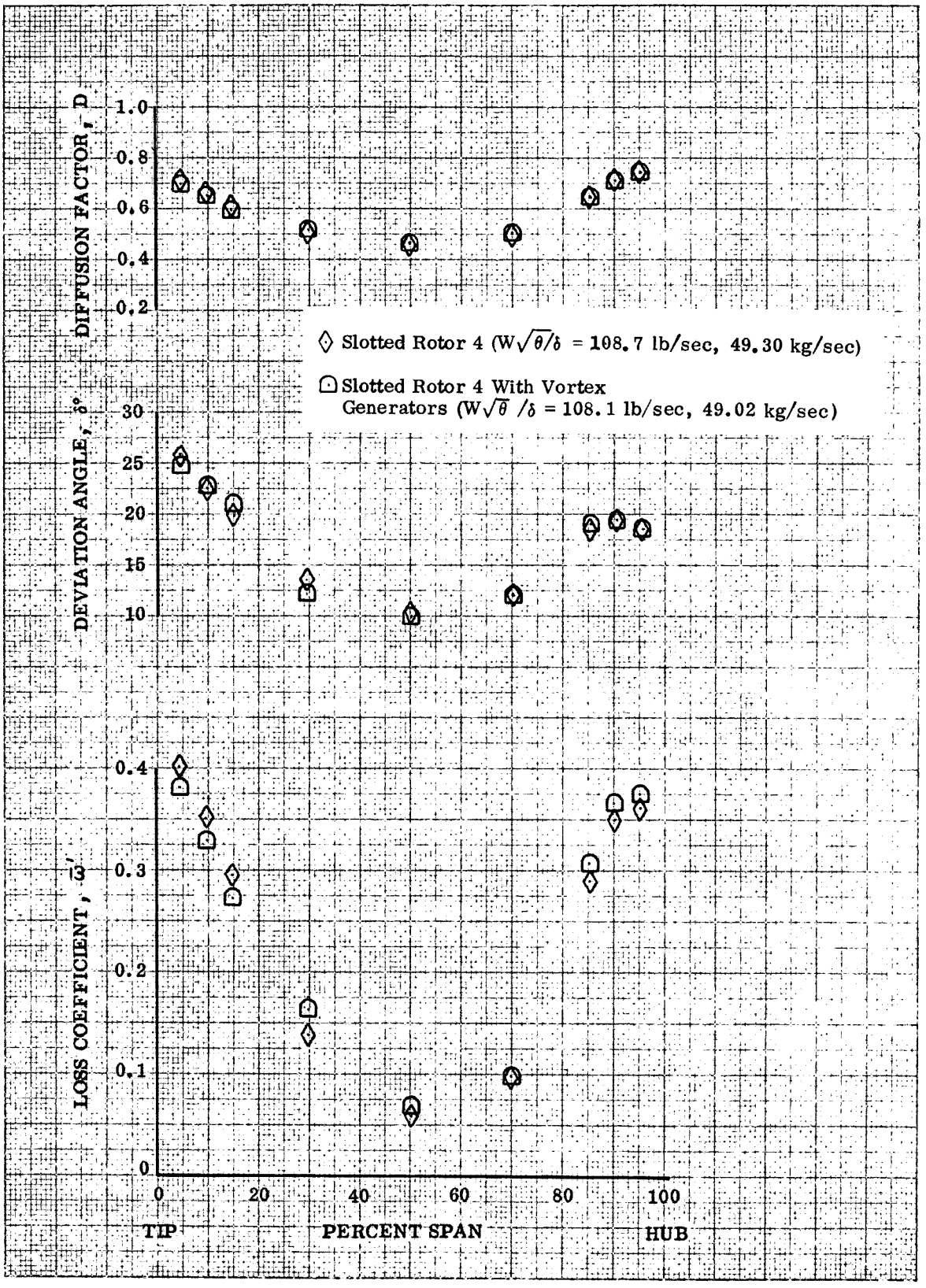

Figure 55. Blade Element Performance for Slotted Rotor 4 With and Without Vortex Generators at Design Equivalent Rotor Speed and Near Design Corrected Flow

DF 89753

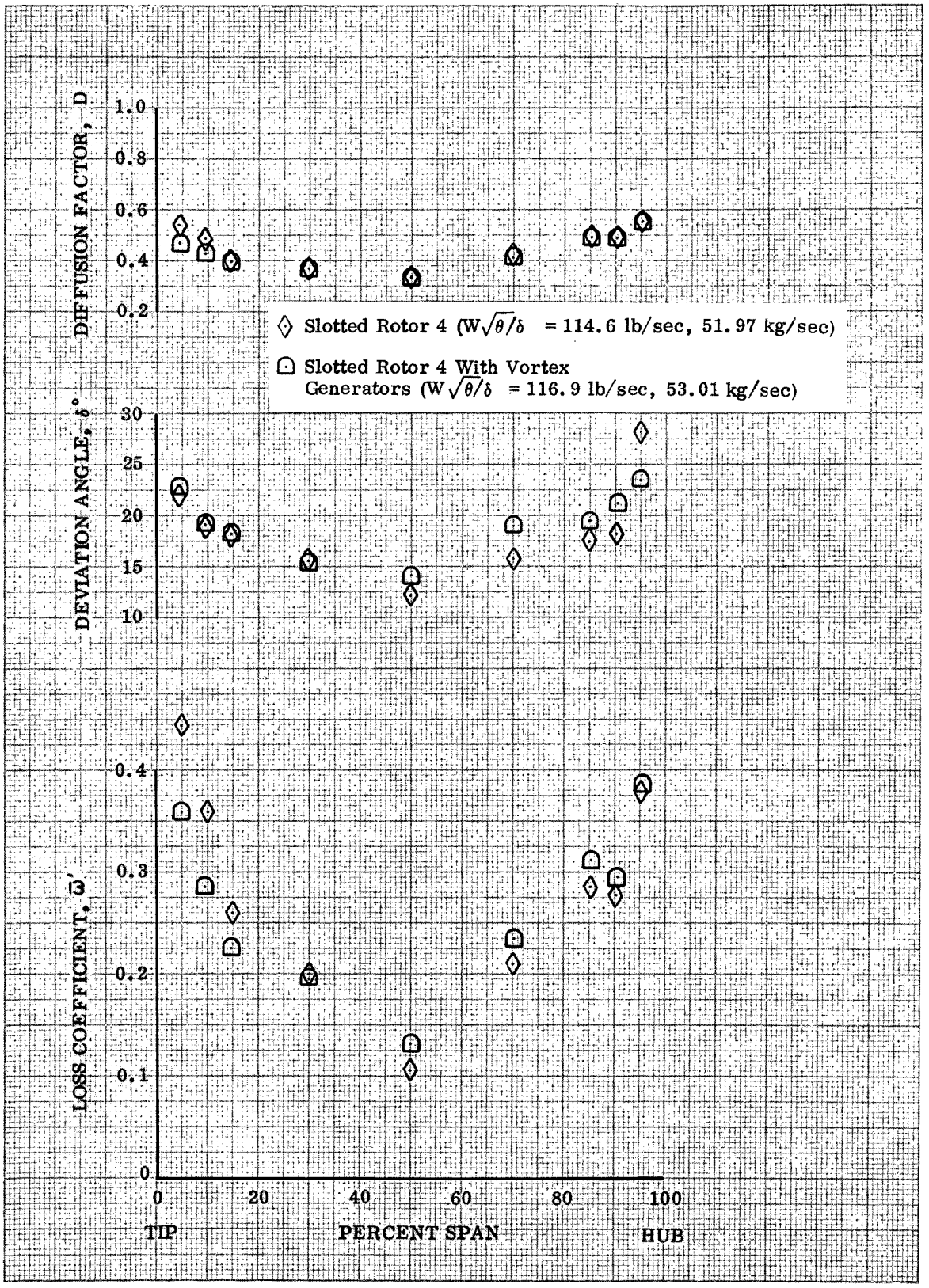

Figure 56. Blade Element Performance for Slotted Rotor 4 With and Without Vortex Generators at Design Equivalent Rotor Speed and Maximum Corrected Flow

DF 89754

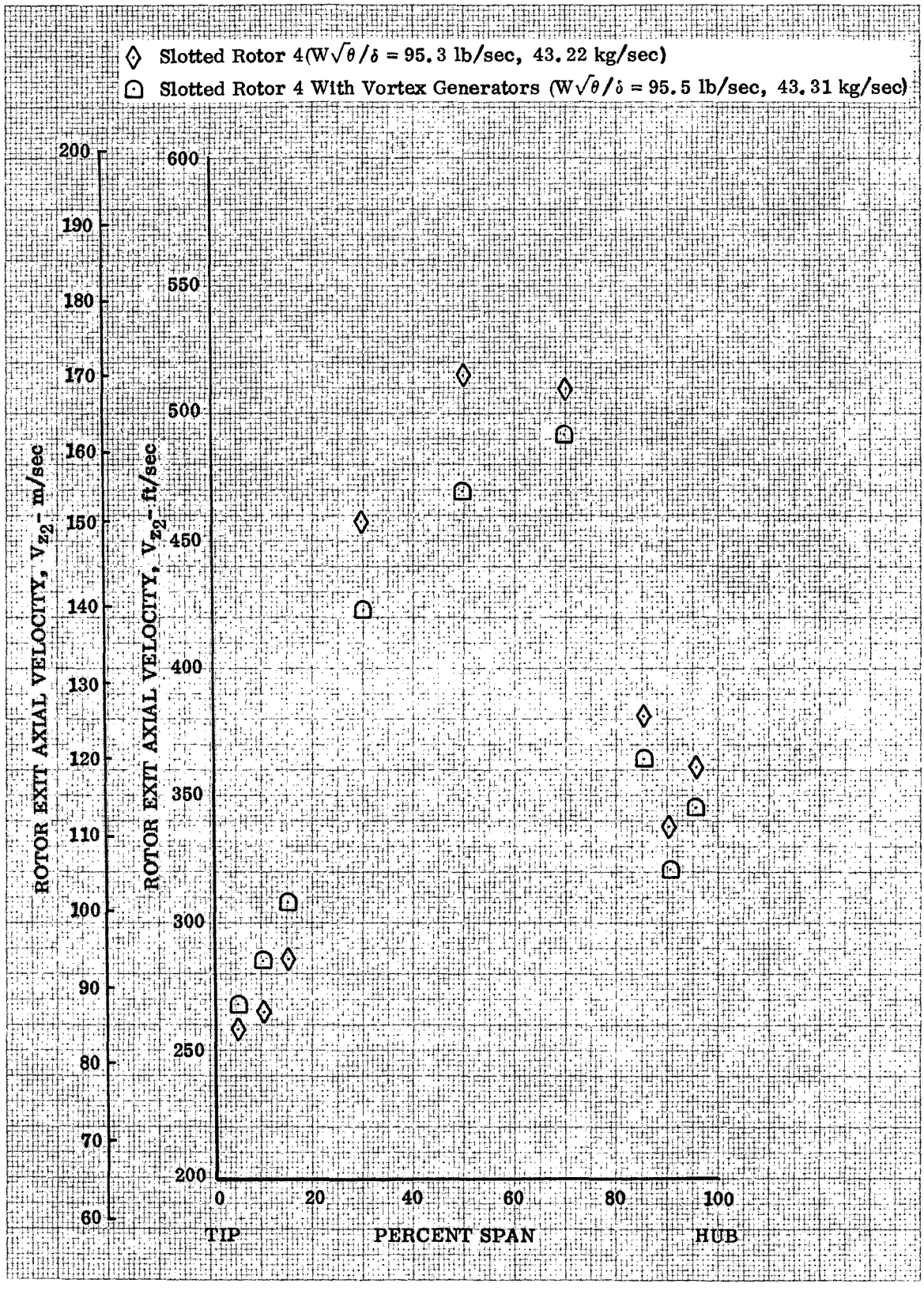

Figure 57. Rotor Exit Axial Velocity for Slotted Rotor 4 With and Without Vortex Generators at Design Equivalent Rotor Speed and Near Stall Corrected Flow

DF 89755

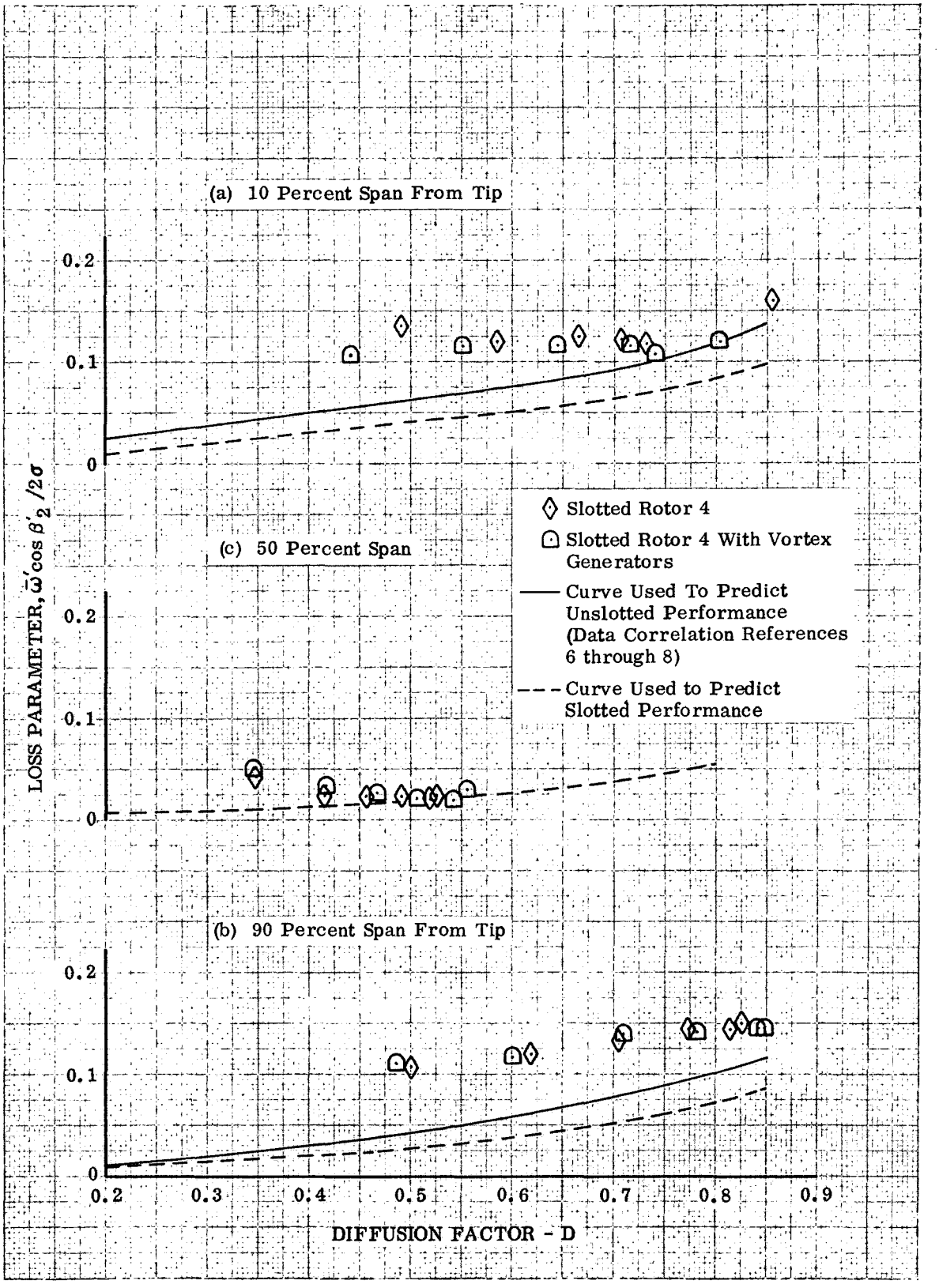

Figure 58 a - c. Loss Parameter Distributions for Slotted Rotor 4 With and Without Vortex Generators at Design Equivalent Rotor Speed DF 89756

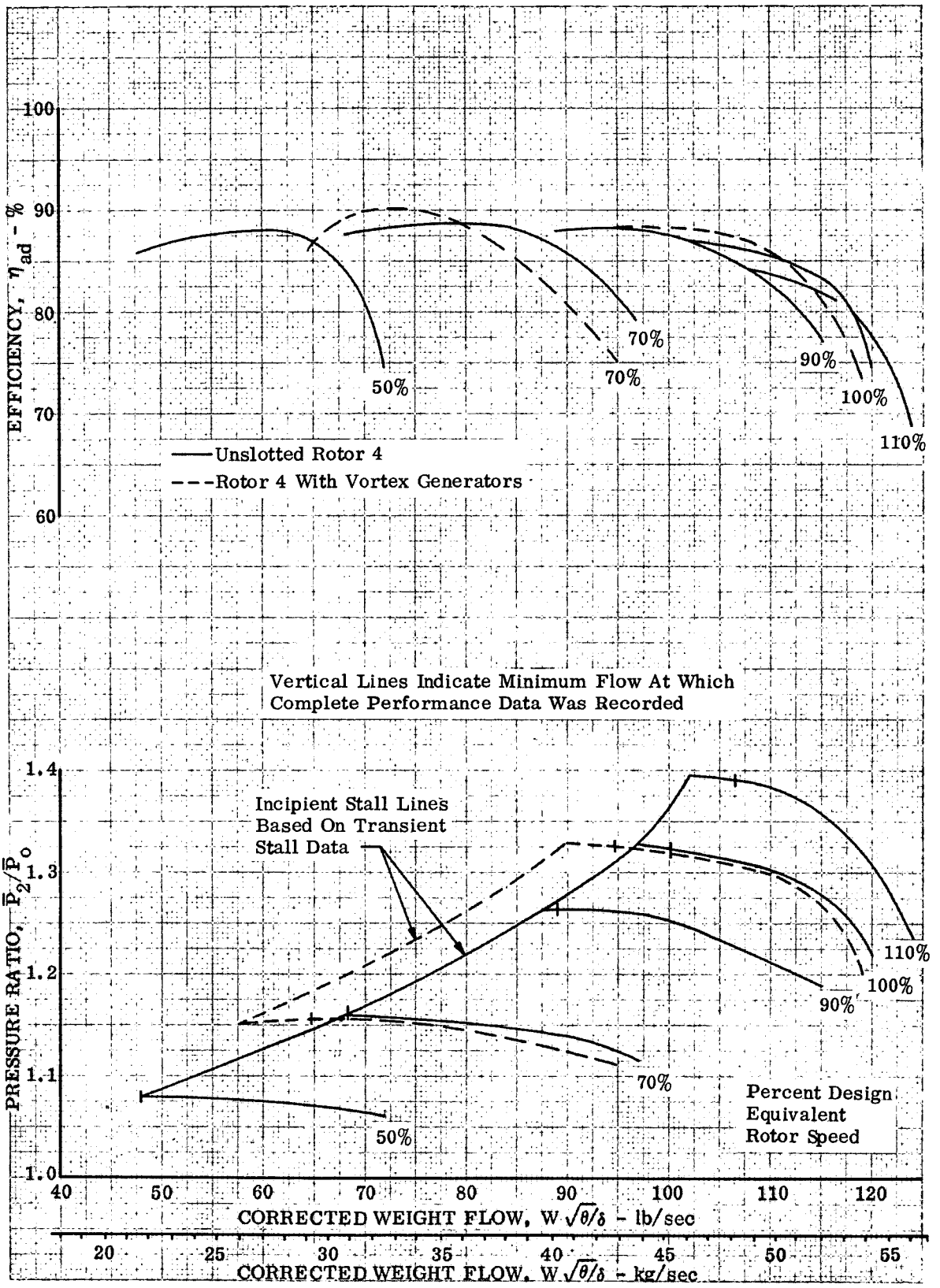

Figure 59. Comparison of Unslotted Rotor 4 Overall Performance With and Without Vortex Generators DF 89757

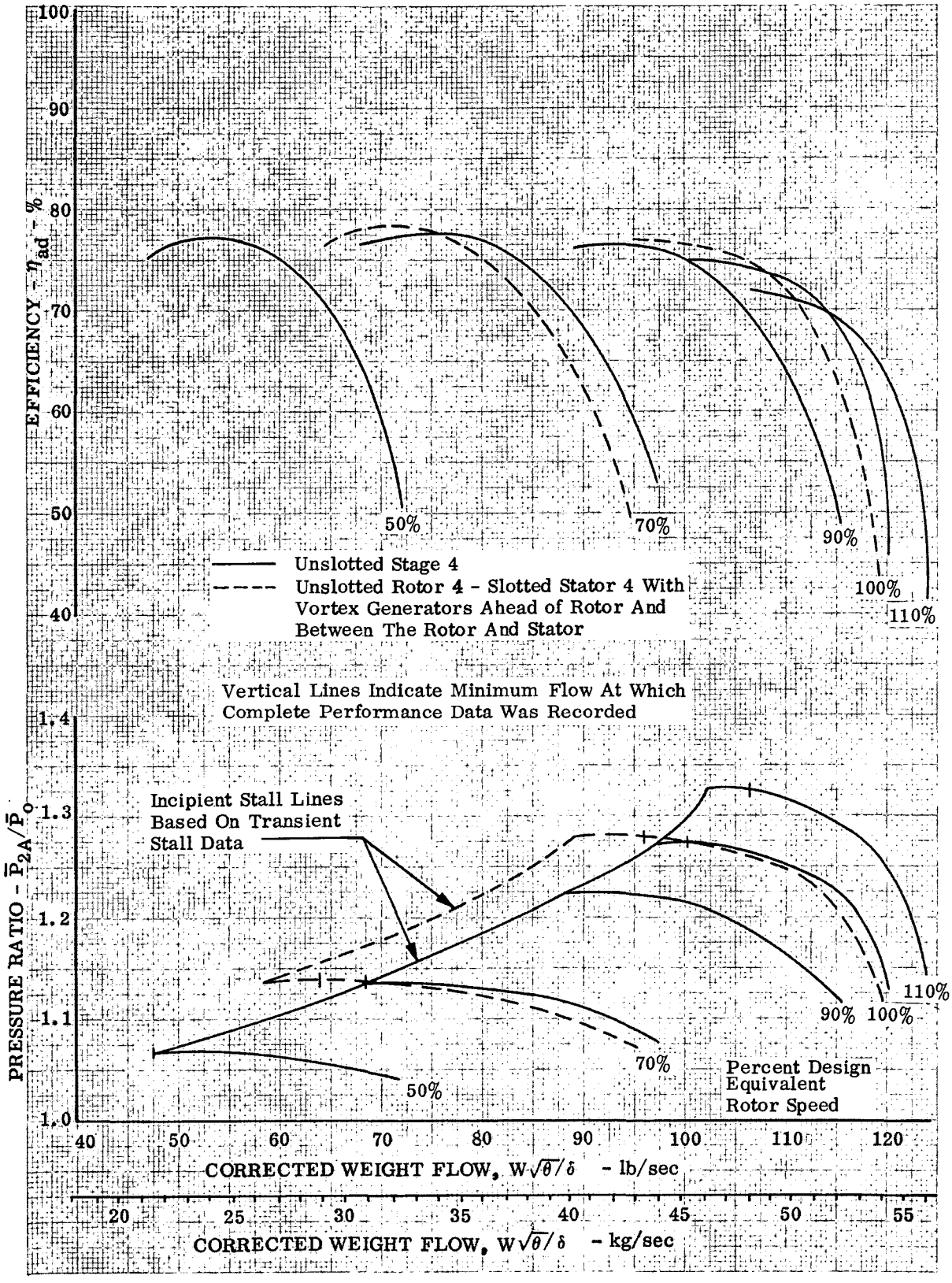

Figure 60. Comparison of Unslotted Stage 4 Overall Performance With the Performance for Unslotted Rotor 4 - Slotted Stator 4 With Vortex Generators DF 89758

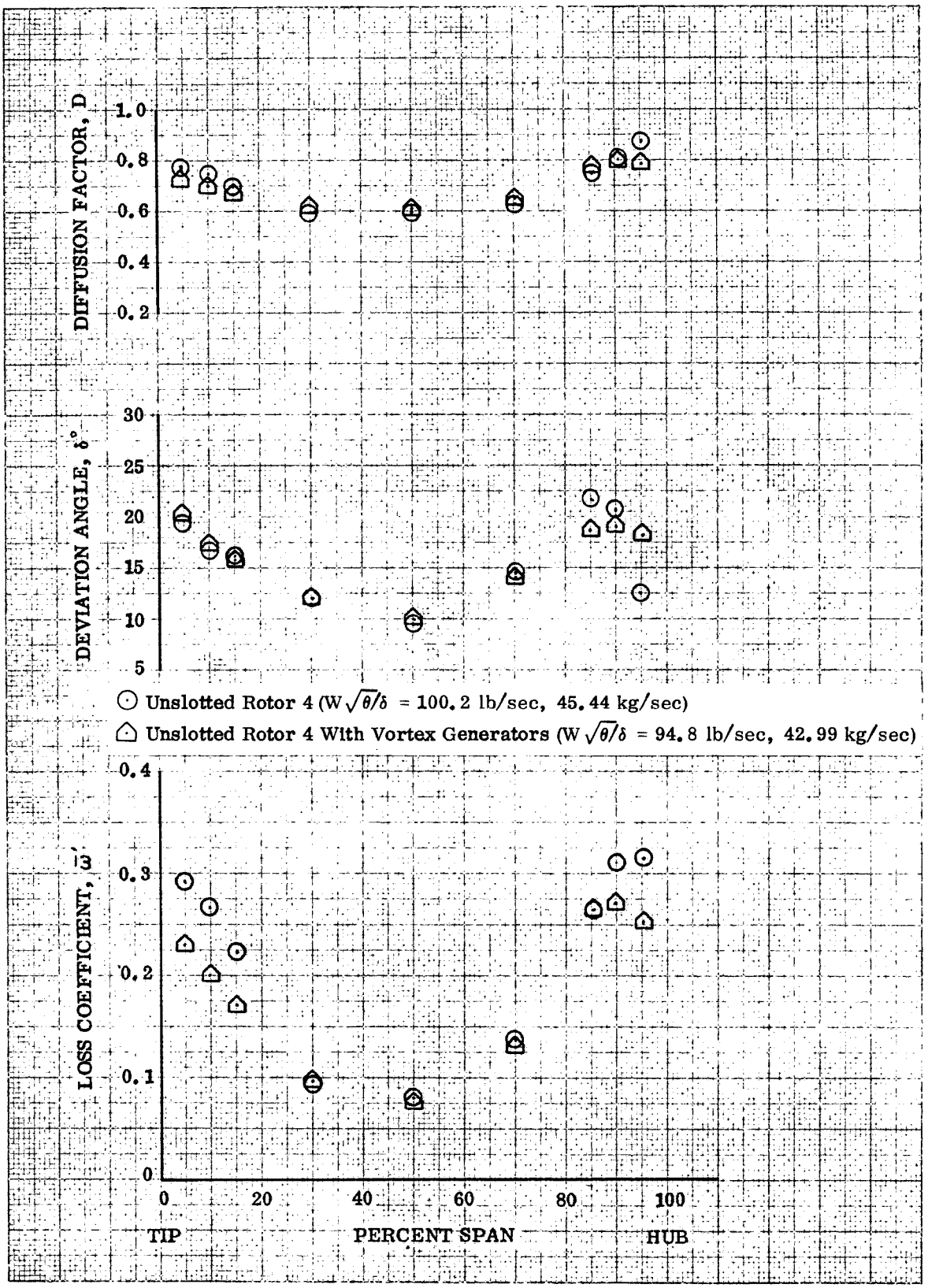

Figure 61. Blade Element Performance for Unslotted Rotor 4 With and Without Vortex Generators at Design Equivalent Rotor Speed and Near Stall Corrected Flow

DF 89759

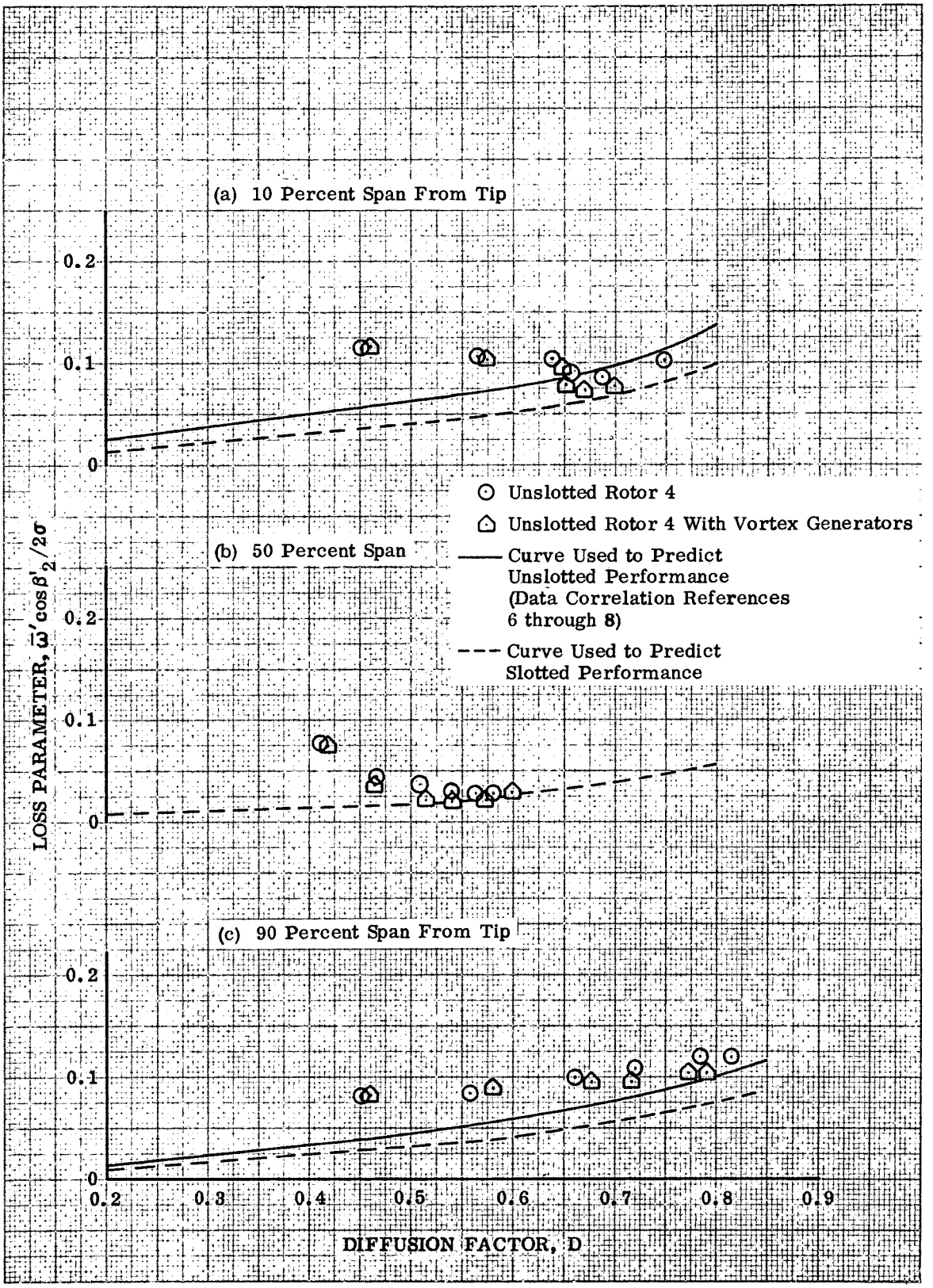

Figure 62 a - c. Loss Parameter Distributions for Unslotted Rotor 4 With and Without Vortex Generators at Design Equivalent Rotor Speed

DF 89760

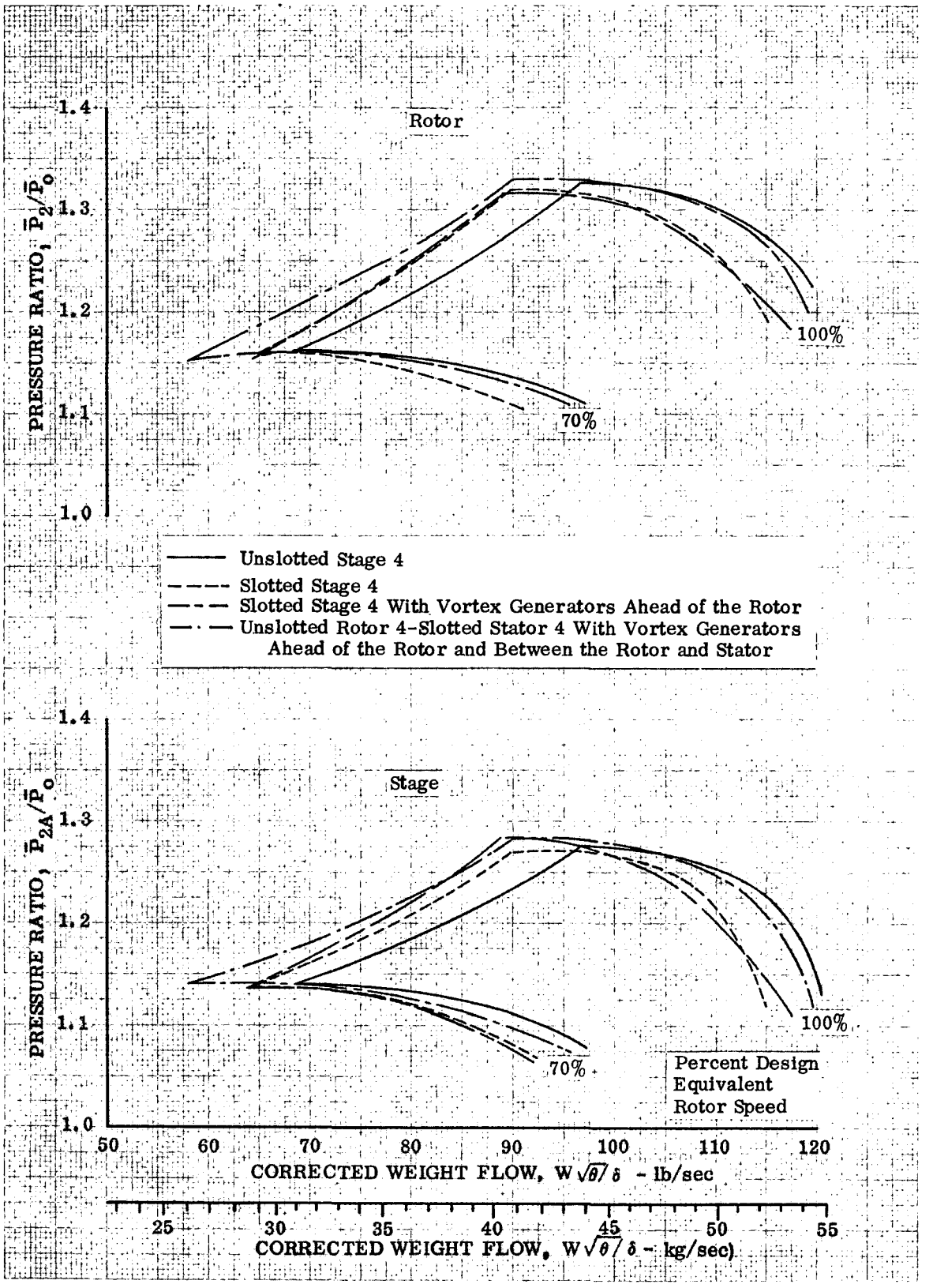

Figure 63. Rotor and Stage Pressure Ratio Comparisons DF 89761

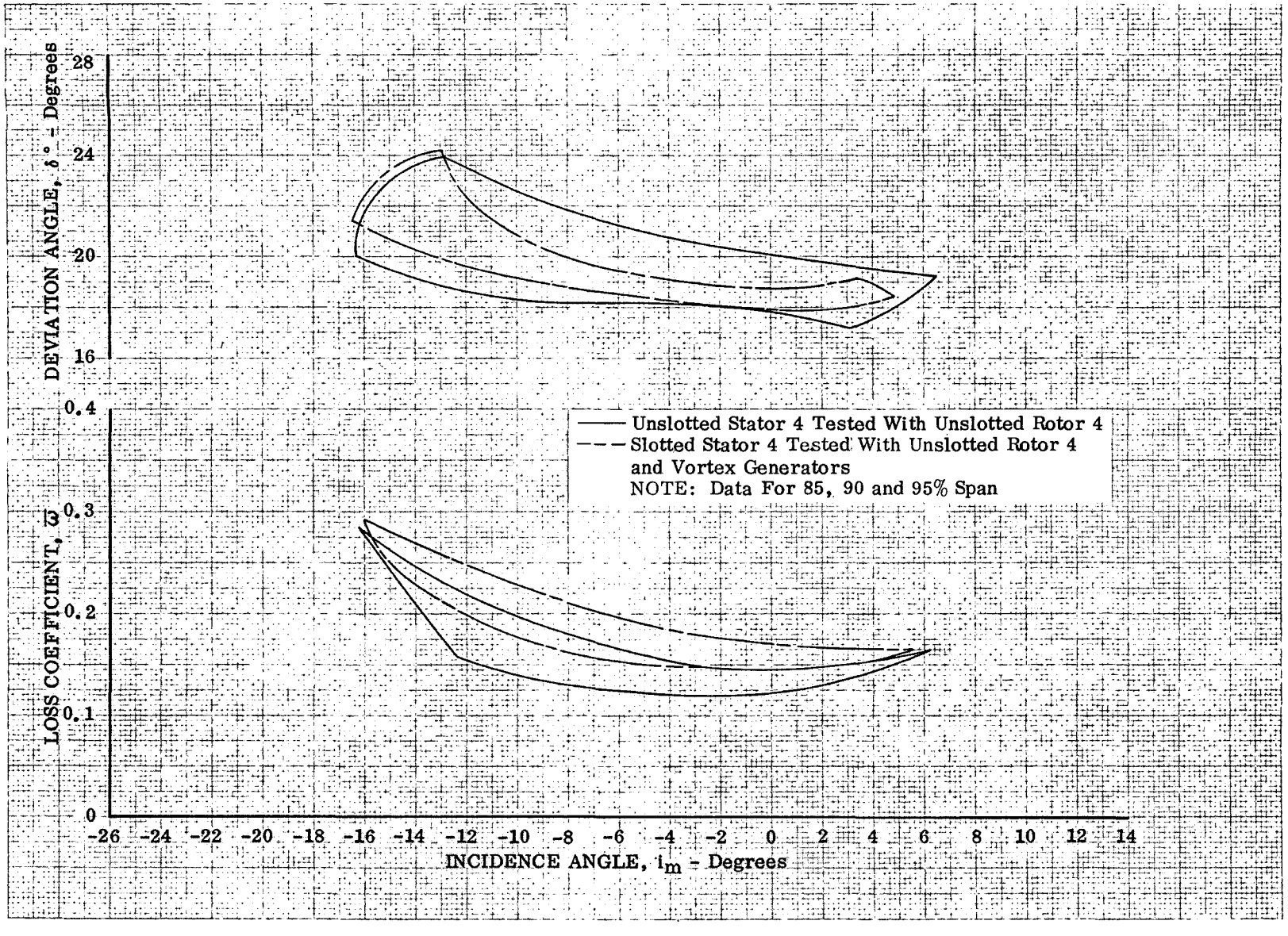

Figure 64. Comparison of the Ranges of the Loss Coefficient and Deviation Angle Data for the Hub Regions of Unslotted and Slotted Stator 4 at Design Equivalent Rotor Speed

DF 89762

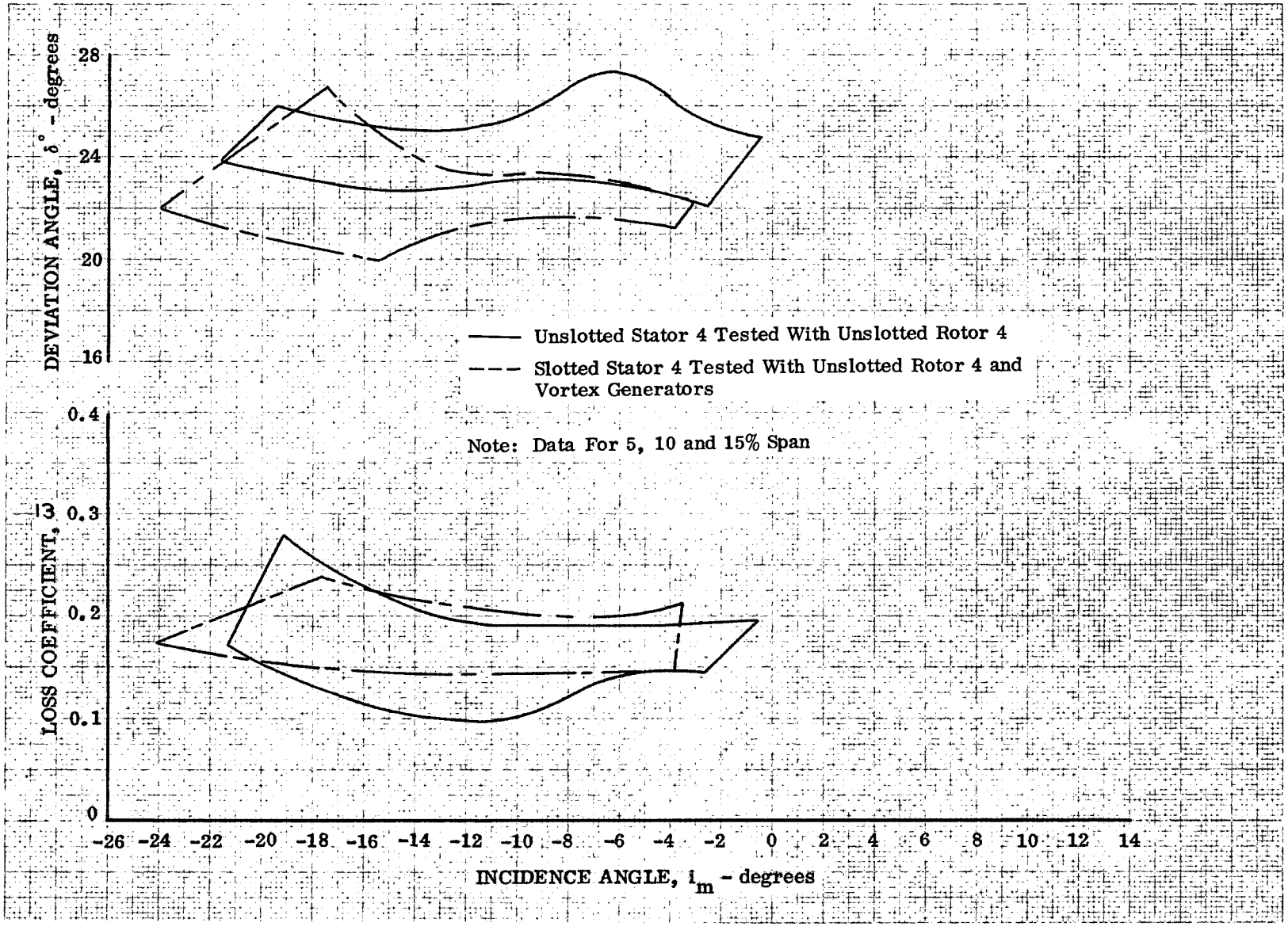

Figure 65. Comparison of the Ranges of the Loss Coefficient and Deviation Angle Data for the Tip Regions of Unslotted and Slotted Stator 4 at Design Equivalent Rotor Speed

DF 89763

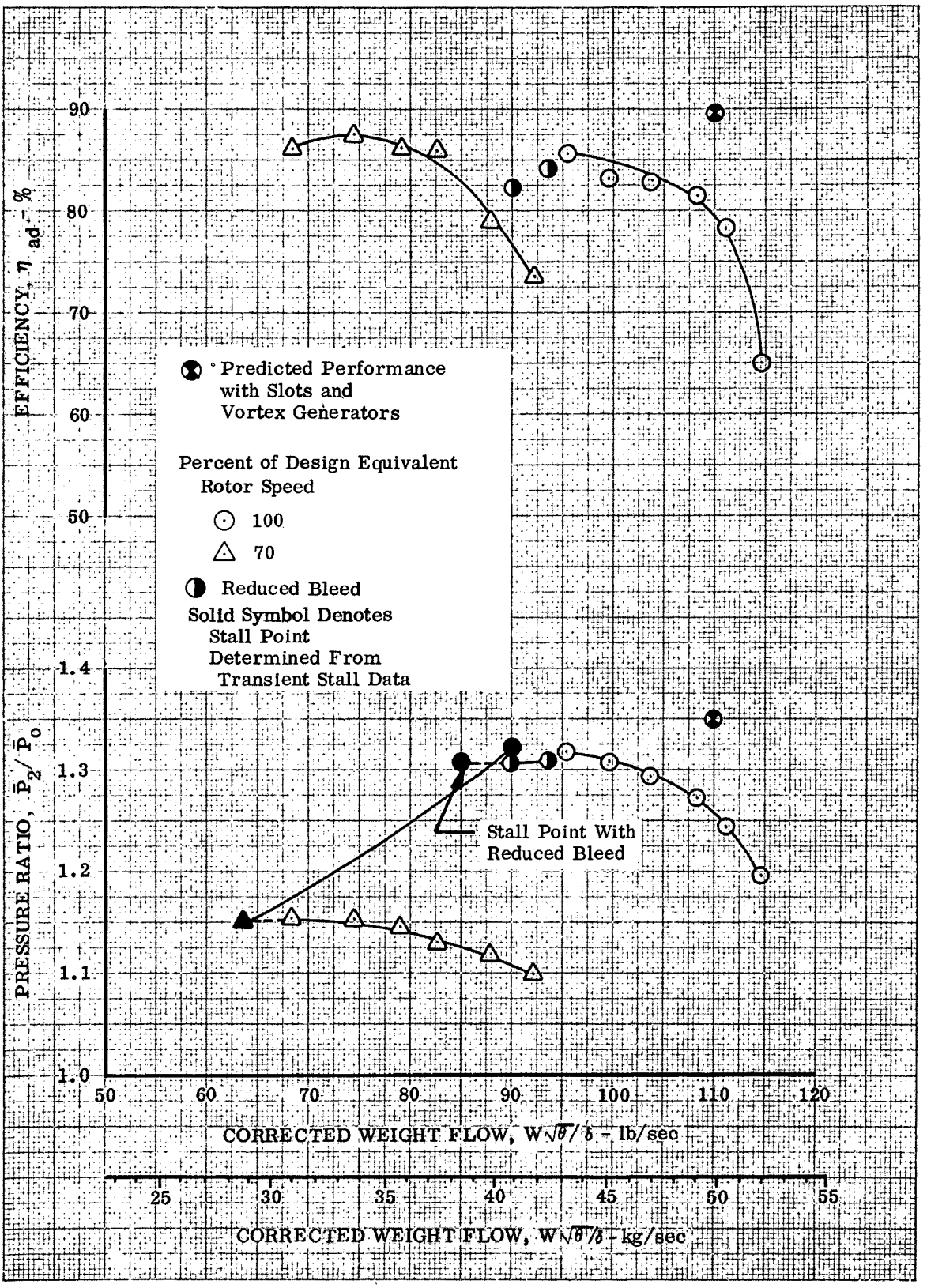

Figure 66. Overall Performance, Slotted Rotor 4 DF 89764

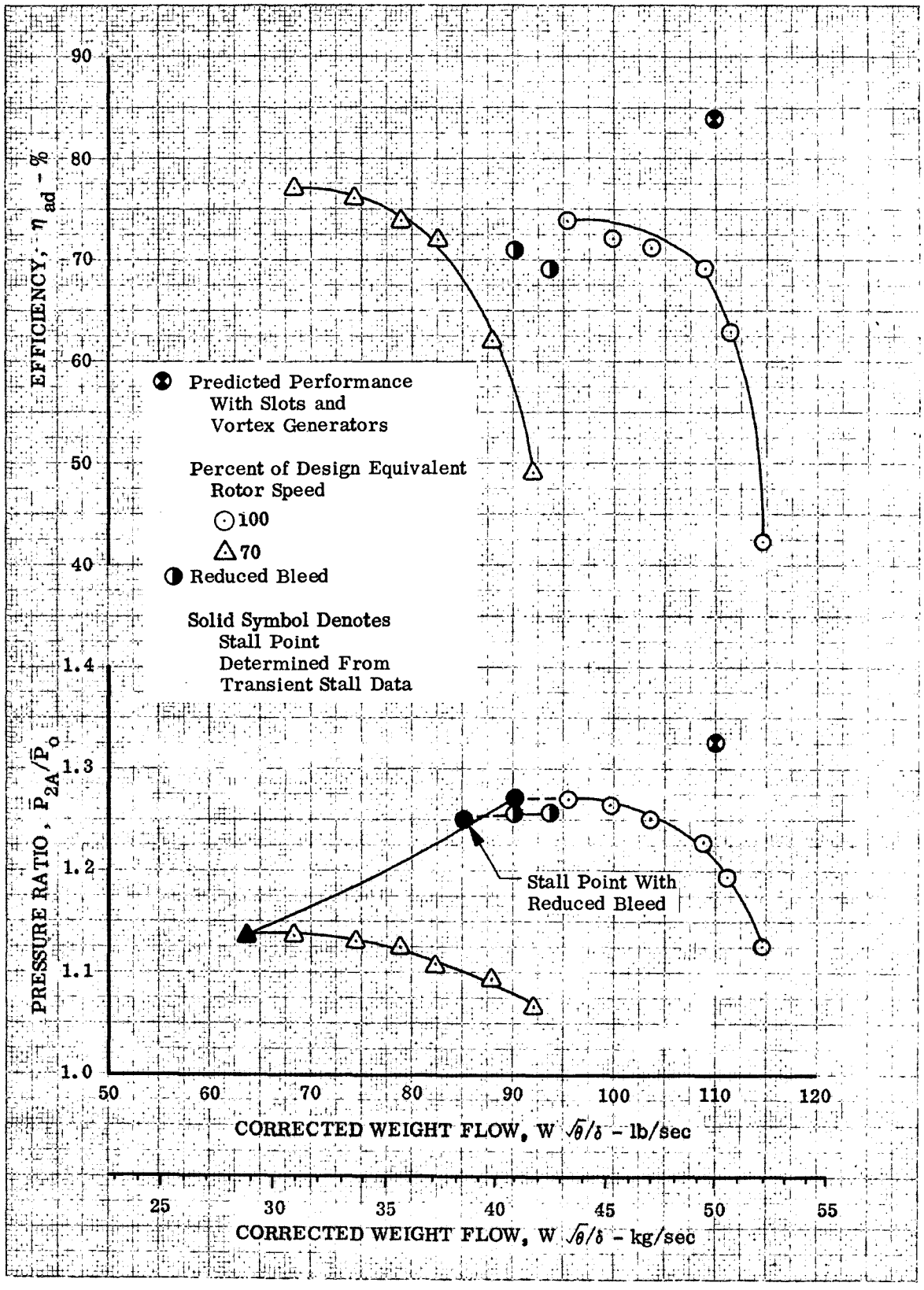

Figure 67. Overall Performance, Slotted Stage 4 DF 89765

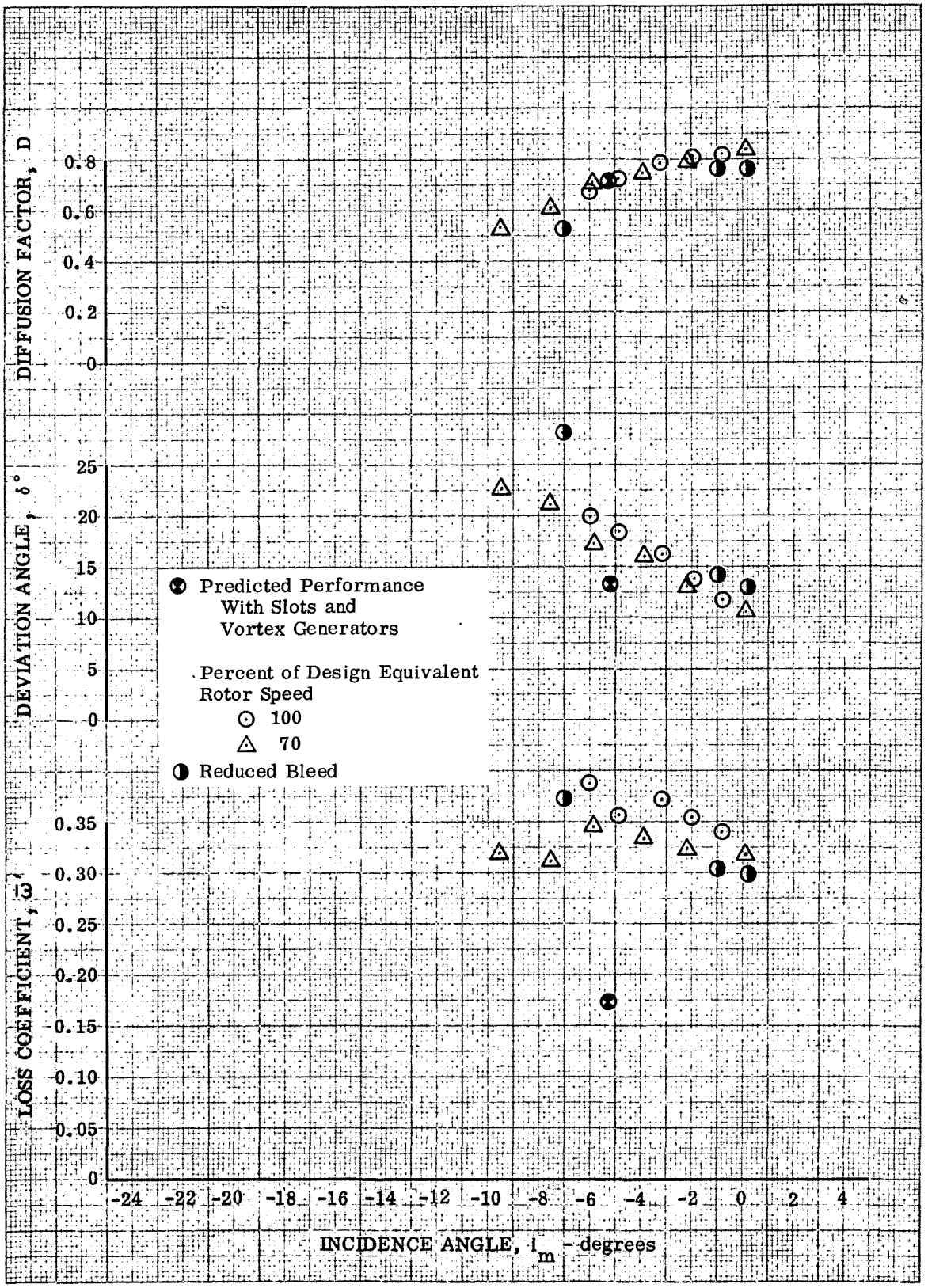

Figure 68a. Slotted Rotor 4 Blade Element Performance, 95% Span From Tip

DF 89766

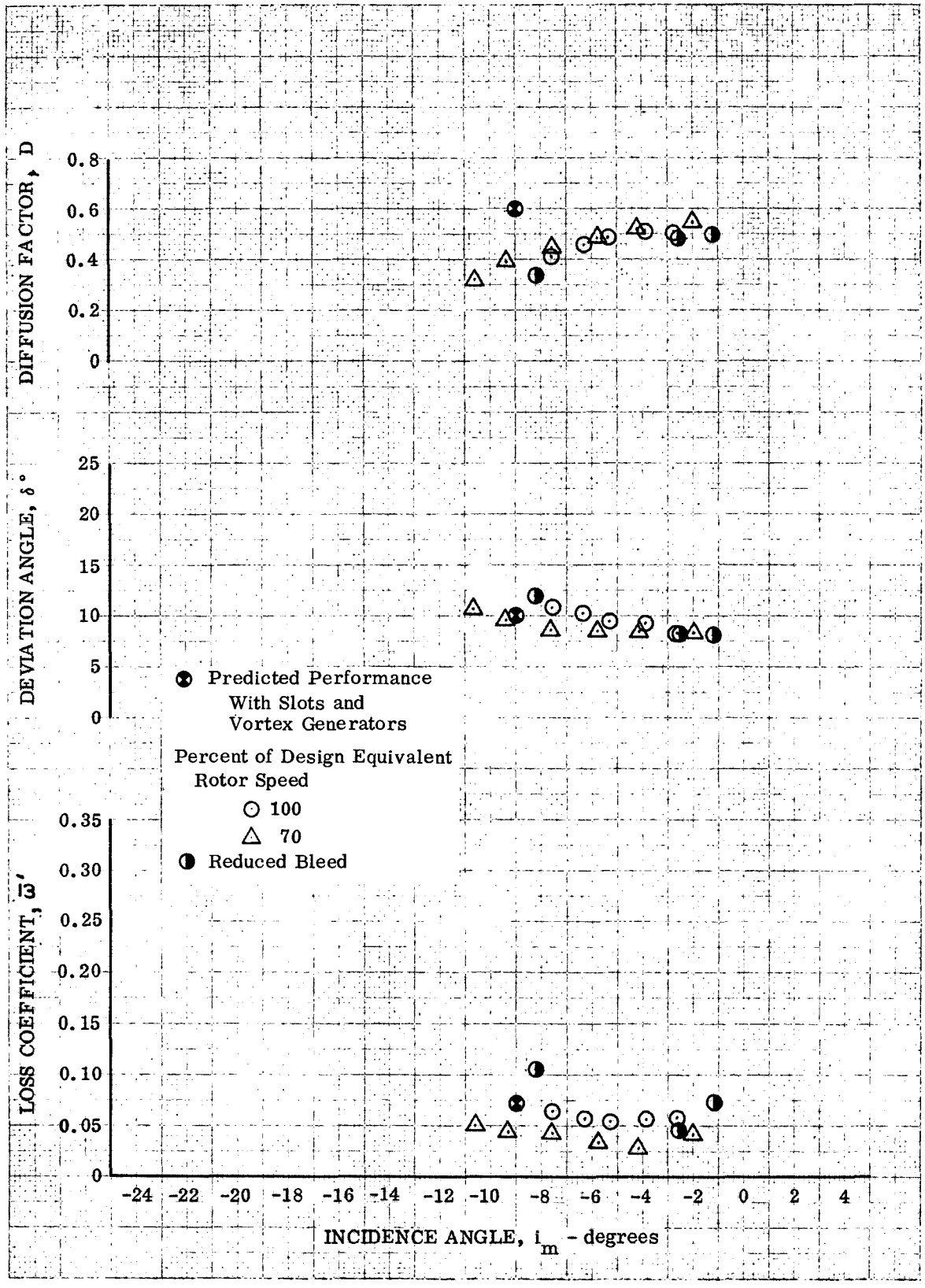

Figure 68b. Slotted Rotor 4 Blade Element Performance, 50% Span From Tip

DF 89767

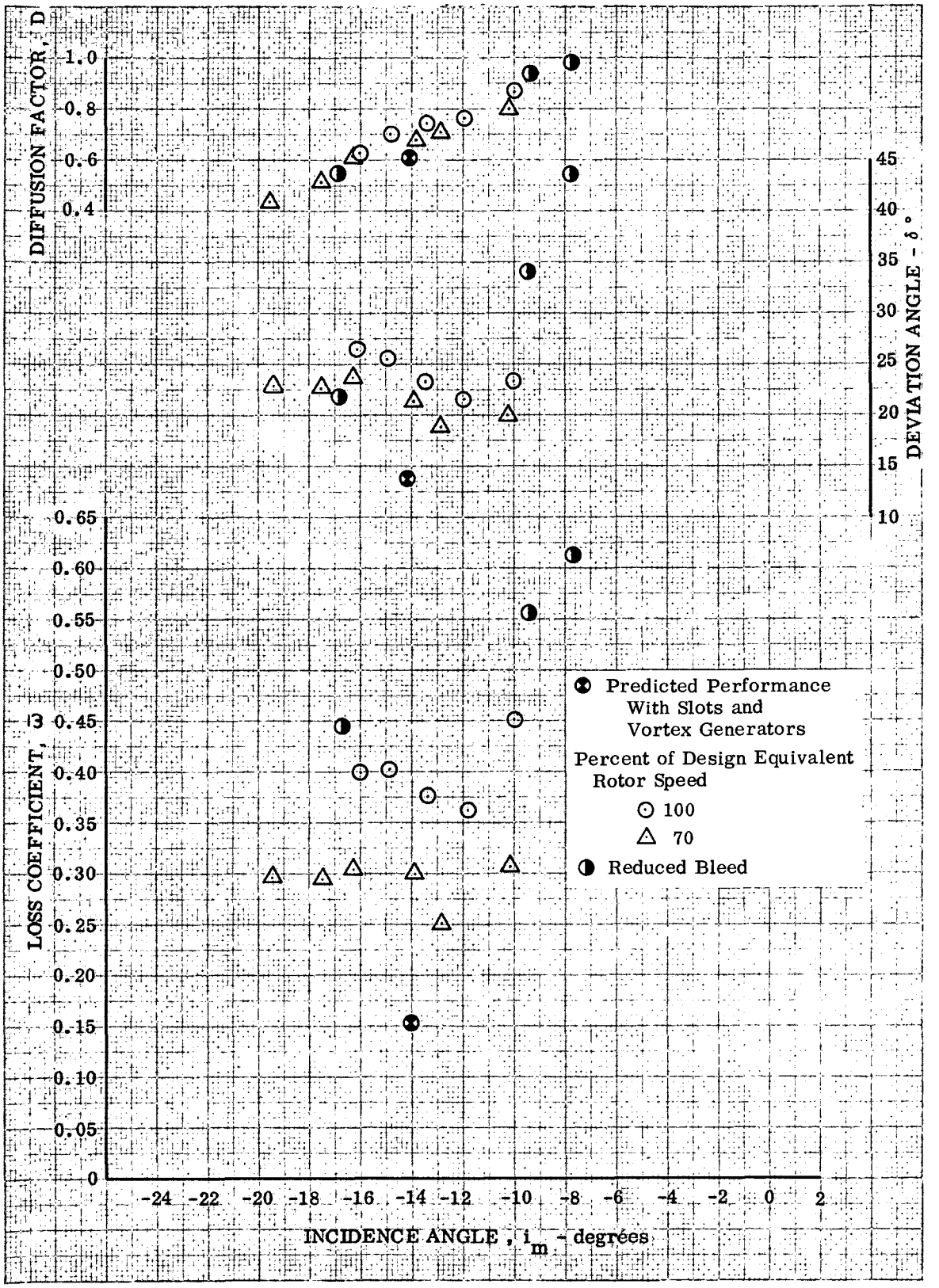

Figure 68c. Slotted Rotor 4 Blade Element Performance, 5% Span From Tip

DF 89768

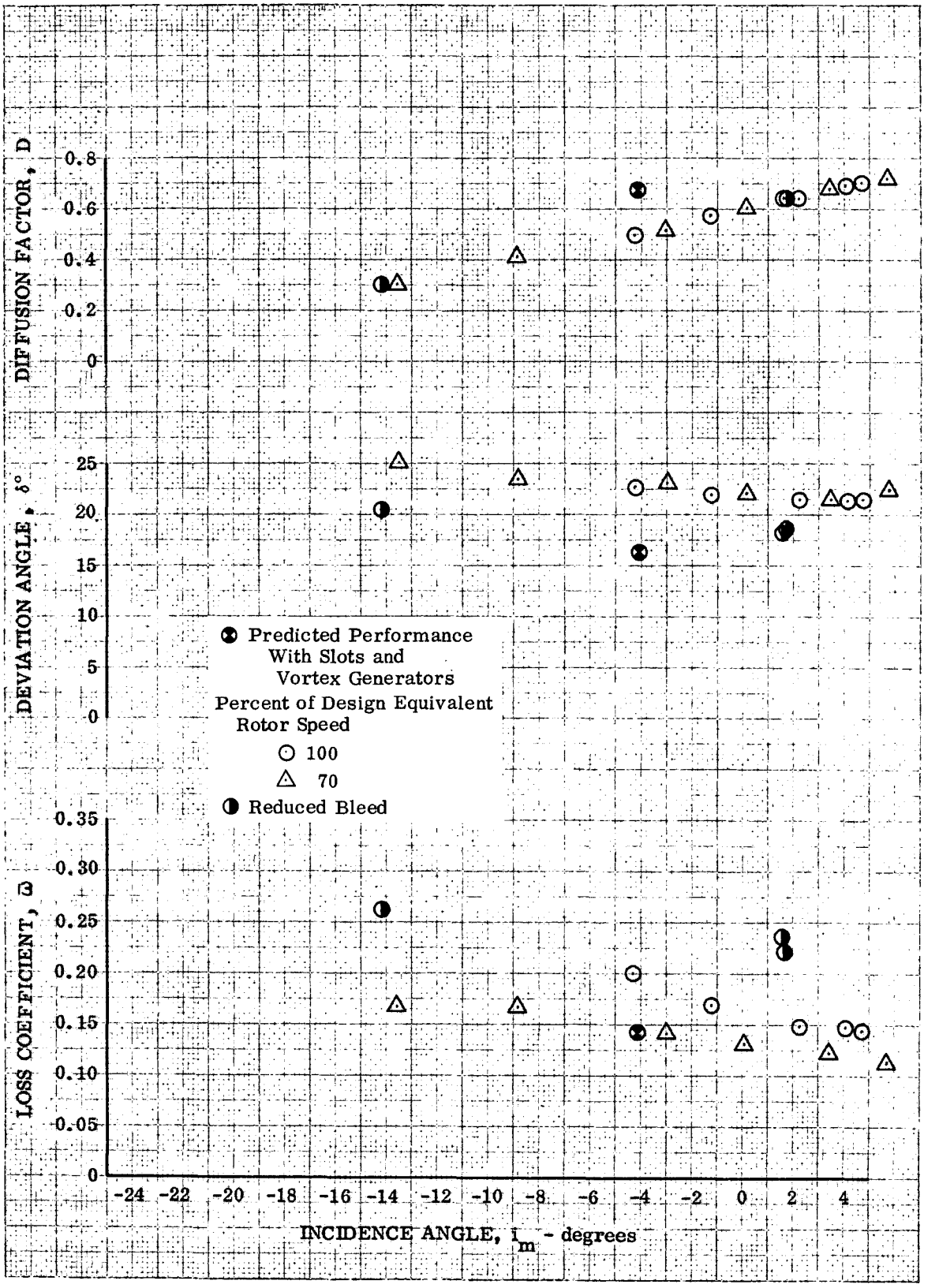

Figure 69a. Slotted Stator 4 Blade Element Performance, 95% Span From Tip

DF 89769

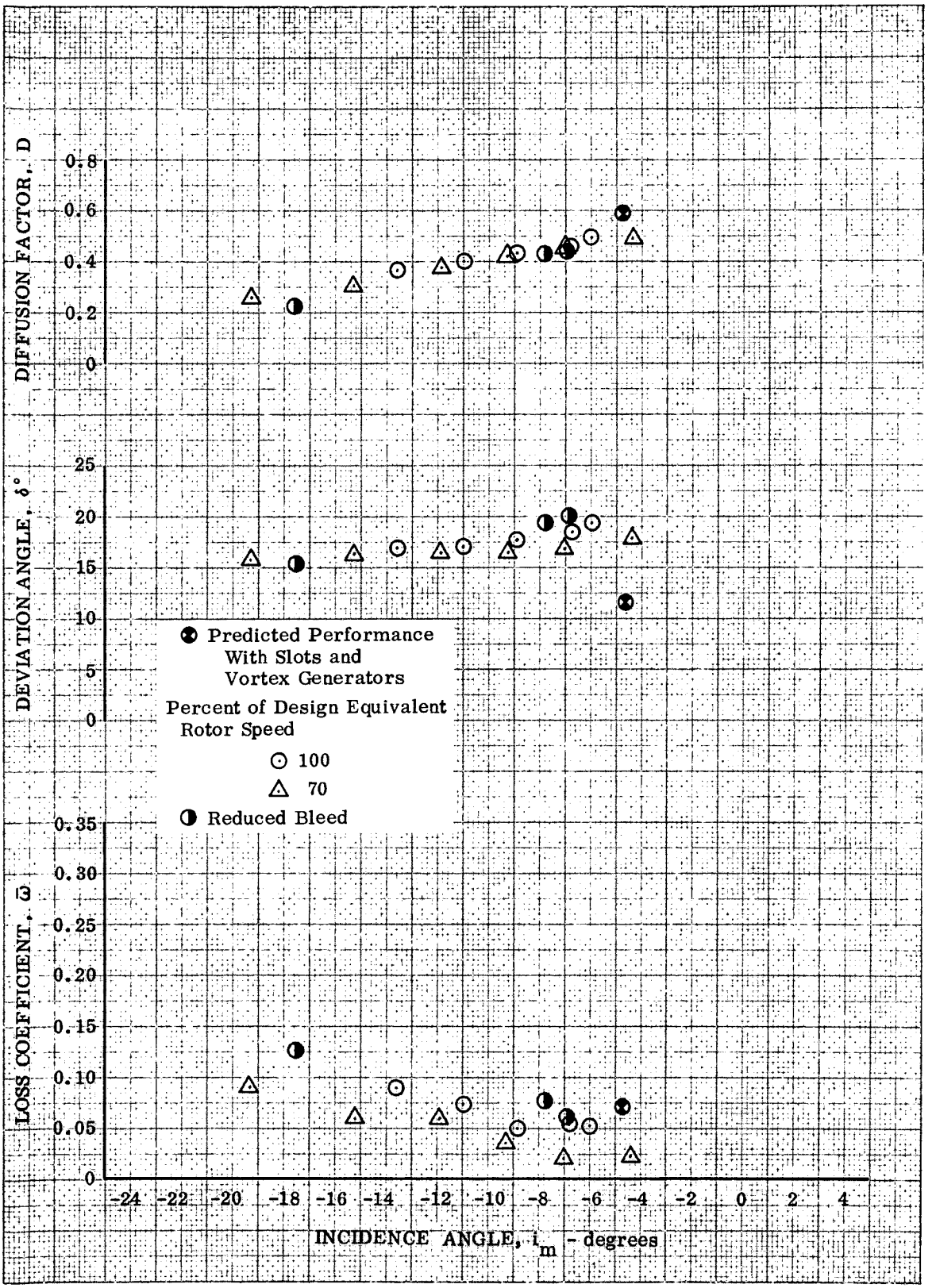

Figure 69b. Slotted Stator 4 Blade Element Performance, 50% Span From Tip

DF 89770

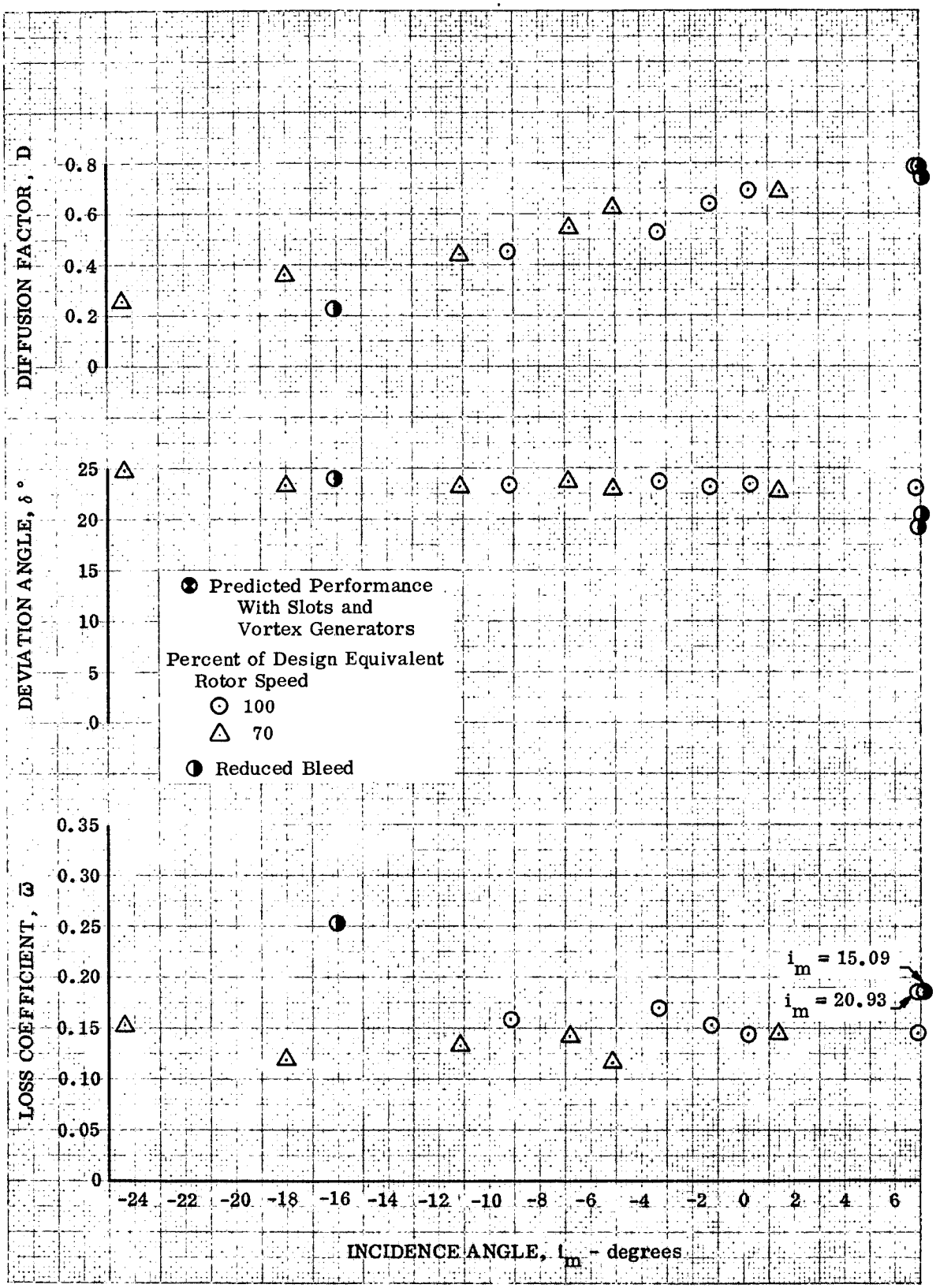

Figure 69c. Slotted Stator 4 Blade Element Performance, 5% Span From Tip

DF 89771

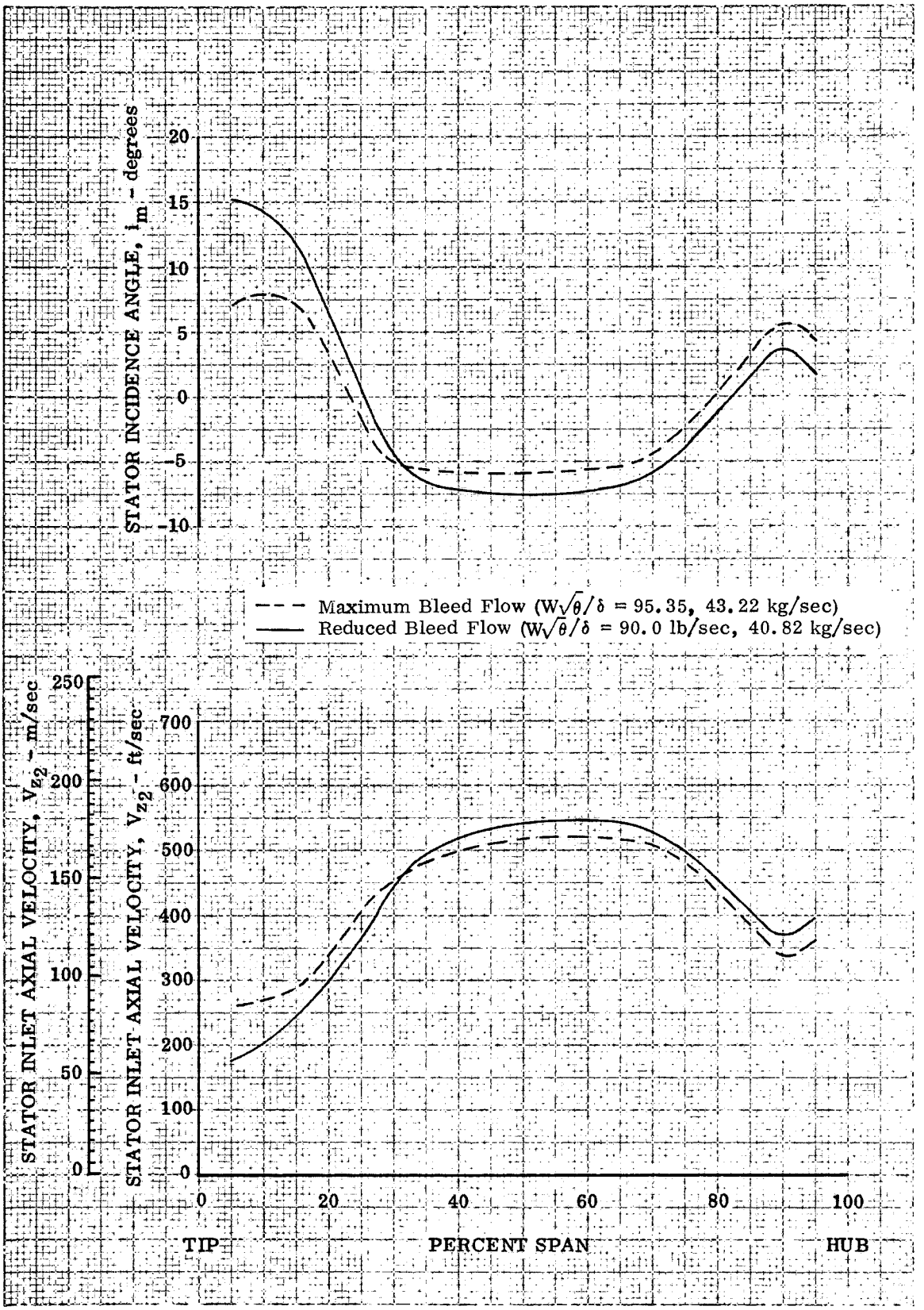

Figure 70. Effect of Bleed Flow on the Slotted Stage 4 Stator Inlet Axial Velocity and Incidence Angle at Design Equivalent Rotor Speed and Near Stall Corrected Flow

DF 89772

APPENDIX A
DESIGN GEOMETRY, VECTOR DIAGRAM, AND PREDICTED PERFORMANCE INFORMATION

Rotor and stator design velocity diagram data, blade element geometry data, and predicted performance for stages 4 and 5 selected based on the assumption that there would be reduced losses due to slots and vortex generators are presented in tables A-1 through A-4. Velocity diagram data and predicted performance for the stages 4 and 5 blading without assuming reduced losses due to slots and vortex generators are given in tables A-5 through A-8. The rotor and stator design geometry from tables A-1 through A-4 are repeated in tables A-5 through A-8. Symbols and performance variables are defined in Appendix B.

Table A-1. Slotted Rotor 4 Blade Element Design Data Along Design Streamlines[1] (English Units)

GEOMETRY DATA

Airfoil: NACA 65 (A = 1.0) — Aspect Ratio: 1.820
No. of Blades: 60 — Chord Length: 2.21 in.

Percent Span From Tip Leading Edge	Trailing Edge	κ_{le} (deg)	κ_{te} (deg)	ϕ (deg)	$\gamma°$ (deg)	0/0*	σ	t/c
97.01	96.90	56.43	-8.50	64.93	23.97	1.286	1.276	0.078
91.02	91.02	56.22	-3.50	59.72	26.36	1.270	1.258	0.076
86.71	86.60	56.28	-0.20	56.48	28.04	1.259	1.243	0.074
71.02	69.60	57.70	9.75	47.95	33.73	1.224	1.197	0.068
50.06	49.10	61.29	16.40	44.89	38.85	1.194	1.143	0.060
29.59	28.40	65.85	19.10	46.75	42.48	1.177	1.093	0.052
14.02	13.50	70.18	19.28	50.90	44.73	1.147	1.060	0.046
9.23	8.50	71.89	19.05	52.84	45.47	1.134	1.050	0.044
3.36	3.36	73.85	18.65	55.20	46.25	1.119	1.040	0.042

VELOCITY DIAGRAM DATA

Corrected Rotor Speed: 4210 rpm — Corrected Weight Flow: 110 lb/sec

Percent Span From Tip Leading Edge	Trailing Edge	V'_{le} (ft/sec)	V_{zle} (ft/sec)	$V'_{\theta le}$ (ft/sec)	β'_{le} (deg)	U_{le} (ft/sec)	V'_{te} (ft/sec)	V_{zte} (ft/sec)	$V'_{\theta te}$ (ft/sec)	β'_{te} (deg)	U_{te} (ft/sec)
97.01	96.90	780.00	489.20	605.10	51.23	604.9	438.80	437.50	37.9	4.82	607.9
91.02	91.02	788.35	490.09	616.70	51.53	615.7	453.25	447.70	71.2	8.95	616.2
86.71	86.60	794.20	492.80	623.60	51.78	624.2	463.90	454.20	95.9	11.75	622.6
71.02	69.60	814.30	496.00	647.80	52.74	647.7	498.40	466.75	174.9	20.40	645.5
50.06	49.10	837.40	488.25	679.80	54.30	680.0	527.25	471.65	234.9	26.47	675.8
29.59	28.40	855.20	473.70	711.30	56.28	711.7	546.75	472.70	272.3	29.83	705.3
14.02	13.50	865.10	454.60	735.00	58.17	735.0	556.80	472.05	292.3	31.55	726.3
9.23	8.80	867.50	446.65	742.65	58.85	742.5	560.30	472.20	297.9	32.05	733.1
3.36	3.36	870.05	436.25	751.80	59.72	751.7	565.75	473.75	303.8	32.58	740.2

DESIGN PERFORMANCE DATA

Pressure Ratio: 1.349 — Efficiency: 89.5%

Percent Span From Tip Leading Edge	Trailing Edge	$\Delta\beta'$ (deg)	M'_{le}	i_m (deg)	D	$\overline{\omega'}$	Loss Parameter	$\delta°$ (deg)	P_{te} (psia)	T_{te} (°R)
97.01	96.90	46.41	0.713	-5.20	0.722	0.176	0.069	13.32	20.197	576.59
91.02	91.02	42.58	0.720	-4.69	0.697	0.149	0.058	12.45	20.116	574.41
86.71	86.60	40.03	0.726	-4.50	0.681	0.131	0.052	11.95	20.057	573.16
71.02	69.60	28.64	0.744	-4.96	0.632	0.089	0.034	10.65	19.834	569.53
50.06	49.10	27.83	0.765	-6.99	0.603	0.073	0.029	10.07	19.766	568.50
29.59	28.40	26.45	0.780	-9.57	0.598	0.094	0.037	10.73	19.762	569.58
14.02	13.50	26.62	0.789	-12.01	0.600	0.127	0.051	12.27	19.719	571.30
9.23	8.80	26.80	0.790	-13.04	0.600	0.139	0.056	13.00	19.714	571.87
3.36	3.36	27.14	0.792	-14.13	0.599	0.155	0.063	13.93	19.683	572.54

[1] Based on the Assumption That There Would be Reduced Losses Due to Slots and Vortex Generators

Table A-1. Slotted Rotor 4 Blade Element Design Data Along Design Streamlines[1] (Metric Units)

GEOMETRY DATA

Airfoil: NACA 65 (A = 1.0) — Aspect Ratio: 1.820
No. of Blades: 60 — Chord Length: 0.0561m

Percent Span From Tip Leading Edge	Trailing Edge	κ_{le} (deg)	κ_{te} (deg)	ϕ (deg)	$\gamma°$ (deg)	$0/0^*$	σ	t/c
97.01	96.90	56.43	-8.50	64.93	23.97	1.286	1.276	0.078
91.02	91.02	56.22	-3.50	59.72	26.36	1.270	1.258	0.076
86.71	86.60	56.28	-0.20	56.48	28.04	1.259	1.243	0.074
71.02	69.60	57.70	9.75	47.95	33.73	1.224	1.197	0.068
50.06	49.10	61.29	16.40	44.89	38.85	1.194	1.143	0.060
29.59	28.40	65.85	19.10	46.75	42.48	1.177	1.093	0.052
14.02	13.50	70.18	19.28	50.90	44.73	1.147	1.060	0.046
9.23	8.80	71.89	19.05	52.84	45.47	1.134	1.050	0.044
3.36	3.36	73.85	18.65	55.20	46.25	1.119	1.040	0.042

VELOCITY DIAGRAM DATA

Corrected Rotor Speed: 4210 rpm — Corrected Weight Flow: 49.89 kg/sec

Percent Span From Tip Leading Edge	Trailing Edge	V'_{le} (m/sec)	V_{zle} (m/sec)	$V'_{\theta le}$ (m/sec)	β'_{le} (deg)	U_{le} (m/sec)	V'_{te} (m/sec)	V_{zte} (m/sec)	$V'_{\theta te}$ (m/sec)	β'_{te} (deg)	U_{te} (m/sec)
97.01	96.90	237.7	149.1	184.4	51.23	184.4	133.8	133.4	11.6	4.82	185.3
91.02	91.02	240.3	149.4	188.0	51.53	187.7	138.2	136.5	21.7	8.95	187.8
86.71	86.60	242.1	150.2	190.1	51.78	190.3	141.4	138.4	29.2	11.75	189.8
71.02	69.60	248.2	151.2	197.5	52.74	197.4	151.9	142.3	53.3	20.40	196.7
50.06	49.10	255.2	148.8	207.2	54.30	207.3	160.7	143.8	71.6	26.47	205.0
29.59	28.40	260.7	144.4	216.8	56.28	216.9	166.7	144.1	83.0	29.83	215.0
14.02	13.50	263.7	138.6	224.0	58.17	224.0	169.7	143.9	89.1	31.55	221.4
9.23	8.80	264.4	136.1	226.4	58.85	226.3	170.8	143.9	90.8	32.05	223.4
3.36	3.36	265.2	133.0	229.2	59.72	229.1	172.4	144.4	92.6	32.58	225.6

DESIGN PERFORMANCE DATA

Pressure Ratio: 1.349 — Efficiency: 89.5%

Percent Span From Tip Leading Edge	Trailing Edge	$\Delta\beta'$ (deg)	M^i_{le}	i_m (deg)	D	$\bar{\omega}'$	Loss Parameter	$\delta°$ (deg)	$P_{te} \times 10^{-6}$ (N/m^2)	T_{te} (°K)
97.01	96.90	46.41	0.713	- 5.20	0.722	0.176	0.069	13.32	0.1393	320.33
91.02	91.02	42.58	0.720	- 4.69	0.697	0.149	0.058	12.45	0.1387	319.12
86.71	86.60	40.03	0.726	- 4.50	0.681	0.131	0.052	11.95	0.1383	318.42
71.02	69.60	28.64	0.744	- 4.96	0.632	0.089	0.034	10.65	0.1368	316.41
50.06	49.10	27.83	0.765	- 6.99	0.603	0.073	0.029	10.07	0.1363	315.83
29.59	28.40	26.45	0.780	- 9.57	0.598	0.094	0.037	10.73	0.1363	316.43
14.02	13.50	26.62	0.789	-12.01	0.600	0.127	0.051	12.27	0.1360	317.39
9.23	8.80	26.80	0.790	-13.04	0.600	0.139	0.056	13.00	0.1360	317.71
3.36	3.36	27.14	0.792	-14.13	0.599	0.155	0.063	13.93	0.1358	318.08

[1] Based on the Assumption That There Would be Reduced Losses Due to Slots and Vortex Generators

Table A-2. Slotted Stator 4 Blade Element Design Data Along Design Streamlines[1] (English Units)

GEOMETRY DATA

Airfoil: NACA 65 (A = 1.0)
No. of Vanes: 58

Aspect Ratio: 1.689
Chord Length: 2.182 in.
Thickness Ratio, t/c: 0.090

Percent Span From Tip Leading Edge	Trailing Edge	κ_{le} (deg)	κ_{te} (deg)	ϕ (deg)	$\gamma°$ (deg)	0/0*	σ
94.87	94.87	53.81	-16.48	70.29	18.67	1.324	1.214
90.07	90.07	51.87	-15.59	67.46	18.14	1.310	1.200
85.00	84.85	50.23	-14.62	64.85	17.81	1.297	1.187
70.27	69.68	47.18	-12.52	59.70	17.33	1.265	1.151
50.40	49.95	46.30	-11.67	57.97	17.32	1.236	1.105
30.27	29.25	48.75	-12.52	61.27	18.12	1.216	1.063
15.27	14.60	52.40	-14.12	66.52	19.14	1.196	1.032
10.27	9.70	53.92	-14.95	68.87	19.49	1.194	1.021
5.00	4.60	55.80	-15.95	81.75	19.93	1.199	1.010

VELOCITY DIAGRAM DATA

Percent Span From Tip Leading Edge	Trailing Edge	V_{le} (ft/sec)	V_{zle} (ft/sec)	$V_{\theta le}$ (ft/sec)	β_{le} (deg)	V_{te} (ft/sec)	V_{zte} (ft/sec)	$V_{\theta te}$ (ft/sec)	β_{te} (deg)
94.87	94.87	735.2	474.2	561.2	49.71	469.0	468.9	0.0	0.0
90.07	90.07	725.0	482.9	540.2	48.15	468.9	468.8	0.0	0.0
85.00	84.85	715.2	491.2	520.4	46.68	468.7	468.7	0.0	0.0
70.27	69.98	690.0	501.1	474.3	43.45	468.9	468.8	0.0	0.0
50.40	49.95	667.9	498.9	443.2	41.59	477.0	476.4	0.0	0.0
30.27	29.25	649.6	481.0	435.2	42.07	489.9	489.9	0.0	0.0
15.27	14.60	631.2	454.8	436.8	43.77	504.9	503.7	0.0	0.0
10.27	9.70	623.8	443.5	437.8	44.52	511.1	510.2	0.0	0.0
5.00	4.60	615.3	429.9	438.5	45.40	518.7	517.5	0.0	0.0

DESIGN PERFORMANCE DATA

Stage Pressure Ratio: 1.324

Stage Efficiency: 83.8%

Percent Span From Tip Leading Edge	Trailing Edge	$\Delta\beta'$ (deg)	M_{le}	i_m (deg)	D	$\overline{\omega}'$	Loss Parameter	$\delta°$ (deg)	P_{te} (psia)
94.87	94.87	49.71	0.652	-4.105	0.676	0.142	0.058	16.48	19.455
90.07	90.07	48.15	0.644	-3.730	0.663	0.132	0.055	15.59	19.455
85.00	84.85	46.68	0.634	-3.555	0.652	0.121	0.051	14.62	19.455
70.27	69.98	43.45	0.612	-3.730	0.620	0.094	0.041	12.52	19.418
50.40	49.95	41.59	0.591	-4.710	0.588	0.072	0.033	11.67	19.440
30.27	29.25	42.07	0.574	-6.680	0.563	0.073	0.034	12.52	19.469
15.27	14.60	43.77	0.557	-8.630	0.537	0.066	0.032	14.12	19.484
10.27	9.70	44.52	0.549	-9.400	0.526	0.062	0.030	14.95	19.484
5.00	4.60	45.40	0.541	-10.405	0.511	0.056	0.028	15.95	19.492

[1] Based on the Assumption That There Would be Reduced Losses Due to Slots and Vortex Generators

Table A-2. Slotted Stator 4 Blade Element Design Data Along Design Streamlines[1] (Metric Units)

GEOMETRY DATA

Airfoil: NACA 65 (A = 1.0)
No. of Vanes: 58

Aspect Ratio: 1.689
Chord Length: 0.0554m
Thickness Ratio, t/c: 0.090

Percent Span From Tip Leading Edge	Trailing Edge	κ_{le} (deg)	κ_{te} (deg)	ϕ (deg)	$\gamma°$ (deg)	0/0*	σ
94.87	94.87	53.81	-16.48	70.29	18.67	1.324	1.214
90.07	90.07	51.87	-15.59	67.46	18.14	1.310	1.200
85.00	84.85	50.23	-14.62	64.85	17.81	1.297	1.187
70.27	69.98	47.18	-12.52	59.70	17.33	1.265	1.151
50.40	49.95	46.30	-11.67	57.97	17.32	1.236	1.105
30.27	29.25	48.75	-12.52	61.27	18.12	1.216	1.063
15.27	14.60	52.40	-14.12	66.52	19.14	1.196	1.032
10.27	9.70	53.92	-14.95	68.87	19.49	1.194	1.021
5.00	4.60	55.80	-15.95	71.75	19.93	1.199	1.010

VELOCITY DIAGRAM DATA

Percent Span From Tip Leading Edge	Trailing Edge	V_{le} (m/sec)	V_{zle} (m/sec)	$V_{\theta le}$ (m/sec)	β_{le} (deg)	V_{te} (m/sec)	V_{zte} (m/sec)	$V_{\theta te}$ (m/sec)	β_{te} (deg)
94.87	94.87	224.1	144.5	171.1	49.71	143.0	142.9	0.0	0.0
90.07	90.07	221.0	147.2	164.7	48.15	142.9	142.9	0.0	0.0
85.00	84.85	218.0	149.7	158.6	46.68	142.9	142.9	0.0	0.0
70.27	69.98	210.3	152.7	144.6	43.45	142.9	142.9	0.0	0.0
50.40	49.95	203.6	152.1	135.1	41.59	145.4	145.2	0.0	0.0
30.27	29.25	198.0	146.6	132.7	42.07	149.3	149.3	0.0	0.0
15.27	14.60	192.4	138.6	133.1	43.77	153.9	153.5	0.0	0.0
10.27	9.70	190.1	135.2	133.4	44.52	155.8	155.5	0.0	0.0
5.00	4.60	187.5	131.0	133.7	45.40	158.1	157.7	0.0	0.0

DESIGN PERFORMANCE DATA

Stage Pressure Ratio: 1.324

Stage Efficiency: 83.8%

Percent Span From Tip Leading Edge	Trailing Edge	$\Delta\beta$ (deg)	M_{le}	i_m (deg)	D	$\bar{\omega}$	Loss Parameter	$\delta°$ (deg)	$P_{te} \times 10^{-6}$ (N/m^2)
94.87	94.87	49.71	0.652	-4.105	0.676	0.142	0.058	16.48	0.1342
90.07	90.07	48.15	0.644	-3.730	0.663	0.132	0.055	15.59	0.1342
85.00	84.85	46.68	0.634	-3.555	0.652	0.121	0.051	14.62	0.1342
70.27	69.98	43.45	0.612	-3.730	0.620	0.094	0.041	12.52	0.1339
50.40	49.95	41.59	0.591	-4.710	0.588	0.072	0.033	11.67	0.1341
30.27	29.25	42.07	0.574	-6.680	0.563	0.073	0.034	12.52	0.1343
15.27	14.60	43.77	0.557	-8.630	0.537	0.066	0.032	14.12	0.1344
10.27	9.70	44.52	0.549	-9.400	0.526	0.062	0.030	14.95	0.1344
5.00	4.60	45.40	0.541	-10.405	0.511	0.056	0.028	15.95	0.1344

[1] Based on the Assumption That There Would be Reduced Losses Due to Slots and Vortex Generators

Table A-3. Slotted Rotor 5 Blade Element Design Data Along Design Streamlines[1] (English Units)

GEOMETRY DATA

Airfoil: NASA 65 (A = 1.0)
No. of Blades: 60

Aspect Ratio: 1,820
Chord Length: 2.21 in.

Percent Span From Tip Leading Edge	Trailing Edge	κ_{le} (deg)	κ_{te} (deg)	ϕ (deg)	$\gamma°$ (deg)	0/0*	σ	t/c
96.41	94.75	60.40	-31.00	91.40	14.70	1.039	1.276	0.078
91.20	89.25	59.90	-22.60	82.50	18.65	1.060	1.258	0.076
86.77	84.80	59.70	-17.00	76.70	21.35	1.079	1.243	0.074
70.84	69.00	60.37	- 2.40	62.77	28.99	1.142	1.197	0.068
50.30	49.40	63.22	7.00	56.22	35.11	1.194	1.143	0.060
29.94	29.75	68.07	9.85	58.22	38.96	1.229	1.093	0.052
13.65	14.40	72.80	10.40	62.40	41.60	1.266	1.060	0.046
9.22	10.00	74.35	10.20	64.15	42.28	1.277	1.050	0.044
3.41	4.70	76.60	9.65	66.95	43.13	1.293	1.040	0.042

VELOCITY DIAGRAM DATA

Corrected Rotor Speed: 4210 rpm

Corrected Weight Flow: 110 lb/sec

Percent Span From Tip Leading Edge	Trailing Edge	V'le (ft/sec)	Vzle (ft/sec)	V'θle (ft/sec)	β'le (deg)	Ule (ft/sec)	V'te (ft/sec)	Vzte (ft/sec)	Vθte (ft/sec)	β'te (deg)	Ute (ft/sec)
96.41	94.75	779.4	485.6	609.1	51.44	608.5	429.2	422.5	- 77.0	-10.30	610.7
91.20	89.25	786.3	487.3	617.3	51.70	616.6	440.6	439.0	- 32.0	- 4.40	618.8
86.77	84.80	792.9	488.7	624.2	51.92	623.7	449.3	449.2	2.0	- 0.00	625.0
70.84	69.00	813.3	491.5	648.3	52.84	648.0	478.4	468.5	96.0	11.40	647.5
50.30	49.40	837.4	488.2	680.2	54.27	680.0	499.8	475.4	167.0	19.40	675.3
29.94	29.75	855.6	474.3	710.8	56.15	711.0	515.3	472.0	202.0	23.40	703.6
13.65	14.40	866.2	455.2	735.3	58.17	736.7	520.8	468.0	221.0	25.30	725.2
9.22	10.00	868.1	448.5	742.8	58.79	743.0	522.9	467.5	227.0	25.70	731.8
3.41	4.70	870.6	437.5	752.0	59.65	752.3	525.2	467.0	233.0	26.20	739.2

DESIGN PERFORMANCE DATA

Pressure Ratio: 1.414

Efficiency = 89.3%

Percent Span From Tip Leading Edge	Trailing Edge	Δβ' (deg)	M'le	i_m (deg)	D	$\overline{\omega}$	Loss Parameter	δ° (deg)	P_{te} (psia)	T_{te} (°R)
96.41	94.75	61.74	0.712	-8.96	0.796	0.200	0.077	20.70	21.550	588.47
91.20	89.25	56.10	0.719	-8.20	0.770	0.173	0.069	18.20	21.328	585.51
86.77	84.80	51.92	0.724	-7.78	0.750	0.153	0.062	17.00	21.168	583.38
70.84	69.00	41.44	0.743	-7.53	0.696	0.107	0.044	13.80	20.788	578.35
50.30	49.40	34.87	0.766	-8.95	0.665	0.082	0.034	12.40	20.627	575.76
29.94	29.75	32.75	0.780	-11.92	0.668	0.107	0.045	13.55	20.616	576.90
13.65	14.40	32.87	0.789	-14.63	0.678	0.141	0.060	14.90	20.608	579.23
9.22	10.00	33.09	0.791	-15.56	0.680	0.154	0.066	15.50	20.601	580.96
3.41	4.70	33.45	0.792	-16.95	0.682	0.170	0.073	16.55	20.589	580.94

[1] Based on the Assumption That There Would be Reduced Losses Due to Slots and Vortex Generators

Table A-3. Slotted Rotor 5 Blade Element Design Data Along Design Streamlines[1] (Metric Units)

GEOMETRY DATA

Airfoil: NASA 65 (A = 1.0)
No. of Blades: 60

Aspect Ratio: 1,820
Chord Length: 0.0561m

Percent Span From Tip Leading Edge	Trailing Edge	κ_{le} (deg)	κ_{te} (deg)	ϕ (deg)	$\gamma°$ (deg)	0/0*	σ	t/c
96.41	94.75	60.40	-31.00	91.40	14.70	1.039	1.276	0.078
91.20	89.25	59.90	-22.60	82.50	18.65	1.060	1.258	0.076
86.77	84.80	59.70	-17.00	76.70	21.35	1.079	1.243	0.074
70.84	69.00	60.37	- 2.40	62.77	28.99	1.142	1.197	0.068
50.30	49.40	63.22	7.00	56.22	35.11	1.194	1.143	0.060
29.94	29.75	68.07	9.85	58.22	38.96	1.229	1.093	0.052
13.65	14.40	72.80	10.40	62.40	41.60	1.266	1.060	0.046
9.22	10.00	74.35	10.20	64.15	42.28	1.277	1.050	0.044
3.41	4.70	76.60	9.65	66.95	43.13	1.293	1.040	0.042

VELOCITY DIAGRAM DATA

Corrected Rotor Speed: 4210 rpm

Corrected Weight Flow: 49.89 kg/sec

Percent Span From Tip Leading Edge	Trailing Edge	V'_{le} (m/sec)	V_{zle} (m/sec)	$V'_{\theta le}$ (m/sec)	β'_{le} (deg)	U_{le} (m/sec)	V'_{te} (m/sec)	V_{zte} (m/sec)	$V'_{\theta te}$ (m/sec)	β'_{te} (deg)	U_{te} (m/sec)
96.41	94.75	237.6	148.0	185.7	51.44	185.5	130.8	128.8	-23.5	-10.30	186.1
91.20	89.25	239.7	148.5	188.2	51.70	187.9	134.3	133.8	- 9.8	- 4.40	188.6
86.77	84.80	241.7	148.9	190.3	51.92	190.1	136.9	136.9	0.6	0.00	190.5
70.84	69.00	247.9	149.8	197.6	52.84	197.5	145.8	142.8	29.3	11.40	197.4
50.30	49.40	255.2	148.8	207.3	54.27	207.3	152.3	144.9	50.9	19.40	205.8
29.94	29.75	260.8	144.6	216.7	56.15	216.7	157.1	143.9	61.6	23.40	214.5
13.65	14.40	264.0	138.7	224.1	58.17	224.5	158.7	142.6	67.4	25.30	221.0
9.22	10.00	264.6	136.7	226.4	58.79	226.5	159.4	142.5	69.2	25.70	223.1
3.41	4.70	265.4	133.4	229.2	59.65	229.3	160.1	142.3	71.0	26.20	225.3

DESIGN PERFORMANCE DATA

Pressure Ratio: 1.414

Efficiency = 89.3%

Percent Span From Tip Leading Edge	Trailing Edge	$\Delta\beta'$ (deg)	M'_{le}	i_m (deg)	D	$\bar{\omega}'$	Loss Parameter	$\delta°$ (deg)	$P_{te} \times 10^{-6}$ (N/m^2)	T_{te} (°K)
96.41	94.75	61.74	0.712	- 8.96	0.796	0.200	0.077	20.70	0.1486	326.93
91.20	89.25	56.10	0.719	- 8.20	0.770	0.173	0.069	18.20	0.1471	325.28
86.77	84.80	51.92	0.724	- 7.78	0.750	0.153	0.062	17.00	0.1460	324.10
70.84	69.00	41.44	0.743	- 7.53	0.696	0.107	0.044	13.80	0.1434	321.31
50.30	49.40	34.87	0.766	- 8.95	0.665	0.082	0.034	12.40	0.1423	319.87
29.94	29.75	32.75	0.780	-11.92	0.668	0.107	0.045	13.55	0.1422	320.50
13.65	14.40	32.87	0.789	-14.63	0.678	0.141	0.060	14.90	0.1421	321.79
9.22	10.00	33.09	0.791	-15.56	0.680	0.154	0.066	15.50	0.1421	322.76
3.41	4.70	33.45	0.792	-16.95	0.682	0.170	0.073	16.55	0.1420	322.74

[1] Based on the Assumption That There Would be Reduced Losses Due to Slots and Vortex Generators

Table A-4. Slotted Stator 5 Blade Element Design Data Along Design Streamlines[1] (English Units)

GEOMETRY DATA

Airfoil: NACA 65 (A = 1.0)
No. of Vanes: 58

Aspect Ratio: 1.689
Chord Length: 2.182 in.
Thickness Ratio t/c: 0.090

Percent Span From Tip Leading Edge	Trailing Edge	κ_{le} (deg)	κ_{te} (deg)	ϕ (deg)	$\gamma°$ (deg)	0/0*	σ
94.74	94.9	66.30	-22.42	88.72	21.94	1.311	1.214
90.13	90.4	62.35	-20.42	82.77	20.97	1.255	1.200
84.87	85.0	59.20	-18.60	77.80	20.30	1.201	1.187
70.39	70.2	53.65	-15.12	68.77	19.27	1.126	1.151
50.66	49.8	51.95	-13.80	65.75	19.08	1.101	1.105
30.92	30.0	55.03	-15.17	70.20	19.93	1.131	1.063
15.79	15.0	59.20	-17.22	76.42	20.99	1.188	1.032
10.53	10.0	61.10	-18.15	79.25	21.48	1.212	1.021
5.13	5.0	63.30	-19.40	82.70	21.95	1.238	1.010

VELOCITY DIAGRAM DATA

Percent Span From Tip Leading Edge	Trailing Edge	V_{le} (ft/sec)	V_{zle} (ft/sec)	$V_{\theta le}$ (ft/sec)	β_{le} (deg)	V_{te} (ft/sec)	V_{zte} (ft/sec)	$V_{\theta te}$ (ft/sec)	β_{te} (deg)
94.74	94.9	821.5	453.1	687.1	56.90	457.1	457.0	0.0	0.0
90.13	90.4	800.5	468.7	655.8	54.50	457.8	457.8	0.0	0.0
84.87	85.0	787.0	481.5	622.5	52.35	458.4	458.3	0.0	0.0
70.39	70.2	747.5	500.0	558.0	48.00	459.2	459.0	0.0	0.0
50.66	49.8	716.0	503.5	510.0	45.40	464.3	464.0	0.0	0.0
30.92	30.0	697.0	482.1	503.0	46.14	474.8	474.6	0.0	0.0
15.79	15.0	680.5	463.8	505.0	47.94	488.2	487.5	0.0	0.0
10.53	10.0	673.0	440.0	506.2	48.77	493.8	493.0	0.0	0.0
5.13	5.0	664.5	426.2	508.0	49.85	500.0	499.2	0.0	0.0

DESIGN PERFORMANCE DATA

Stage Pressure Ratio: 1.375

Stage Efficiency: 81.7%

Percent Span From Tip Leading Edge	Trailing Edge	$\Delta\beta$ (deg)	M_{le}	i_m (deg)	D	$\overline{\omega}$	Loss Parameter	$\delta°$ (deg)	P_{te} (psia)
94.74	94.9	56.90	0.728	-9.40	0.789	0.215	0.089	22.42	20.175
90.13	90.4	54.50	0.712	-7.85	0.771	0.193	0.080	20.42	20.189
84.87	85.0	52.35	0.695	-6.85	0.751	0.167	0.070	18.60	20.204
70.39	70.2	48.00	0.662	-5.65	0.710	0.116	0.050	15.12	20.189
50.66	49.8	45.40	0.633	-6.55	0.676	0.090	0.041	13.80	20.175
30.92	30.0	46.14	0.614	-8.89	0.659	0.092	0.043	15.17	20.175
15.79	15.0	47.94	0.597	-11.26	0.643	0.096	0.047	17.22	20.182
10.53	10.0	48.77	0.590	-12.33	0.636	0.097	0.048	18.15	20.189
5.13	5.0	49.85	0.582	-13.45	0.626	0.098	0.049	19.40	20.175

[1] Based on the Assumption That There Would be Reduced Losses Due to Slots and Vortex Generators

Table A-4. Slotted Stator 5 Blade Element Design Data Along Design Streamlines[1] (Metric Units)

GEOMETRY DATA

Airfoil: NACA 65 (A = 1.0)
No. of Vanes: 58

Aspect Ratio: 1.689
Chord Length: 0.0554m
Thickness Ratio t/c: 0.090

Percent Span From Tip Leading Edge	Trailing Edge	κ_{le} (deg)	κ_{te} (deg)	ϕ (deg)	$\gamma°$ (deg)	0/0*	σ
94.74	94.9	66.30	-22.42	88.72	21.94	1.311	1.214
90.13	90.4	62.35	-20.42	82.77	20.97	1.255	1.200
84.87	85.0	59.20	-18.60	77.80	20.30	1.201	1.187
70.39	70.2	53.65	-15.12	68.77	19.27	1.126	1.151
50.66	49.8	51.95	-13.80	65.75	19.08	1.101	1.105
30.92	30.0	55.03	-15.17	70.20	19.93	1.131	1.063
15.79	15.0	59.20	-17.22	76.42	20.99	1.188	1.032
10.53	10.0	61.10	-18.15	79.25	21.48	1.212	1.021
5.13	5.0	63.30	-19.40	82.70	21.95	1.238	1.010

VELOCITY DIAGRAM DATA

Percent Span From Tip Leading Edge	Trailing Edge	V_{le} (m/sec)	V_{zle} (m/sec)	$V_{\theta le}$ (m/sec)	β_{le} (deg)	V_{te} (m/sec)	V_{zte} (m/sec)	$V_{\theta te}$ (m/sec)	β_{te} (deg)
94.74	94.9	250.4	138.1	209.4	56.90	139.3	139.3	0.0	0.0
90.13	90.4	244.0	142.9	199.9	54.50	139.5	139.5	0.0	0.0
84.87	85.0	239.9	146.8	189.7	52.35	139.7	139.7	0.0	0.0
70.39	70.2	227.8	152.4	170.1	48.00	140.0	139.9	0.0	0.0
50.66	49.8	218.2	153.5	155.4	45.40	141.5	141.4	0.0	0.0
30.92	30.0	212.4	146.9	153.3	46.14	144.7	144.7	0.0	0.0
15.79	15.0	207.4	141.4	153.9	47.94	148.8	148.6	0.0	0.0
10.53	10.0	205.1	134.1	154.3	48.77	150.5	150.3	0.0	0.0
5.13	5.0	202.5	129.9	154.8	49.85	152.4	152.2	0.0	0.0

DESIGN PERFORMANCE DATA

Stage Pressure Ratio: 1.375

Stage Efficiency: 81.7%

Percent Span From Tip Leading Edge	Trailing Edge	$\Delta\beta$ (deg)	M_{le}	i_m (deg)	D	$\bar{\omega}$	Loss Parameter	$\delta°$ (deg)	$P_{te} \times 10^{-6}$ (N/m^2)
94.74	94.9	56.90	0.728	- 9.40	0.789	0.215	0.089	22.42	0.1391
90.13	90.4	54.50	0.712	- 7.85	0.771	0.193	0.080	20.42	0.1392
84.87	85.0	52.35	0.695	- 6.85	0.751	0.167	0.070	18.60	0.1393
70.39	70.2	48.00	0.662	- 5.65	0.710	0.116	0.050	15.12	0.1392
50.66	49.8	45.40	0.633	- 6.55	0.676	0.090	0.041	13.80	0.1391
30.92	30.0	46.14	0.614	- 8.89	0.659	0.092	0.043	15.17	0.1391
15.79	15.0	47.94	0.597	-11.26	0.643	0.096	0.047	17.22	0.1392
10.53	10.0	48.77	0.590	-12.33	0.636	0.097	0.048	18.15	0.1392
5.13	5.0	49.85	0.582	-13.45	0.626	0.098	0.049	19.40	0.1391

[1]Based on the Assumption That There Would be Reduced Losses Due to Slots and Vortex Generators

Table A-5. Unslotted Rotor 4 Blade Element Design Data Along Design Streamlines[1] (English Units)

GEOMETRY DATA

Airfoil: NACA 65 (A = 1.0)
No. of Blades: 60

Aspect Ratio: 1.820
Chord Length: 2.21 in.

Percent Span From Tip Leading Edge	Trailing Edge	κ_{le} (deg)	κ_{te} (deg)	ϕ (deg)	$\gamma°$ (deg)	0/0*	σ	t/c
97.01	96.90	56.43	-8.50	64.93	23.97	1.286	1.276	0.078
91.02	91.02	56.22	-3.50	59.72	26.36	1.270	1.258	0.076
86.71	86.60	56.28	-0.20	56.48	28.04	1.259	1.243	0.074
71.02	69.60	57.70	9.75	47.95	33.73	1.224	1.197	0.068
50.06	49.10	61.29	16.40	44.89	38.85	1.194	1.143	0.060
29.59	28.40	65.85	19.10	46.75	42.48	1.177	1.093	0.052
14.02	13.50	70.18	19.28	50.90	44.73	1.147	1.060	0.046
9.23	8.80	71.89	19.05	52.84	45.47	1.134	1.050	0.044
3.36	3.36	73.85	18.65	55.20	46.25	1.119	1.040	0.042

VELOCITY DIAGRAM DATA

Corrected Rotor Speed 4210 rpm

Corrected Weight Flow: 110 lb/sec

Percent Span From Tip Leading Edge	Trailing Edge	V'_{le} (ft/sec)	V_{zle} (ft/sec)	$V'_{\theta le}$ (ft/sec)	β'_{le} (deg)	U_{le} (ft/sec)	V'_{te} (ft/sec)	V_{zte} (ft/sec)	$V'_{\theta te}$ (ft/sec)	β'_{te} (deg)	U_{te} (ft/sec)
96.8	94.9	780.1	488.3	608.3	51.25	608.3	413.8	411.4	44.3	6.14	610.7
92.2	89.8	786.4	489.6	615.4	51.49	615.4	437.1	430.9	73.4	9.67	618.0
87.4	84.6	793.0	491.0	622.8	51.75	622.8	459.6	448.0	102.5	12.89	625.3
72.0	69.3	812.7	492.7	646.3	52.68	646.3	519.7	487.1	181.3	20.41	647.2
50.5	49.1	836.8	488.5	679.4	54.28	679.4	560.3	501.6	249.6	26.45	676.1
28.9	29.1	855.8	474.1	712.4	56.36	712.4	561.7	487.2	279.5	29.84	704.5
13.4	14.4	865.4	454.8	736.3	58.30	736.3	545.6	464.7	286.0	31.61	725.4
8.4	9.6	867.9	446.9	744.0	59.01	744.0	540.0	457.5	287.0	32.11	732.3
3.4	4.9	870.0	438.2	751.6	59.76	751.6	535.0	450.9	287.9	32.56	739.1

DESIGN PERFORMANCE DATA

Pressure Ratio: 1.335

Efficiency: 86.8%

Percent Span From Tip Leading Edge	Trailing Edge	$\Delta\beta'$ (deg)	M'_{le}	i_m (deg)	Df	$\bar{\omega}'$	Loss Parameter	$\delta°$ (deg)	P_{te} (psia)	Tte (°R)
96.8	94.9	45.11	0.712	- 5.15	0.754	0.261	0.102	14.44	19.65	576.3
92.2	89.8	41.82	0.718	- 4.76	0.718	0.222	0.087	14.17	19.67	574.7
87.4	84.6	38.86	0.724	- 4.50	0.684	0.186	0.073	13.69	19.69	573.1
72.0	69.3	32.27	0.742	- 4.92	0.599	0.097	0.038	11.11	19.70	568.9
50.5	49.1	30.83	0.764	- 6.97	0.555	0.057	0.022	10.15	19.66	566.7
28.9	29.1	26.52	0.781	- 9.44	0.575	0.106	0.042	10.69	19.54	568.5
13.4	14.4	26.69	0.788	-12.15	0.615	0.184	0.074	12.36	19.38	571.8
8.4	9.6	26.90	0.790	-13.09	0.628	0.211	0.085	13.11	19.33	573.0
3.4	4.9	27.20	0.791	-14.24	0.641	0.238	0.097	13.88	19.28	574.2

[1] No Assumed Reduction in Losses Due to Slots and Vortex Generators

Table A-5. Unslotted Rotor 4 Blade Element Design Data Along Design Streamlines[1] (Metric Units)

GEOMETRY DATA

Airfoil: NACA 65 (A = 1.0)
No. of Blades: 60

Aspect Ratio: 1.820
Chord Length: 0.0561m

Percent Span From Tip Leading Edge	Trailing Edge	κ_{le} (deg)	κ_{te} (deg)	ϕ (deg)	$\gamma°$ (deg)	0/0*	σ	t/c
97.01	96.90	56.43	-8.50	64.93	23.97	1.286	1.276	0.078
91.02	91.02	56.22	-3.50	59.72	26.36	1.270	1.258	0.076
86.71	86.60	56.28	-0.20	56.48	28.04	1.259	1.243	0.074
71.02	69.60	57.70	9.75	47.95	33.73	1.224	1.197	0.068
50.06	49.10	61.29	16.40	44.89	38.85	1.194	1.143	0.060
29.59	28.40	65.85	19.10	46.75	42.48	1.177	1.093	0.052
14.02	13.50	70.18	19.28	50.90	44.73	1.147	1.060	0.046
9.23	8.80	71.89	19.05	52.84	45.47	1.134	1.050	0.044
3.36	3.36	73.85	18.65	55.20	46.25	1.119	1.040	0.042

VELOCITY DIAGRAM DATA

Corrected Rotor Speed: 4210 rpm

Corrected Weight Flow: 49.89 kg/sec

Percent Span From Tip Leading Edge	Trailing Edge	V'_{le} (m/sec)	V_{zle} (m/sec)	$V'_{\theta le}$ (m/sec)	β'_{le} (deg)	U_{le} (m/sec)	V'_{te} (m/sec)	V_{zte} (m/sec)	$V'_{\theta te}$ (m/sec)	β'_{te} (deg)	U_{te} (m/sec)
96.8	94.9	237.8	142.7	185.4	51.25	185.4	126.1	125.4	13.5	6.14	186.1
92.2	89.8	239.7	149.2	187.6	51.49	187.6	133.2	131.3	22.4	9.67	188.4
87.4	84.6	241.7	149.7	189.8	51.75	189.8	140.1	136.6	31.2	12.89	190.6
72.0	69.3	247.6	150.2	197.0	52.68	197.0	158.4	148.5	55.3	20.41	197.3
50.5	49.1	255.1	148.9	207.1	54.28	207.1	170.8	152.9	76.1	26.45	206.1
28.9	29.1	260.2	144.5	217.1	56.36	217.1	171.2	148.5	85.2	29.84	214.7
13.4	14.4	263.8	138.6	224.4	58.30	224.4	166.3	141.6	87.2	31.61	221.1
8.4	9.6	264.5	136.2	226.8	59.01	226.8	164.6	139.4	87.5	32.11	223.2
3.4	4.9	265.2	133.6	229.1	59.76	229.1	164.0	137.4	87.8	32.56	225.3

DESIGN PERFORMANCE DATA

Pressure Ratio: 1.335

Efficiency: 86.8%

Percent Span From Tip Leading Edge	Trailing Edge	$\Delta\beta'$ (deg)	M'_{le}	i_m (deg)	D_f	$\bar{\omega}'$	Loss Parameter	$\delta°$ (deg)	$P_{te} \times 10^{-6}$ (N/m^2)	T_{te} (°K)
96.8	94.9	45.11	0.712	- 5.15	0.754	0.261	0.102	14.44	0.1355	320.17
92.2	89.8	41.82	0.718	- 4.76	0.718	0.222	0.087	14.17	0.1357	319.28
87.4	84.6	38.86	0.724	- 4.50	0.684	0.186	0.073	13.69	0.1358	318.39
72.0	69.3	32.27	0.742	- 4.92	0.599	0.097	0.038	11.11	0.1359	316.06
50.5	49.1	30.83	0.764	- 6.97	0.555	0.057	0.022	10.15	0.1356	314.83
28.9	29.1	26.52	0.781	- 9.44	0.575	0.106	0.042	10.69	0.1348	315.83
13.4	14.4	26.69	0.788	-12.15	0.615	0.184	0.074	12.36	0.1337	317.67
8.4	9.6	26.90	0.790	-13.09	0.628	0.211	0.085	13.11	0.1333	318.33
3.4	4.9	27.20	0.791	-14.24	0.641	0.238	0.097	13.88	0.1330	319.00

[1] No Assumed Reduction in Losses Due to Slots and Vortex Generators

Table A-6. Unslotted Stator 4 Blade Element Design Data Along Design Streamlines[1] (English Units)

GEOMETRY DATA

Airfoil: NACA 65 (A = 1.0)
No. of Vanes: 58

Aspect Ratio: 1.689
Chord Length: 2.182 in.
Thickness Ratio, t/c: 0.090

Percent Span From Tip Leading Edge	Trailing Edge	κ_{le} (deg)	κ_{te} (deg)	ϕ (deg)	$\gamma°$ (deg)	0/0*	σ
94.87	94.87	53.81	-16.48	70.29	18.67	1.324	1.214
90.07	90.07	51.87	-15.59	67.46	18.14	1.310	1.200
85.00	84.85	50.23	-14.62	64.85	17.81	1.297	1.187
70.27	69.98	47.18	-12.52	59.70	17.33	1.265	1.151
50.40	49.95	46.30	-11.67	57.97	17.32	1.236	1.105
30.27	29.25	48.75	-12.52	61.27	18.12	1.216	1.063
15.27	14.60	52.40	-14.12	66.52	19.14	1.196	1.032
10.27	9.70	53.92	-14.95	68.87	19.49	1.194	1.021
5.0	4.60	55.80	-15.95	71.75	19.93	1.199	1.010

VELOCITY DIAGRAM DATA

Percent Span From Tip Leading Edge	Trailing Edge	V_{le} (ft/sec)	V_{zle} (ft/sec)	$V_{\theta le}$ (ft/sec)	β_{le} (deg)	V_{te} (ft/sec)	V_{zte} (ft/sec)	$V_{\theta te}$ (ft/sec)	β_{te} (deg)
95.1	94.5	723.3	449.4	566.7	51.59	371.1	371.1	0.0	0.0
90.2	88.8	719.0	468.6	545.3	49.33	410.1	410.1	0.0	0.0
85.3	83.4	714.2	485.3	523.9	47.19	442.7	442.7	0.0	0.0
70.4	67.8	700.9	521.9	467.8	41.87	505.7	505.7	0.0	0.0
50.7	47.6	681.4	529.5	428.9	39.01	520.3	520.3	0.0	0.0
30.8	27.7	656.3	497.8	427.6	40.66	518.7	518.7	0.0	0.0
15.6	13.5	629.5	448.2	442.0	44.60	520.0	520.0	0.0	0.0
10.4	9.0	619.4	428.2	447.6	46.27	521.9	521.9	0.0	0.0
5.2	4.6	608.2	405.6	453.2	48.17	524.7	524.7	0.0	0.0

DESIGN PERFORMANCE DATA

Stage Pressure Ratio: 1.305

Stage Efficiency: 79.7%

Percent Span From Tip Leading Edge	Trailing Edge	$\Delta\beta$ (deg)	M_{le}	i_m (deg)	D	$\bar{\omega}$	Loss Parameter	$\delta°$ (deg)	P_{te} (psia)
95.1	94.5	51.59	0.639	-2.41	0.810	0.318	0.131	16.55	18.15
90.2	88.8	49.33	0.636	-2.54	0.746	0.264	0.110	15.52	18.44
85.3	83.4	47.19	0.632	-3.12	0.690	0.211	0.089	14.70	18.71
70.4	67.8	41.87	0.622	-5.33	0.569	0.094	0.041	12.50	19.28
50.7	47.6	39.01	0.605	-7.29	0.522	0.063	0.029	11.57	19.39
30.8	27.7	40.66	0.580	-8.06	0.517	0.075	0.035	12.51	19.24
15.6	13.5	44.60	0.553	-7.70	0.515	0.075	0.036	14.14	19.11
10.4	9.0	46.27	0.543	-7.63	0.512	0.074	0.036	14.93	19.07
5.2	4.6	48.17	0.532	-7.58	0.506	0.072	0.036	15.90	19.03

[1] No Assumed Reduction in Losses Due to Slots and Vortex Generators

Table A-6. Unslotted Stator 4 Blade Element Design Data Along Design Streamlines[1] (Metric Units)

GEOMETRY DATA

Airfoil: NACA 65 (A = 1.0)
No. of Vanes: 58

Aspect Ratio: 1.689
Chord Length: 0.0554m
Thickness Ratio, t/c: 0.090

Percent Span From Tip Leading Edge	Trailing Edge	κ_{le} (deg)	κ_{te} (deg)	ϕ (deg)	$\gamma°$ (deg)	0/0*	σ
94.87	94.87	53.81	-16.48	70.29	18.67	1.324	1.214
90.07	90.07	51.87	-15.59	67.46	18.14	1.310	1.200
85.00	84.85	50.23	-14.62	64.85	17.81	1.297	1.187
70.27	69.98	47.18	-12.52	59.70	17.33	1.265	1.151
50.40	49.95	46.30	-11.67	57.97	17.32	1.236	1.105
30.27	29.25	48.75	-12.52	61.27	18.12	1.216	1.063
15.27	14.60	52.40	-14.12	66.52	19.14	1.196	1.032
10.27	9.70	53.92	-14.95	68.87	19.49	1.194	1.021
5.0	4.60	55.80	-15.95	71.75	19.93	1.199	1.010

VELOCITY DIAGRAM DATA

Percent Span From Tip Leading Edge	Trailing Edge	V_{le} (m/sec)	V_{zle} (m/sec)	$V_{\theta le}$ (m/sec)	β_{le} (deg)	V_{te} (m/sec)	V_{zte} (m/sec)	$V_{\theta te}$ (m/sec)	β_{te} (deg)
95.1	94.5	220.5	137.0	172.7	51.59	113.1	113.1	0.0	0.0
90.2	88.8	219.2	142.8	166.2	49.33	125.0	125.0	0.0	0.0
85.3	83.4	217.7	147.9	159.7	47.19	134.9	134.9	0.0	0.0
70.4	67.8	213.6	159.1	142.6	41.87	154.1	154.1	0.0	0.0
50.7	47.6	207.7	161.4	130.7	39.01	158.6	158.6	0.0	0.0
30.8	27.7	200.0	151.7	130.3	40.66	158.1	158.1	0.0	0.0
15.6	13.5	191.9	136.6	134.7	44.60	158.5	158.5	0.0	0.0
10.4	9.0	188.8	130.5	136.4	46.27	159.1	159.1	0.0	0.0
5.2	4.6	185.4	123.6	138.1	48.17	159.9	159.9	0.0	0.0

DESIGN PERFORMANCE DATA

Stage Pressure Ratio: 1.305

Stage Efficiency: 79.7%

Percent Span From Tip Leading Edge	Trailing Edge	$\Delta\beta$ (deg)	M_{le}	i_m (deg)	D	$\bar{\omega}$	Loss Parameter	$\delta°$ (deg)	$P_{te} \times 10^{-6}$ (N/m^2)
95.1	94.5	51.59	0.639	-2.41	0.810	0.318	0.131	16.55	0.1252
90.2	88.8	49.33	0.636	-2.54	0.746	0.264	0.110	15.52	0.1272
85.3	83.4	47.19	0.632	-3.12	0.690	0.211	0.089	14.70	0.1290
70.4	67.8	41.87	0.622	-5.33	0.569	0.094	0.041	12.50	0.1330
50.7	47.6	39.01	0.605	-7.29	0.522	0.063	0.029	11.57	0.1337
30.8	27.7	40.66	0.580	-8.06	0.517	0.075	0.035	12.51	0.1327
15.6	13.5	44.60	0.553	-7.70	0.515	0.075	0.036	14.14	0.1318
10.4	9.0	46.27	0.543	-7.63	0.512	0.074	0.036	14.93	0.1315
5.2	4.6	48.17	0.532	-7.58	0.506	0.072	0.036	15.90	0.1313

[1]No Assumed Reduction in Losses Due to Slots and Vortex Generators

Table A-7. Unslotted Rotor 5 Blade Element Design Data Along Design Streamlines[1] (English Units)

GEOMETRY DATA

Airfoil: NACA 65 (A = 1.0)
No. of Blades: 60

Aspect Ratio: 1.820
Chord Length: 2.21 in.

Percent Span From Tip Leading Edge	Trailing Edge	κ_{le} (deg)	κ_{te} (deg)	ϕ (deg)	$\gamma°$ (deg)	0/0*	σ	t/c
96.41	94.75	60.40	-31.00	91.40	14.70	1.039	1.276	0.078
91.20	89.25	59.90	-22.60	82.50	18.65	1.060	1.258	0.076
86.77	84.80	59.70	-17.00	76.70	21.35	1.079	1.243	0.074
70.84	69.00	60.37	- 2.40	62.77	28.99	1.142	1.197	0.068
50.30	49.40	63.22	7.00	56.22	35.11	1.194	1.143	0.060
29.94	29.75	68.07	9.85	58.22	38.96	1.229	1.093	0.052
13.65	14.40	72.80	10.40	62.40	41.60	1.266	1.060	0.046
9.22	10.00	74.35	10.20	64.15	42.28	1.277	1.050	0.044
3.41	4.70	76.60	9.65	66.05	43.13	1.2	1.040	0.042

VELOCITY DIAGRAM DATA

Equivalent Rotor Speed: 4210 rpm

Corrected Weight Flow: 110 lb/sec

Percent Span From Tip Leading Edge	Trailing Edge	V'_{le} (ft/sec)	V_{zle} (ft/sec)	$V'_{\theta le}$ (ft/sec)	β'_{le} (deg)	U_{le} (ft/sec)	V'_{te} (ft/sec)	V_{zte} (ft/sec)	$V'_{\theta te}$ (ft/sec)	β'_{te} (deg)	U_{te} (ft/sec)
96.39	94.83	775.3	479.3	608.8	51.77	608.8	384.2	373.9	-69.0	-10.8	610.6
92.31	89.41	781.5	481.2	614.9	51.94	614.9	418.9	419.6	-31.5	- 5.1	618.2
87.50	84.37	788.8	483.7	622.5	52.13	622.5	447.1	447.1	2.5	- 0.1	625.6
71.70	69.38	811.8	491.1	646.6	52.79	646.6	503.3	494.1	93.5	10.8	646.8
50.24	49.48	838.7	490.8	679.6	54.15	679.6	529.9	500.6	73.0	19.1	675.3
28.85	29.59	857.4	475.6	712.6	56.19	712.4	529.6	485.0	209.5	23.2	703.7
13.10	14.86	866.5	454.7	736.8	58.21	736.5	510.2	458.6	219.0	25.2	724.7
8.65	9.88	868.7	448.1	743.3	58.74	743.2	497.8	444.7	217.5	25.7	731.7
3.37	4.91	870.8	441.4	751.4	59.61	751.3	481.3	427.7	214.0	26.2	738.8

DESIGN PERFORMANCE DATA

Pressure Ratio: 1.401

Efficiency = 87.3%

Percent Span From Tip Leading Edge	Trailing Edge	$\Delta\beta$ (deg)	M'_{le}	i_m (deg)	D	$\bar{\omega}'$	Loss Parameter	$\delta°$ (deg)	P_{te} (psia)	T_{te} (°R)
96.39	94.83	62.57	0.708	- 8.63	0.851	0.325	0.125	20.20	20.684	587.9
92.31	89.41	57.04	0.714	- 8.06	0.801	0.262	0.104	19.00	20.801	586.0
87.50	84.37	52.23	0.721	- 7.57	0.759	0.210	0.085	17.70	20.882	583.8
71.70	69.38	41.99	0.742	- 7.51	0.663	0.101	0.041	13.80	20.828	578.1
50.24	49.48	35.05	0.766	- 9.07	0.632	0.074	0.030	12.00	20.603	575.0
28.85	29.59	32.99	0.784	-12.21	0.650	0.115	0.048	13.30	20.479	576.6
13.10	14.86	33.01	0.790	-14.79	0.692	0.187	0.080	14.80	20.335	579.5
8.65	9.88	33.04	0.791	-15.86	0.715	0.221	0.095	15.50	20.263	581.0
3.37	4.91	33.41	0.793	-16.99	0.745	0.264	0.114	16.60	20.184	583.0

[1] No Assumed Reduction in Losses Due to Slots and Vortex Generators

Table A-7. Unslotted Rotor 5 Blade Element Design Data Along Design Streamlines[1] (Metric Units)

GEOMETRY DATA

Airfoil: NACA 65 (A = 1.0)
No. of Blades: 60

Aspect Ratio: 1.820
Chord Length: 0.0561m

Percent Span From Tip Leading Edge	Trailing Edge	κ_{le} (deg)	κ_{te} (deg)	ϕ (deg)	$\gamma°$ (deg)	0/0*	σ	t/c
96.41	94.75	60.40	-31.00	91.40	14.70	1.039	1.276	0.078
91.20	89.25	59.90	-22.60	82.50	18.65	1.060	1.258	0.076
86.77	84.80	59.70	-17.00	76.70	21.35	1.079	1.243	0.074
70.84	69.00	60.37	- 2.40	62.77	28.99	1.142	1.197	0.068
50.30	49.40	63.22	7.00	56.22	35.11	1.194	1.143	0.060
29.94	29.75	68.07	9.85	58.22	38.96	1.229	1.093	0.052
13.65	14.40	72.80	10.40	62.40	41.60	1.266	1.060	0.046
9.22	10.00	74.35	10.20	64.15	42.28	1.277	1.050	0.044
3.41	4.70	76.60	9.65	66.05	43.13		1.040	0.092

VELOCITY DIAGRAM DATA

Equivalent Rotor Speed: 4210 rpm

Corrected Weight Flow: 49.89 kg/sec

Percent Span From Tip Leading Edge	Trailing Edge	V'_{le} (m/sec)	V_{zle} (m/sec)	$V'_{\theta le}$ (m/sec)	β'_{le} (deg)	U_{le} (m/sec)	V'_{te} (m/sec)	V_{zte} (m/sec)	$V'_{\theta te}$ (m/sec)	β'_{te} (deg)	U_{te} (m/sec)
96.39	94.83	236.3	146.1	185.6	51.77	185.6	117.1	114.0	-21.0	-10.8	186.1
92.31	89.41	238.2	146.7	187.4	51.94	187.4	127.7	127.9	- 9.6	- 5.1	188.4
87.50	84.37	240.4	147.4	189.7	52.13	189.7	136.3	136.3	0.8	- 0.1	190.7
71.70	69.38	247.4	149.7	197.1	52.79	197.1	153.4	150.6	28.5	10.8	197.1
50.24	49.48	255.6	149.6	207.1	54.15	207.1	161.5	152.6	22.3	19.1	205.8
28.85	29.59	261.3	145.0	217.2	56.19	217.2	161.4	147.8	63.9	23.2	214.5
13.10	14.86	264.1	138.6	224.6	58.21	224.6	155.5	139.8	66.8	25.2	220.9
8.65	9.88	264.8	136.6	226.5	58.74	226.5	151.7	135.5	66.3	25.7	223.0
3.37	4.91	265.4	134.5	229.0	59.61	229.0	146.7	130.4	65.2	26.2	225.2

DESIGN PERFORMANCE DATA

Pressure Ratio: 1.401

Efficiency = 87.3%

Percent Span From Tip Leading Edge	Trailing Edge	$\Delta\beta$ (deg)	M'_{le}	i_m (deg)	D	$\bar{\omega}'$	Loss Parameter	$\delta°$ (deg)	$P_{te} \times 10^{-6}$ (N/m^2)	T_{te} (°K)
96.39	94.83	62.57	0.708	- 8.63	0.851	0.325	0.125	20.20	0.1427	326.61
92.31	89.41	57.04	0.714	- 8.06	0.801	0.262	0.104	19.00	0.1435	325.56
87.50	84.37	52.23	0.721	- 7.57	0.759	0.210	0.085	17.70	0.1440	324.33
71.70	69.38	41.99	0.742	- 7.51	0.663	0.101	0.041	13.80	0.1437	321.17
50.24	49.48	35.05	0.766	- 9.07	0.632	0.074	0.030	12.00	0.1421	319.44
28.85	29.59	32.99	0.784	-12.21	0.650	0.115	0.048	13.30	0.1412	320.33
13.10	14.86	33.01	0.790	-14.79	0.692	0.187	0.080	14.80	0.1403	321.94
8.65	9.88	33.04	0.791	-15.86	0.715	0.221	0.095	15.50	0.1398	322.78
3.37	4.91	33.41	0.793	-16.99	0.745	0.264	0.114	16.60	0.1392	323.89

[1] No Assumed Reduction in Losses Due to Slots and Vortex Generators

Table A-8. Unslotted Stator 5 Blade Element Design Data Along Design Streamlines[1] (English Units)

GEOMETRY DATA

Airfoil: NACA 65 (A = 1.0)
No. of Blades: 58

Aspect Ratio: 1.689
Chord Length: 2.182 in.
Thickness, t/c = 0.090

Percent Span From Tip Leading Edge	Trailing Edge	κ_{le} (deg)	κ_{te} (deg)	ϕ (deg)	$\gamma°$ (deg)	0/0*	σ
94.74	94.90	66.30	-22.42	88.72	21.90	1.311	1.214
90.13	90.40	62.35	-20.42	82.77	20.87	1.255	1.200
84.87	85.00	59.20	-18.60	77.80	20.23	1.201	1.187
70.39	70.10	53.65	-15.12	68.77	19.32	1.126	1.151
50.66	49.80	51.95	-13.80	65.75	19.13	1.101	1.105
30.92	30.00	55.03	-15.17	70.20	19.95	1.131	1.063
15.79	15.00	59.20	-17.22	76.42	21.10	1.188	1.032
10.53	10.00	61.10	-18.15	79.25	21.57	1.212	1.021
5.13	5.00	63.30	-19.40	82.70	22.00	1.238	1.010

VELOCITY DIAGRAM DATA

Percent Span From Tip Leading Edge	Trailing Edge	V_{le} (ft/sec)	V_{zle} (ft/sec)	$V_{\theta le}$ (ft/sec)	β_{le} (deg)	V_{te} (ft/sec)	V_{zte} (ft/sec)	$V_{\theta te}$ (ft/sec)	β_{te} (deg)
94.73	94.40	784.5	388.7	679.5	60.41	283.5	278.5	0.0	0.0
89.86	88.38	782.8	427.9	655.0	57.01	381.0	373.5	0.0	0.0
84.59	82.84	778.9	463.6	626.0	53.58	439.0	441.5	0.0	0.0
70.03	68.49	759.9	520.4	554.0	46.77	509.5	507.5	0.0	0.0
50.73	48.88	732.8	531.2	504.5	43.53	515.0	515.5	0.0	0.0
30.83	28.71	708.6	503.6	498.0	44.59	507.0	506.5	0.0	0.0
15.81	13.87	683.3	454.7	509.0	48.17	496.5	495.5	0.0	0.0
10.54	8.54	671.6	427.8	516.5	50.33	492.5	491.5	0.0	0.0
5.01	5.18	660.3	395.6	527.5	53.12	490.0	489.0	0.0	0.0

DESIGN PERFORMANCE DATA

Stage Pressure Ratio: 1.353

Stage Efficiency: 78.1%

Percent Span From Tip Leading Edge	Trailing Edge	$\Delta\beta$ (deg)	M_{le}	i_m (deg)	D	$\bar{\omega}$	Loss Parameter	P_{te} (psia)	$\delta°$ (deg)
94.73	94.40	60.41	0.690	- 5.89	0.999	0.422	0.174	18.310	22.40
89.86	88.38	57.01	0.690	- 5.19	0.864	0.316	0.132	19.035	20.30
84.59	82.84	53.58	0.688	- 5.42	0.775	0.237	0.100	19.560	18.50
70.03	68.49	46.77	0.674	- 6.73	0.649	0.116	0.050	20.190	15.00
50.73	48.88	43.53	0.649	- 8.42	0.610	0.079	0.036	20.200	13.80
30.83	28.71	44.59	0.626	-10.44	0.618	0.094	0.044	20.045	15.27
15.81	13.87	48.17	0.600	-11.03	0.636	0.118	0.057	19.810	17.20
10.54	8.54	50.33	0.588	-10.77	0.646	0.129	0.063	19.700	18.20
5.01	5.18	53.12	0.576	-10.18	0.654	0.137	0.068	19.630	19.40

[1] No Assumed Reduction in Losses Due to Slots and Vortex Generators

Table A-8. Unslotted Stator 5 Blade Element Design Data Along Design Streamlines[1] (Metric Units)

GEOMETRY DATA

Airfoil: NACA 65 (A = 1.0)
No. of Blades: 58

Aspect Ratio: 1.689
Chord Length: 0.0554m
Thickness, t/c = 0.090

Percent Span From Tip Leading Edge	Trailing Edge	κ_{le} (deg)	κ_{te} (deg)	ϕ (deg)	$\gamma°$ (deg)	0/0*	σ
94.74	94.90	66.30	-22.42	88.72	21.90	1.311	1.214
90.13	90.40	62.35	-20.42	82.77	20.87	1.255	1.200
84.87	85.00	59.20	-18.60	77.80	20.23	1.201	1.187
70.39	70.10	53.65	-15.12	68.77	19.32	1.126	1.151
50.66	49.80	51.95	-13.80	65.75	19.13	1.101	1.105
30.92	30.00	55.03	-15.17	70.20	19.95	1.131	1.063
15.79	15.00	59.20	-17.22	76.42	21.10	1.188	1.032
10.53	10.00	61.10	-18.15	79.25	21.57	1.212	1.021
5.13	5.00	63.30	-19.40	82.70	22.00	1.238	1.010

VELOCITY DIAGRAM DATA

Percent Span From Tip Leading Edge	Trailing Edge	V_{le} (m/sec)	V_{zle} (m/sec)	$V_{\theta le}$ (m/sec)	β_{le} (deg)	V_{te} (m/sec)	V_{zte} (m/sec)	$V_{\theta te}$ (m/sec)	β_{te} (deg)
94.73	94.40	239.1	118.5	207.1	60.41	86.4	84.9	0.0	0.0
89.86	88.38	238.6	130.4	199.6	57.01	116.1	113.8	0.0	0.0
84.59	82.84	237.4	141.3	190.8	53.58	133.8	134.6	0.0	0.0
70.03	68.49	231.6	158.6	168.9	46.77	155.3	154.7	0.0	0.0
50.73	48.88	223.4	161.9	153.8	43.53	157.0	157.1	0.0	0.0
30.83	28.71	216.0	153.5	151.8	44.59	154.5	154.4	0.0	0.0
15.81	13.87	208.3	138.6	155.1	48.17	151.3	151.0	0.0	0.0
10.54	8.54	204.7	130.4	157.4	50.33	150.1	149.8	0.0	0.0
5.01	5.18	201.3	120.6	160.8	53.12	149.4	149.0	0.0	0.0

DESIGN PERFORMANCE DATA

Stage Pressure Ratio: 1.353

Stage Efficiency: 78.1%

Percent Span From Tip Leading Edge	Trailing Edge	$\Delta\beta$ (deg)	M_{le}	i_m (deg)	D	$\bar{\omega}$	Loss Parameter	$P_{te} \times 10^{-6}$ (N/m^2)	$\delta°$ (deg)
94.73	94.40	60.41	0.690	- 5.89	0.999	0.422	0.174	0.1263	22.40
89.86	88.38	57.01	0.690	- 5.19	0.864	0.316	0.132	0.1313	20.30
84.59	82.84	53.58	0.688	- 5.42	0.775	0.237	0.100	0.1349	18.50
70.03	68.49	46.77	0.674	- 6.73	0.649	0.116	0.050	0.1393	15.00
50.73	48.88	43.53	0.649	- 8.42	0.610	0.079	0.036	0.1393	13.80
30.83	28.71	44.59	0.626	-10.44	0.618	0.094	0.044	0.1383	15.27
15.81	13.87	48.17	0.600	-11.03	0.636	0.118	0.057	0.1366	17.20
10.54	8.54	50.33	0.588	-10.77	0.646	0.129	0.063	0.1369	18.20
5.01	5.18	53.12	0.576	-10.18	0.654	0.137	0.068	0.1354	19.40

[1] No Assumed Reduction in Losses Due to Slots and Vortex Generators

APPENDIX B
DEFINITION OF SYMBOLS AND PERFORMANCE VARIABLES

a_o'	Inlet relative stagnation velocity of sound, ft/sec (m/sec)
c	Chord length, in. (m)
C_p	Specific heat at constant pressure, Btu/lb_m - °R(J/kg-°K)
d	Diameter, in. (m)
D	Diffusion factor
g	Gravitation constant, 32.2 lb_m-ft/lb_f-sec^2 (kg-m^2/N-sec^2)
i_m	Incidence angle, deg (based on equivalent circular arc meanline)
J	Mechanical equivalent of heat, 778.2 ft-lb_f (10,558.7 J)
L	Loading parameter
M	Absolute Mach number
N	Rotor speed, rpm
O	Minimum blade passage gap, in. (m)
O^*	Critical blade passage gap, in. (m)
P	Total pressure, psia (N/m^2)
p	Static pressure, psia (N/m^2)
R	Radius, in. (m)
S	Blade passage gap (leading edge), in. (m)
t	Blade maximum thickness, in. (m)
T	Total temperature, °R (°K)
T_s	Static temperature, °R (°K)
TP	Turning parameter
U	Rotor speed, ft/sec (m/sec)

V	Velocity, ft/sec (m/sec)
W	Actual flowrate, lb_m/sec (kg/sec)
β	Air angle, deg from axial direction
$\Delta\beta$	Turning, $\beta_1 - \beta_2$, deg
γ	Ratio of specific heats
γ°	Blade-chord angle, deg from axial direction
δ	Ratio of total pressure to NASA standard sea level pressure of 14.694 psia (101,312.2 N/m^2)
δ°	Deviation angle, deg (based on equivalent circular arc meanline)
η_{ad}	Adiabatic efficiency
θ	Ratio of total temperature to NASA standard sea level temperature of 518.7°R (228.16°K)
κ	Blade metal angle, deg from axial direction (based on equivalent circular arc meanline)
σ	Solidity, c/S
ϕ	Blade camber angle, $\kappa_{le} - \kappa_{te}$, deg
$\bar{\omega}$	Loss coefficient
$\bar{\omega}\cos\beta/2\sigma$	Loss parameter

Subscripts:

0	Compressor inlet (bellmouth)
1	Rotor inlet
2	Rotor exit
2A	Stator exit
c	Cascade critical
fs	Freestream value
id	Isentropic condition
m	Mean, mass, or minimum loss

le	Leading edge
te	Trailing edge
s	Static condition
z	Axial component
θ	Tangential component

Superscripts:

'	Related to rotor blade
—	Mass average value

Definition of Overall Performance Variables

Pressure Ratio:

$$\text{Rotor: } \frac{\bar{P}_2}{\bar{P}_o} \qquad \text{Stage: } \frac{\bar{P}_{2A}}{\bar{P}_o}$$

Corrected Flow:

$$\frac{W\sqrt{\theta}}{\delta}$$

Equivalent Rotor Speed:

$$N/\sqrt{\theta}$$

Adiabatic Efficiency:

$$\text{Rotor: } \frac{(\bar{P}_2/\bar{P}_o)^{\frac{\gamma-1}{\gamma}} - 1}{\bar{T}_{2A}/518.7 - 1} \qquad \text{Stage: } \frac{(\bar{P}_2/\bar{P}_o)^{\frac{\gamma-1}{\gamma}} - 1}{\bar{T}_{2A}/518.7 - 1}$$

Incidence Angle:

$$\text{Rotor: } i_m = \beta'_1 - \kappa_{le} \qquad \text{Stator: } i_m = \beta_2 - \kappa_{le}$$

Diffusion Factor:

$$\text{Rotor: } D = 1 - \frac{V'_2}{V'_1} + \frac{d_2 V_{\theta 2} - d_1 V_{\theta 1}}{(d_1 + d_2)\, V'_1 \sigma}$$

$$\text{Stator: } D = 1 - \frac{V'_{2A}}{V_2} + \frac{d_2 V_{\theta 2} - d_{2A} V_{\theta 2A}}{(d_2 + d_{2A})\, V_2 \sigma}$$

Deviation Angle:

$$\text{Rotor:} \quad \delta^\circ = \beta_2' - \kappa_{te} \qquad \text{Stator:} \quad \delta^\circ = \beta_{2A} - \kappa_{te}$$

Loss Coefficient:

$$\text{Rotor:} \quad \bar{\omega}' = \frac{P'_{2id} - P'_2}{P'_1 - p_1}$$

where:

$$P'_{2id} = P'_1 \left\{ 1 + \frac{\gamma - 1}{2} \left(\frac{U_2^2}{a'^2_{0_1}} \right) \left[1 - \left(\frac{d_1}{d_2} \right)^2 \right] \right\}^{\frac{\gamma}{\gamma - 1}}$$

P' is found from $p/P' = \left[1 + \frac{\gamma - 1}{2} M'^2 \right]^{\frac{\gamma}{1 - \gamma}}$

and M' is calculated using trigonometric functions and the measurements of U, β, P, and p.

$$\text{Stator:} \quad \bar{\omega} = \frac{P_{2_1} - \bar{P}_{2A}}{P_{2_1} - p_2}$$

where:

P_{2_1} = the wake rake freestream total pressure

Loading Parameter

$$L = \frac{\Delta V_\theta \cos \beta_m}{\sigma V_{z\ avg}}$$

where:

$$\beta_m = \arctan \left[0.5 \left(\tan \beta'_1 + \tan \beta'_2 \right) \right]$$

$$Vz_{avg} = 0.5 \left(V_{z1} + V_{z2} \right)$$

$$\Delta V_\theta = \left(V'_{\theta 1} - V'_{\theta 2} \right)$$

Turning Parameter

$$TP = \phi + i_m$$

APPENDIX C
REFERENCES

1. Rockenbach, R. W., "Single-Stage Experimental Evaluation of Slotted Rotor and Stator Blading, Part IX - Final Report," NASA CR-54553, PWA FR-2289, 26 September 1968.

2. Rockenbach, R. W. and J. A. Brent, "Single-Stage Experimental Evaluation of Compressor Blading With Slots and Wall Flow Fences," NASA CR-72635, PWA FR-3597, 1 April 1971.

3. Rockenbach, R. W., J. A. Brent, and B. A. Jones, "Single-Stage Experimental Evaluation of Compressor Blading With Slots and Vortex Generators, Part I - Design of Stages 4 and 5," NASA CR-72626, PWA FR-3461, 20 March 1970.

4. Brent, J. A., "Single-Stage Experimental Evaluation of Compressor Blading With Slots and Vortex Generators, Part III - Data and Performance for Stage 4," NASA CR-72741, PWA FR-3840, 29 December 1970.

5. Brent, J. A. and B. A. Jones, "Single-Stage Experimental Evaluation of Compressor Blading With Slots and Vortex Generators, Part II - Data and Performance for Stage 5 Without Slots or Vortex Generators," NASA CR-72634, PWA FR-3481, 20 March 1970.

6. Linder, C. G. and B. A. Jones, "Single-Stage Experimental Evaluation of Slotted Rotor and Stator Blading, Part III - Data and Performance for Slotted Rotor 1," NASA CR-54546, PWA FR-2110, February 1967.

7. Linder, C. G. and B. A. Jones, "Single-Stage Experimental Evaluation of Slotted Rotor and Stator Blading, Part IV - Data and Performance for Slotted Rotor 2," NASA CR-54547, PWA FR-2111, February 1967.

8. Linder, C. G. and B. A. Jones, "Single-Stage Experimental Evaluation of Slotted Rotor and Stator Blading, Part V - Data and Performance for Slotted Rotor 3 - Slotted Stator 2," NASA CR-54547, PWA FR-2285, August 1967.

9. Linder, C. G. and B. A. Jones, "Single-Stage Experimental Evaluation of Slotted Rotor and Stator Blading, Part VI - Data and Performance for Slotted Stator 1," NASA CR-54549, PWA FR-2286, July 1967.

10. Linder, C. G. and B. A. Jones, "Single-Stage Experimental Evaluation of Slotted Rotor and Stator Blading, Part VII - Data and Performance for Slotted Stator 2, " NASA CR-54550, PWA FR-2287, September 1967.

11. Linder, C.G. and B.A. Jones, "Single-Stage Experimental Evaluation of Slotted Rotor and Stator Blading, Part VIII - Data and Performance for Slotted Stator 2," NASA CR-54550, PWA FR-2287, September 1967.

12. Aerodynamic Design of Axial Flow Compressors (Revised), NASA SP-36, 1965.

13. Smith, Austin G., "On the Generation of the Streamwise Component of Vorticity for Flows in Rotating Passages," The Aeronautical Quarterly, November 1957.

14. Lakshminarayana, B., "Methods of Predicting the Tip Clearance Effects in Axial Flow Turbomachinery," The American Society of Mechanical Engineers Paper No. 69-WA/FE-26, Winter Annual Meeting of the Fluids Engineering Division, November 16-20, 1969.

15. Herzig, Howard F., Arthur G. Hansen, and George R. Costello, "A Visualization Study of Secondary Flows in Cascades," NACA Rep. 1163, 1954.

Distribution List

CONTRACT NAS3-10481

			Copies
1.	NASA-Lewis Research Center 21000 Brookpark Road Cleveland, Ohio 44135 Attention:		
	Report Control Office	MS 5-5	1
	Technical Utilization Office	MS 3-19	1
	Library	MS 60-3	2
	Fluid System Components Division	MS 5-3	1
	Compressor Branch	MS 5-9	5
	Dr. B. Lubarsky	MS 3-3	1
	R. S. Ruggeri	MS 5-9	1
	M. J. Hartmann	MS 5-9	1
	W. A. Benser	MS 5-9	1
	D. M. Sandercock	MS 5-9	1
	L. J. Herrig	MS 7-1	1
	T. F. Gelder	MS 5-9	1
	C. L. Ball	MS 5-9	1
	L. Reid	MS 5-9	1
	L. W. Schopen	MS 500-206	1
	S. Lieblein	MS 100-1	1
	C. L. Meyer	MS 60-4	1
	J. H. Povolny	MS 60-4	1
	A. W. Goldstein	MS 7-1	1
	C. H. Voit	MS 5-3	1
	E. E. Bailey	MS 5-9	1
2.	NASA Scientific and Technical Information Facility P. O. Box 33 College Park, Maryland 20740 Attention: NASA Representative		2
3.	NASA Headquarters Washington, D. C. 20546 Attention: N. F. Rekos (RLC)		1
4.	U. S. Army Aviation Material Laboratory Fort Eustes, Virginia 23604 Attention: John White		1

		Copies
5.	Headquarters Wright Patterson AFB, Ohio 45433	
	Attention: J. L. Wilkins, SESOS	1
	S. Kobelak, APTP	1
	R. P. Carmichael, SESSP	1
6.	Department of the Navy Naval Air Systems Command Propulsion Division, AIR 536 Washington, D. C. 20360	1
7.	Department of Navy Bureau of Ships Washington, D. C. 20360 Attention: G. L. Graves	1
8.	NASA-Langley Research Center Technical Library Hampton, Virginia 23365	
	Attention: Mark R. Nichols	1
	John V. Becker	1
9.	The Boeing Company Commercial Airplane Group Attention: G. J. Schott Organization: G-8410, M.S. 73-24 P. O. Box 3707 Seattle, Washington 98124	1
10.	Douglas Aircraft Company 3855 Lakewood Boulevard Long Beach, California 90801 Attention: J. E. Merriman	
	Technical Information Center C1-250	1
11.	Pratt & Whitney Aircraft Florida Research & Development Center P. O. Box 2691 West Palm Beach, Florida 33402	
	Attention: J. Brent	1
	H. D. Stetson	1
	W. R. Alley	1
	R. E. Davis	1
	R. W. Rockenbach	1
	B. A. Jones	1
	J. A. Fligg	1

		Copies
12.	Pratt & Whitney Aircraft 400 Main Street East Hartford, Connecticut 06108	
	Attention: R. E. Palatine	1
	T. G. Slaiby	1
	H. V. Marman	1
	M. J. Keenan	1
	B. B. Smyth	1
	A. A. Mikolajczak	1
	Library (UARL)	1
	W. M. Foley (UARL)	1
13.	Allison Division, GMC Department 8894, Plant 8 P. O. Box 894 Indianapolis, Indiana 46206	
	Attention: J. N. Barney	1
	G. E. Holbrook	1
	B. A. Hopkins	1
	R. J. Loughery	1
	Library	1
	J. L. Dillard	1
	P. Tramm	1
14.	Northern Research and Engineering 219 Vassar Street Cambridge, Massachusetts 02139	
	Attention: K. Ginwala	1
15.	General Electric Company Flight Propulsion Division Cincinnati, Ohio 45215	
	Attention: J. W. Blanton J-19	1
	W. G. Cornell K-49	1
	D. Prince H-79	1
	E. E. Hood/J. C. Pirtle J-165	1
	J. F. Klapproth H-42	1
	J. W. McBride H-44	1
	L. H. Smith H-50	1
	S. N. Suciu H-32	1
	J. B. Taylor J-168	1
	Technical Information Center N-32	1
	Marlen Miller H-50	1
	C. C. Koch H-79	1

		Copies
16.	General Electric Company 1000 Western Avenue West Lynn, Massachusetts 01905	
	Attention: D. P. Edkins - Bldg. 2-40	1
	F. F. Ehrich - Bldg. 2-40	1
	L. H. King - Bldg. 2-40	1
	R. E. Neitzel - Bldg. 2-40	1
	Dr. C. W. Smith Library - Bldg. 2-40M	1
17.	Curtiss-Wright Corporation Wright Aeronautical Wood-Ridge, New Jersey 07075	
	Attention: S. Lombardo	1
	G. Provenzale	1
18.	AiResearch Manufacturing Company 402 South 36th Street Phoenix, Arizona 85034	
	Attention: Robert O. Bullock	1
	John H. Deman	1
	Jack Erwin - Dept. 32-1 - J	1
	Don Seylor - Dept. 32-1 - J	1
	Jack Switzer - Dept. 32-1 - M	1
19.	AiResearch Manufacturing Company 2525 West 190th Street Torrance, California 90509	
	Attention: Linwood C. Wright	1
	Library	1
20.	Union Carbide Corporation Nuclear Division Oak Ridge Gaseous Diffusion Plant P. O. Box "P" Oak Ridge, Tennessee 37830	
	Attention: R. G. Jordan	1
	D. W. Burton, K-1001, K-25	1
21.	Avco Corporation Lycoming Division 550 South Main Street Stratford, Connecticut 06497	
	Attention: Clause W. Bolton	1

Copies

22. Teledyne Cae
1330 Laskey Road
Toledo, Ohio 43601
Attention: Eli H. Benstein — 1
Howard C. Walch — 1

23. Solar
San Diego, California 92112
Attention: P. A. Pitt — 1
Mrs. L. Walper — 1

24. Goodyear Atomic Corporation
Box 628
Piketon, Ohio 45661
Attention: C. O. Langebrake — 2

25. Iowa State University of
Science and Technology
Ames, Iowa 50010
Attention: Professor George K. Serovy
Dept. of Mechanical Engineering — 1

26. Hamilton Standard Division of
United Aircraft Corporation
Windsor Locks, Connecticut 06096
Attention: Mr. Carl Rohrbach
Head of Aerodynamics and
Hydrodynamics

27. Westinghouse Electric Corporation
Small Steam and Gas Turbine Engineering B-4
Lester Branch
P. O. Box 9175
Philadelphia, Pennsylvania 19113
Attention: Mr. S. M. DeCorso — 1

28. J. Richard Joy
Supervisor, Analytical Section
Williams Research Corporation
P. O. Box 95
Walled Lake, Michigan 48088 — 1

29. Technical Library
Lockheed Missile and Space Company
P. O. Box 879
Mountain View, California 94040 — 1

		Copies
31.	James Furlong Chrysler Corporation Research Office Dept. 9000 P. O. Box 1118 Detroit, Michigan 48231	1
32.	Elliott Company Jeannette, Pennsylvania 15644 Attention: J. Rodger Schields Director-Engineering	1
33.	R. H. Carmody Dresser Industries Inc. Clark Gas Turbine Division 16530 Peninsula Boulevard P. O. Box 9989 Houston, Texas 77015	1
34.	California Institute of Technology Pasadena, California 91109 Attention: Professor Duncan Rannie	1
35.	Massachusetts Institute of Technology Cambridge, Massachusetts 02139 Attention: Dr. J. L. Kerrebrock	1
36.	Caterpillar Tractor Company Peoria, Illinois 61601 Attention: J. Wiggins	1
37.	Professor B. Lakshminarayana Department of Aerospace Engineering 233 Hammond Building Penn State University University Park, Pennsylvania 16802	1
38.	Dr. Meherwan P. Boyce P. E. Department of Mechanical Engineering Texas A&M University College Station, Texas 77843	1
39.	National Technical Information Center Springfield, Virginia 22151	14